PEOPLES' FRIENDSHIP UNIVERSITY OF RUSSIA

*published as a manuscript*

**Shehak Sattar**

# MODEL OF THERMOMECHANICAL STRESSES IN THERMOELECTRIC SYSTEMS

2.3.1. System Analysis, Management and Information Processing, Statistics

Dissertation
For the degree of
Ph.D. candidate of technical sciences

Scientific supervisor:
Doctor of Technical Sciences
Victor Vasilyevich Belyaev

**Moscow – 2022**

Федеральное государственное автономное образовательное учреждение высшего образования
«РОССИЙСКИЙ УНИВЕРСИТЕТ ДРУЖБЫ НАРОДОВ»

*на правах рукописи*

**Саттар Шехак**

# МОДЕЛЬ ТЕРМОМЕХАНИЧЕСКИХ НАПРЯЖЕНИЙ В ТЕРМОЭЛЕКТРИЧЕСКИХ СИСТЕМАХ

2.3.1. Системный анализ, управление и обработка информации, Статистика

Диссертация
на соискание ученой степени кандидата технических наук

Научный руководитель:
доктор технических наук
Беляев Виктор Васильевич

Москва 2022 г.

# Contents

## List of Abbreviation

| No. | Abbreviation | Meaning |
|---|---|---|
| 1 | TE | Thermoelectric |
| 2 | TEG | Thermoelectric generator |
| 3 | CTE | Coefficient of thermal expansion |
| 4 | NASA | National Aeronautics and Space Administration |
| 5 | RTG | Radioisotope Thermoelectric generator |
| 6 | MHW | multihundred-watt |
| 7 | MMRTG | Multi-Mission Radioisotope Thermoelectric Generator |
| 8 | eMMRTG | Enhanced Multi-Mission Radioisotope Thermoelectric Generator |
| 9 | TESI | Teledyne Energy Systems, Inc |
| 10 | JPL | Jet Propulsion Laboratory |
| 11 | MRL | Mean residual life |
| 12 | SKD | Skutterudite materials |
| 13 | FEM | Finite Element method |
| 14 | IMC | Intermetallic compound |
| 15 | LAST | lead–antimony–silver–tellurium |
| 16 | MTBF | Mean time between failure |
| 17 | CDF | cumulative probability function |
| 18 | PDF | probability density function |
| 19 | MPa | Mega Pascal |
| 20 | MRVR | Fast Multi-output relevance vector regression |
| 21 | HT | High Temperature |
| 22 | LT | Low Temperature |
| 23 | CAGR | Compound annual growth rate |

# INTRODUCTION

## Relevance of Research

Despite the relatively low efficiency and limited reliability, the thermo-electric generators (TEG) have found their application in the creation of backup or emergency sources of electricity. Many countries, companies and universities are actively investing on thermoelectric research. Generally thermoelectric devices are being used as power source for spacecrafts, monitoring distant areas through wireless networks, monitoring gas pipelines, cathodic protection stations and gas distribution points.

Several studies have shown that to predict sustainability of the thermoelectric device thermally induced stresses are bottlenecks, especially for high temperature thermoelectric devices. Due to lack of technological solution, numerical analysis plays a significant role to optimize device geometry and boundary conditions under stress load. Despite the fact that two decades of research has widen the range of material selection but thermoelectric device has not yet seen success in any large-scale terrestrial applications. Much of the conducted studies focus on the influence of device's design, material's phase transition and shape of the thermoelectric device. But there are very few available studies which can quantify the effect of thermo-mechanical stresses on device's reliability. The existing literature on thermoelectric reliability rely on accelerated life testing (AFT) and mean time between failure (MTBF) methods. These methods conclude the reliability of the device based on statistical failure data without considering factors of failure. These methods don't provide enough characterizations of thermoelectric devices.

Third popular method, to analysis and measure reliability of the devices, is Weibull distribution, which is the most suitable model for modules operating gradient is T > 300 C. Most of the cases, where Weibull distribution is applicable, are flaw, fracture, and volume defect failures. But as the range of data increases and size of devices decrease, Weibull distribution has higher relative error compared to lognormal distribution. Different universities (for example Korea Advanced Institute of Science and Technology, School of

Technology, Oxford Brookes, University, Lulea University of Technology, Sweden) are actively publishing experimental- simulation based papers to demonstrate authenticity of the lognormal distribution for high stress bodies (Devices or system) over Weibull distribution. And many researchers (for example Jin Seon Kim, M.T. Todinov etc.) has demonstrate that by considering material characteristics under stress load lognormal is one of suitable alternatives. The proposed research is the first attempt to model the reliability of thermoelectric system by considering lognormal distribution.

**Degree of development of the research topic**

Studies, the results of which are published in the modern literature, do not quantify the effect of thermomechanical loads on the reliability of the device. The existing literature on thermoelectric reliability was based on the Accelerated Endurance Test (AFT) method and the mean time between failures (MTBF). Both methods are based on the number of thermal cycles to failure, which does not provide qualitative information about the reliability of the device. Ephraim Sukhir presented a detailed research paper using a model of shear stress and shear deformation, but it only provides deformation (or bending) of the device. The model cannot predict the survivability of the device. Recently, Naveen Kishore Curry published a numerical and finite element analysis concerning the reliability of a thermoelectric device. Although the model provides a qualitative study of reliability, the model uses a statistical theory of fracture based on Weibull analysis based on destruction data. This model is specifically used for brittle materials such as ceramics. As the data range increases and the size of the devices decreases, the Weibull distribution has a higher relative error compared to the lognormal distribution. In this direction , various organizations in Russia and abroad (for example, the Korea Advanced Institute of Science and Technology, Oxford Brookes University, UK, Luleå University of Technology, Sweden) have published results based on experimental modeling, demonstrating reliability of lognormal distribution for bodies with high voltage according to the Weibull distribution. Many researchers (Jin Sung Kim (National University of Pukyong, South Korea); M.T. Todinov (Oxford Brookes University), etc.) have shown that when considering the characteristics of the material

logarithmically normal voltage is one of the suitable alternatives.

The problems of thermoelectric reliability and the need for the right model, emphasizing the reliability of the thermoelectric device, are in demand now more than ever. There is no significant work providing mathematical work regarding the requirements for a thermoelectric device, which was the motive for the research work.

Our research aims to optimize a mathematical model to predict thermomechanical stresses in a thermoelectric system, offering a suitable solution to compensate for excessive thermomechanical stresses without compromising the performance of the optimized system. To study the possibilities of the mathematical model and the influence of geometry, boundary conditions and the space between the branches on the thermoelectric device, simulations were carried out in MATLAB and the finite element method. The results obtained show that the ratio of length to thickness of a given thermoelectric branch has a significant effect on the voltages in the system, whereas the shape has a negligible effect. The effect of thermoelectric stresses on mechanical reliability is estimated using the parametric and nonparametric logarithmic-normal distribution instead of Weibull, based on the analysis of the theory of failures.

## Target of Research

Mathematical model for thermoelectric module to enhance their operating life optimized by reducing thermo-mechanical stresses without compromising their performance.

## Subject of Research

Development of mathematical model to measuring thermo-mechanical stresses and predict reliability of the thermoelectric device. The contemplation of geometry, boundary conditions and space between each leg for thermoelectrical modules, for both unsegmented and segmented modules.

## Tasks

1. Develop an optimized mathematical model to present relationship between heat fluxes, electrical power, and efficiency of the device. Find the impact of Joule heat on thermal conductivity and charge carriers in the given volume and surface.
2. Developing an optimized mathematical model to measure plane stress and strain, shearing stresses, stress function and study thermoelastic behavior of thermoelectric legs. Compile the results in MATLAB and develop characteristics of thermoelectric leg, for segmented and unsegmented devices.
3. Developing an optimized mathematical model to predict the reliability of thermoelectric devices using parametric lognormal mean residual life and nonparametric Lognormal kernel distribution.
4. Developing a comprehensive comparative discussion to illustrate the maximum likelihood using Bayesian nonparametric Lognormal-Kernel inference method regarding to Monte Carlo simulation, Weibull's distribution, and Lognormal mean residual life for various shapes for the survival function on MATLAB.

## The Scientific Novelty

Our study presents the following innovative results

1. Mathematical model can predict precise characteristics of the thermoelectric device and influence of thermally induced stress on mechanical properties. Naotake's plate theory was first time optimized and applied on thermoelectric device to measure stresses.
2. Our research work first time presents a mathematical model to calculate precise number of thermoelectric legs in device. MATLAB simulation and COMSOL solution shows that by increasing space between legs can compensate excessive thermally induced stresses.
3. Our research work provides first time an optimistic way of utilizing lognormal distribution to calculate lifetime of device using parametric and non-parametric lognormal distribution.
4. Additionally, first time we have mathematically derived a non-parametric survival

function to find mean residual life of devices that are working at medium and higher temperature gradient by using discrete data.

## Theoretical significance

The developed methodology, the mathematical description of thermomechanical stresses, elements of thermoelectric devices, as well as the created software and computing tools will serve to further develop scientific research aimed at improving the technologies for generating thermoelectricity and their reliability.

## Practical Significance

Implementation of the mathematical model has following practical significance:

1. The optimized model demonstrates possible model to increase life of thermoelectric system in future, without compromising its efficiency. By increasing lifetime of the device will save project cost and increase material compatibility factor.
2. By managing stresses in thermoelectric device, thermoelectric systems will play more significant role in future space projects, waste heat production industries, buildings, and cars.
3. The mathematical model ultimately prescribes number of legs in device and their sustainable height to thickness ratio for log operating life.
4. The temperature gradient can be designed according to survive able thermal stresses and vice-versa.
5. Lognormal distribution mean residual life and non-parametric survival function are newly introduced and will play a distinctive role in thermoelectric systems compare to Weibull failure theory.

## Methodology and methods of research

The work is based on the methods of mathematical modeling and system analysis in the selection of optimal solutions. The basis of the developed mathematical models is represented by the fundamental laws of the physical phenomena under study. Generally accepted, certified databases are used to describe thermodynamic properties. Numerical methods for solving systems of equations were used to organize the computational process.

## Fundamental Principles Submitted to Defense

1. Model can is used to measure thermo-mechanical stresses by analyzing resultant forces and resultant moment per unit thickness, induced due to thermal stresses.
2. The model considers two basic boundary conditions to measure thermal expansion of each material. The expansion is direct product of temperature-deformation relation under given boundary conditions.
3. The relationship between principle of energy conservation, local conservation of mass theory and maximum stress principle investigated by changing the TE geometrical parameters to compensate thermally induced stresses and sustain reliability of the device.
4. The optimized lognormal parametric mean residual life and non-parametric survival function derived under Bayesian inference method criteria to measure the reliability of thermoelectric systems instead of Weibull distribution.

## Degree of reliability of the results

- the developed models are based on facts and verified data, are consistent with the published experimental and theoretical results on the topic of the dissertation;
- generally accepted methods of optimization and modeling based on theories that have confirmed their applicability were used;
- established the qualitative and quantitative coincidence of the author's results with the results presented in independent sources on this topic;
- modern proven methods of processing initial information were used.

## Evaluations of Work

Basic concepts and results were discussed and presented at different international scientific conferences, seminars and department sessions:

1. New approaches and technologies for designing, manufacturing, testing and industrial design of rocket and space products. Proceedings of the II International Youth Conference. Publishing house: Diona Limited Liability Company (Moscow).
2. XVI Interstate Conference “Thermoelectric and their applications” October 2018, Saint-Petersburg, Russia
3. 38$^{th}$ international conference on Thermoelectric and 4$^{th}$ Asian conference on Thermoelectric, South Korea (ICT/ACT 2019)
4. Advances in the Astronautical Sciences, RUDN, Moscow Russia. 2020
5. International multidisciplinary conference “Perspective element base of micro- and nanoelectronics using Modern Achievements in Theoretical Physics” 2019.
6. International conference on "Perspective of elemental base of micro- and nanoelectronics using modern achievements of theoretical physics" 2021
7. XVII Interstate Conference “Thermoelectric and Their Applications” (ISCTA 2021) St. Petersburg, Russia September 13 – 16, 2021

## Publications

This work includes 6 publications: 5 published in (SCOPUS, WOS) indexed journals, 1 in (VAK, RUDN list) indexed journals

## Personal contribution

The author took the lead contribution from selecting the research topic to obtaining the overall results. The author personally developed the theoretical basis, models, optimization criteria and all technical details, performed coding, performed numerical

simulations, received, analyzed, and summarized the results, and then wrote the manuscript. The Author's contribution is predominant where he has participated in all stages of research: task setting, realization, and discussed research results in scientific publications and conferences.

## Structure and Volume of work

This work consists of introduction, a literature review chapter and 3 other chapters, conclusion, glossary, and References. The total volume of the dissertation is 104 pages, including 84 references, 40 figures, 5 tables, and 94 formulas.

# Chapter 1. Literature Review

The search for more sustainable energy is an ever-growing global concern because of escalating global warming associated with consumption of fossil fuel. Among the other feasible technologies, thermoelectric (TE) energy is an interesting viable alternative because the TE devices can convert given heat, through different sources, into electric power using the Seebeck affect without requiring moving components. Due to the absence of moving parts, and, as a result, the reliability that allows such systems to operate in unattended mode for a long period of time (decades), today there is practically no alternative to such generators in space exploration.

Despite the relatively low efficiency, the conventional thermo-electric generators (TEG) have found their application in the creation of backup or emergency sources of electricity. Specifically, Russian government is using TEGs as power source for monitoring distant areas through wireless networks, monitoring gas pipelines, cathodic protection stations and gas distribution points.

Figure 1.1 (a) & (b) shows the trending Global thermoelectric generators market, which has plan to grow from USD 460 million in 2019 to USD 741 million by 2025, at a CAGR of 8.3% during the forecast period [1]. Since TE devices plan a significant role in industries and space, the need to improve the efficiency of TE devices is growing as well. Globally, the TEG market has application in automotive, aerospace, defense, industrial, consumer, healthcare, oil & gas, mining, and telecommunications sectors. Among these, the industrial sector has acquired the highest CAGR during the forecast period. Many industries have invested significant amount of investment in the growth of TE technologies in the past few years. Continuous improvement in the efficiency of the TE modules and system, the stringent standards for environmental conservation the thermoelectric generator are expected to be popular among both developing and developed countries (See figure 1.1 (b)).

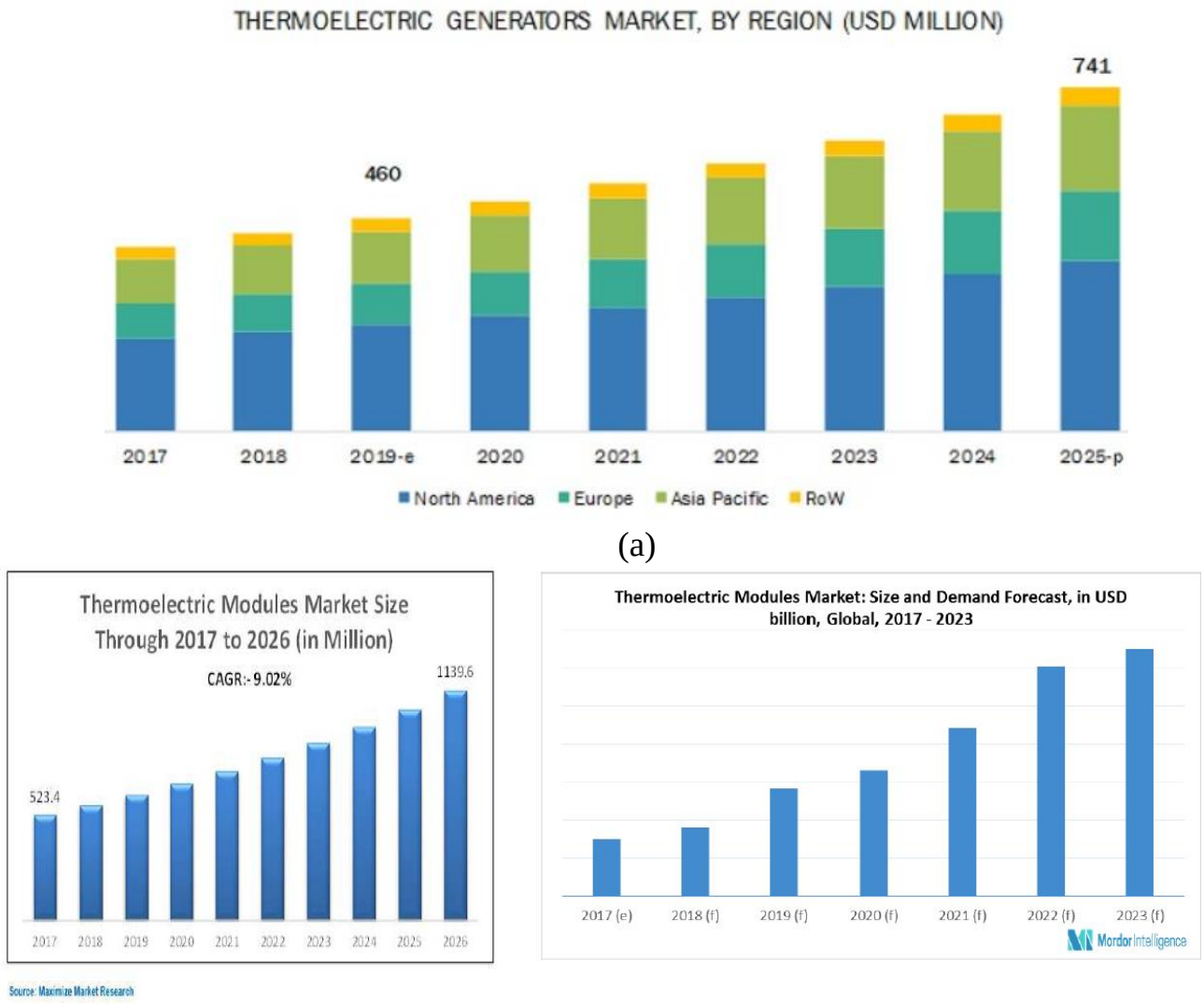


Figure 1.1 The Trending Global Thermoelectric Generators Market

The range of Applications regarding to material, temperature and efficiency are listed in below in table 1.1. The table entails 9 major material categories that are currently being utilized in commercial applications.

Table. No. 1.1

| **Material Type** | **Efficiency(η%) Range** | **Temperature Range** | **Major Applications** |
|---|---|---|---|
| Bismuth Chalcogenides | 3-5 | 20 – 200°C | -Medical Instruments<br>-Wearable Thermoelectric Generators<br>-Printing Technology<br>-Solar concentration thermoelectric generator |
| Group IV Tellurides | 2-7 | 200-600 | -Wireless Networks, -Monitoring gas pipelines,<br>-Cathodic protection stations<br>-Gas distribution points |

| | | | |
|---|---|---|---|
| Silicon-Germanium Alloys | 5-7.8 | 600C – 1000°C | -Space Technologies<br>-High Temperature sensors<br>- Monitoring distant area |
| Skutterudites | 2- 8 | 300-700°C | - Space Technologies<br>-Waste heat Energy Industries<br>- Automobile (Waste Heat Energy) |
| $Mg_2B_{IV}$ Solid Solutions | 1- 5.3 | 200-500°C | -Solar thermoelectric generators<br>- Kitchen |
| Silicides | 2-5 | 300-700°C | -Aircraft<br>- Waste Heat Energy<br>- Refrigerators<br>- Unmanned Aerial Vehicles |
| Clathrates | 0.3-1 | 300-700°C | -Stove<br>- Radio<br>- CdZnTe detector |
| Half-Heussler Compounds | 1- 8.7 | 300-700°C | -Automobile Exhaust heat Energy<br>- Motorcycles |
| Oxides | 0.3 upto 1 | 400-1000°C | High Temperature waste heart recovery |

The main challenge TE devices currently encounter is regarding to temperature gradient. In this regard two different types of TE devices are concerned.

## 1.2 Conventional *vs* Segmented TE Devices

Mainly there are two different TE devices are commercially being used (a) Conventional (unsegmented) and (b) Segmented TE devices (block diagrams are shown in figure 1.2). As shown in figure 1.2 (a) Conventional Thermoelectric devices are simple to operate but their applications are limited due to low conversation efficiencies. They mostly work under 300 $^{o}$ C and suitable for devices which run on low power. But TE devices efficiency doesn't only depend on the total conversion of heat into energy, derived as "figure of merit (FOM)", but also by its overall ability to work at different temperature span. Thus, conventional TE devices usually operate well only within a certain temperature range. In order to optimize figure of merit and performance, new TE materials are discovered (or tested) to utilize them at higher temperature gradient. To realize the approaches segmentation

(or Cascade) TE generators have been introduced. As shown in figure 1.2 (b), in the segmentation TE module, each module-leg (n- and p-Type) is made of at least two different materials. These materials are connected physically parallel while electrically and thermally in series.

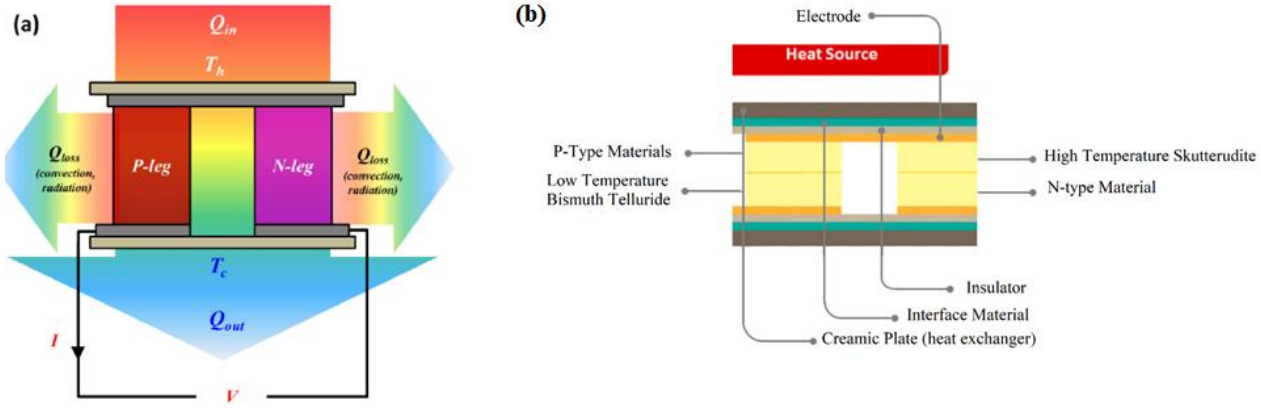


Figure 1.2 (a & b) Conventional *vs* Segmented TE device diagram

Significant efforts have been dedicated for material development and optimization of structures. Yet, after decades of research and work, hardly conventional TE devices can provide high power supply for terrestrial and space applications. Although conventional TE devices are widely being used as waste heat recovery generator in industries, automobiles, aircrafts and helicopters, ships and decentralized domestic areas. But they generally have FOM ~ 1 and create relatively low performance, occupies larger area and manufacturing cost is high with conversation efficiencies of only 3-6%[2]. This is due to a fact that transport properties of conventional TE modules are strongly interdependent. For example, Seebeck coefficient is accompanied with lowering the electrical conductivity and vice versa. Moreover, increasing the electrical conductivity unavoidably leads to an increase in the electronic part of the thermal conductivity[3]. This limits their commercialization merely to niche areas where the reliability and scalability are superior to the operation efficiency.

In order to overcome conventional device limitations, new methods, such as Nano-structuring, band structuring, phonon, and electron engineering, has opened new horizons of optimizing TE device design and efficiency. One of the outcomes of these developments is segmentation of multiple materials to enhance their conversation efficiency from medium to higher temperature. The emergence of segmented devices was primarily driven from the fact

that the properties of TE materials essentially depend on temperature. Each material can achieve maximum conversation efficiency within certain sufficiently narrow temperature range. Thus, materials were chosen for segmentation in such a way that maximum conversation efficiency could be achieved within operational temperature range. The results have revealed that by segmentation TE device can achieve higher conversation efficiency, that is up to 20% [4].

This enhancement has increased market demand and range of applications. Figure [1.3] shows the rising demand of segmented thermoelectric generators in recent era. Although, successive laboratory experiments on segmentation have managed to bring the demand of TEGs in supply-line as a renewable energy source, but still the market share of TEG doesn't exceed more than 5%. Most of the commercially available TE generators are conventional devices and have limited efficiency (see figure 1.5 (b)) but it is expected that till 2025 TE devices will not only gain market space in industrial areas, automobile companies but introduce more stable segmented TEGs and TECs. Figure 1.3 demonstrates that, in near future, more segmented TE devices will be commercially produced as compared to conventional TE devices.

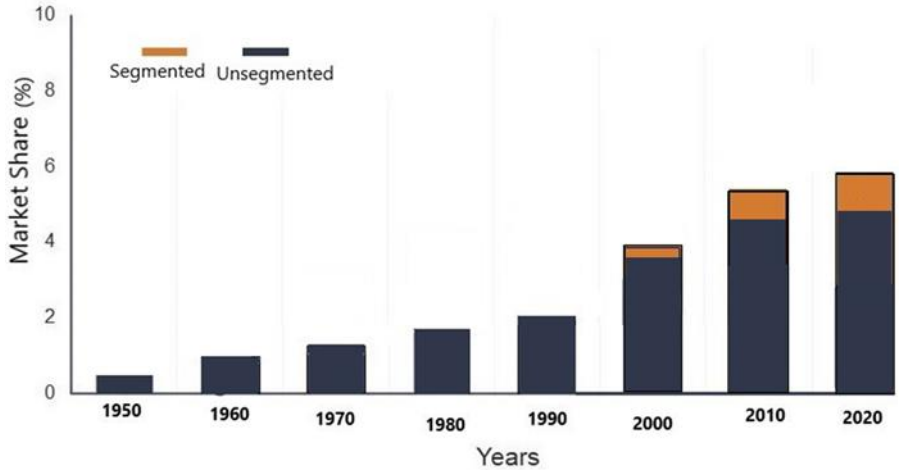


Figure 1.3 Rising demand of Segmented TE devices

Assumably the segmented devices have their own challenges which halt their commercialization. These challenges come mainly from two main factors which are consistently reported after analyzing failed devices. In this regard current challenges are described below in detail.

## 1.3 Current Challenges

The efficiency of the TE device is governed by the properties of TE material and temperature gradient across the device. Temperature gradient, from hot to cold side, controls the limits of Carnot efficiency and TE material plays a significant role to set the upper limits of FOM, i.e., how close the efficiency could be to Carnot efficiency. Figure1.4 shows the difference between Carnot efficiency and attainable FOM.

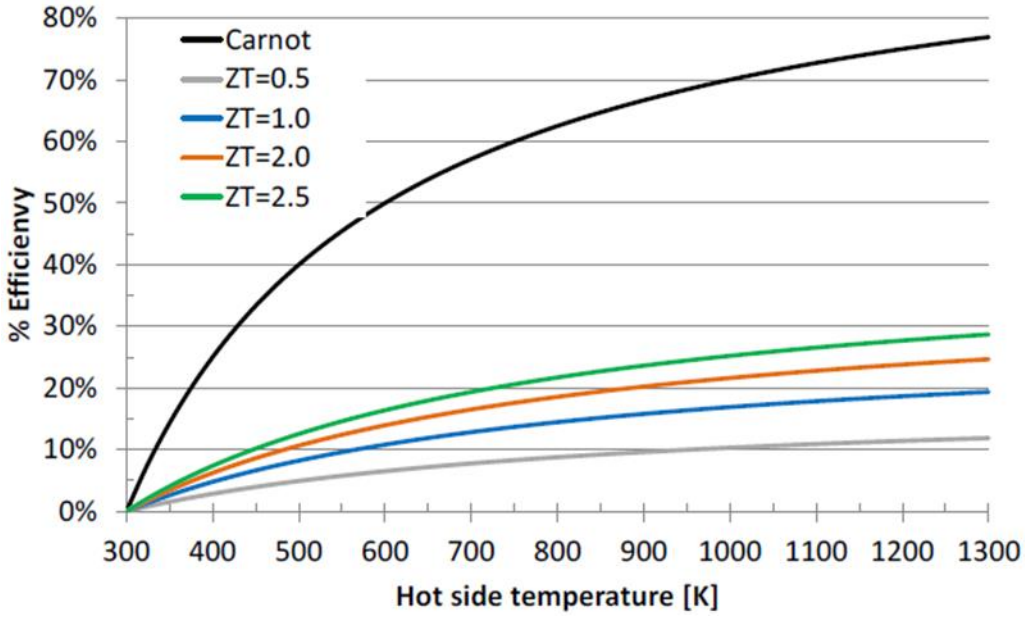


Figure 1.4 Maximum FOM of a TE device compared to Carnot efficiency

The relevant TE material properties which play significant role to define maximum FOM are [5]

a) Seebeck coefficient
b) thermal conductivity
c) Electrical resistivity

These properties vary with temperature and define possible limits of FOM. Thus, the desire to achieve Carnot (high) efficiency from a TE device, we must achieve high FOM at higher temperature. The desire to achieve higher FOM, the use of conventional TE device (built by same material throughout) not possible. Alternative to conventional TE device (Ideally), segmented TE devices, in the case where high temperature materials joined with

low temperature material, can give us maximum efficiency.

Combing different material raise the compatibility problems. Under practical working conditions there are various compatibility factors that influence the performance of a TE device. These factors play a crucial role during continuous heat cycles[6]. These factors are[7]

1. Low Electrical conductivity
2. Low thermal conductivity
3. Mismatch of CTE with neighboring TE material
4. Inability to reduce total electrical and thermal resistance
5. High contact resistance at the interface between contact layer and the TE layer
6. Unstable at the working (high) temperature
7. Unable to form strong mechanical bonds between TE materials
8. Low yield strength of TE material than to solder at operating temperature.

Statistical analysis, based on different literature (articles)[8] [9][10], shows that the compatibility factors has significant effect on FOM of devices. Laboratorial research suggests that at higher temperature most of the devices can't stand long heat-cycling [11]. Conventional TE devices during rapid (or frequent) changes in temperature causes reduction in the Seebeck coefficient and increase in thermal resistivity. Whereas segmented TE devices encounter decreases in the Seebeck coefficient, inter-layer diffusion at the solder (both n- and p-type module), sublimation and microcrack[12]. The statistical analysis has shown (see figure 1.5 (a)) that majority of the TE devices are limited between 1 to 1.8 FOM. Whereas temperature gradient lye between 300 to 500 C. As the temperature gradient increases, number of devices with 2 or above FOM decrease. Even the highest FOM of TE device is between 300 to 400 C, that is 2.8 FOM. Whereas figure 1.5 (b) shows variation of FOM as per leg. This factor has been highlighted by P. Ponnusamya[13], where she has demonstrated the effect of temperature on charge carrier density of leg. The non-constancy of temperature dependance, thermal conductivity significantly deflects FOM from linear one.

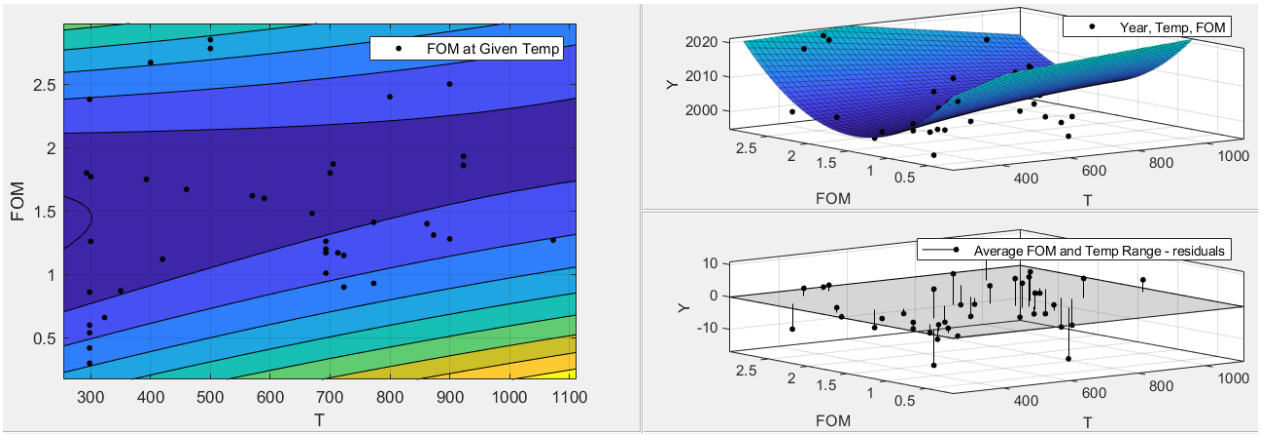


(a)

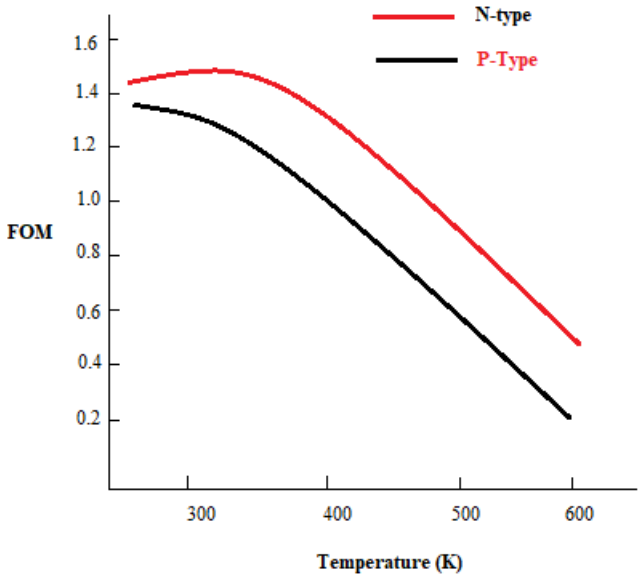


(b)

Figure 1.5 (a) FOM with respect to temperature per year (b) Currently Commercially available TEGs

Not only FOM, rapid temperature change during operational hours also distorts leg geometry, dimensions (length and space between n-p type legs), metallization and thickness of barrier layer [14]. These challenges are known as "Operational Thermo-Mechanical Stresses". One of the major factor impact of frequent (or rapid) temperature change is that it make the TE devices vulnerable to diffusion of impurities at the interfaces and edges[15] leading to cracks, deformation, and fatigue (shown in below in block diagram figure 1.6).

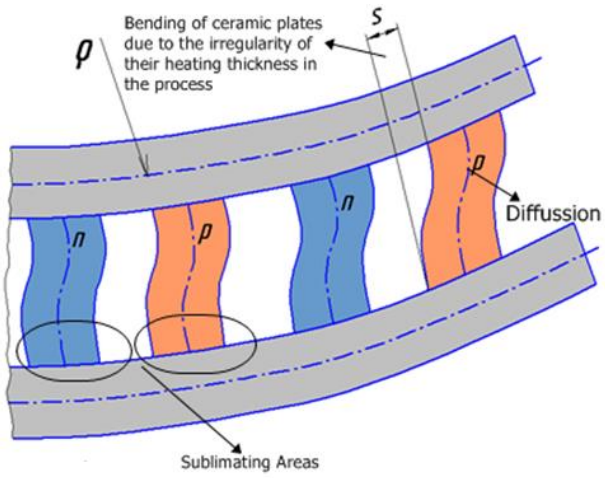


Figure 1.6 Deformation of Structure due to Stress at TEG legs due to Bending, diffusion and sublimation area of TE leg

Block diagram, shown in Figure 1.6, shows the bending or deformation of leg due to thermos-mechanical stress risen during rapid thermal cycling. Plus, the effect of thermo-mechanical stress can also cause sublimation and oxidation, in most of the cases when temperature goes beyond 500C. This is because higher temperature gradient causes thermally induced expansion, which leads to sublimation, bending, crack and deformation. Whereas increase in oxidation reaction leads to incline in thermal stresses, causing spallation of leg. In this regard, statistical analyzes are conducted to understand main challenges regarding to factor effecting structural stability (See table 1.2)

Table 1.2 Overview of Unsegmented devices [16]

| **Material Type** | **Popular Unsegmented Compositions** | **Efficiency (η %) Range** | **Temperature Range** | **Failure Reasons** | **Future Challenges** |
|---|---|---|---|---|---|
| Bismuth Chalcogenides | $Bi_2Te_3$, $Sb_2Te_3$, $Bi_2Se_3$ | 3-5 | 100 – 250°C | -Cracks are found after 4500 thermal cycles [[17]] | -Minimize thermally induced Stress |
| Group IV Tellurides | PbTe, GeTe, SiTe | 2-7 | 200-600 | - Pb, Te sublimate<br>- Low resistance Contacts<br>- Cracks | - Minimize thermally induced Stress<br>- Enhance material Compatibility factor |
| Silicon-Germanium Alloys | SiGe | 5-7.8 | 600C – 1000°C | -Stable Mechanical structure but Sublimates | - Minimize thermally induced Stress |
| Skutterudites | $Ce_{0.45}Co_{2.5}Fe_{1.5}Sb_{12}$ (P)<br>$Yb_{0.25}Co_4Sb_{12}/Yb_2O_3$ (N) | 2- 8 | 300-700°C | -Sublimation<br>-Diffusion<br>-Oxidation | - Minimize thermally induced Stress<br>- Enhance material Compatibility factor |
| $Mg_2B_{IV}$ Solid Solutions | $Mg_2$(Si-Sn) | 1- 5.3 | 200-500°C | -Decomposes and oxidizes<br>-Intermetallic Compounds<br>-Low resistance contact<br>-oxidation | - Minimize thermally induced Stress<br>- Enhance material Compatibility factor |
| Silicides | $MnSi_1$ (HMS)<br>$FeSi_2$, $CrSi_2$, CoSi, $Ru_2Si_3$<br>$Fe_2VAl_{0.9}Si_{0.1}$(P)<br>$Fe_2V_{0.9}Ti_{0.1}Al$ (N) | 2-5 | 300-700°C | - Low mechanical strength due to metallic compounds<br>- Intermetallic Compounds<br>- Interlayer diffusion | - Minimize thermally induced Stress<br>- Enhance material Compatibility factor |
| Clathrates | $In_{0.25}Co_3Fe_1Sb_{12}$ (P)<br>$In_{0.25}Co_{3.95}Ni_{0.05}Sb_{12}$ (N) | 0.3-1 | 300-700°C | -Unstable contact due to Intermetallic Compounds | - Minimize thermally induced Stress |

| | | | | | |
|---|---|---|---|---|---|
| | | | | -Sublimation | - Enhance material Compatibility factor |
| Half-Heussler Compounds | $Hf_{0.3}Zr_{0.7}CoSn_{0.3}Sb_{0.7}$ (P)<br>$Hf_{0.6}Zr_{0.4}NiSn_{0.995}Sb_{0.005}$ (N) | 1- 8.7 | 300-700°C | -Oxidation causes cracks and weakens the Mechanical structure | - Minimize thermally induced Stress |
| Oxides | $Ca_3Co_4O_9$ (P)<br>$Zn_{0.98}Al_{0.02}O$ (N) | 0.3 upto | 400-1000°C | Parasitic Losses | - Enhance material Compatibility factor |

Table 1.3 overview of Unsegmented devices [16], [18]–[20]

| **Material Type** | **Popular Segmented Compositions** | **Temperature Range** | **Efficiency (η %) Range** | **Failure Reasons** | **Current Challenges** |
|---|---|---|---|---|---|
| Bismuth Chalcogenides | -$Bi_{0.4}Sb_{1.6}Te_3$ /$CeFe_{3.5}Co_{0.5}Sb_{12}$ (N)<br>-$Bi_2Te_3$ /$CoSb_3$ (P) | 100-973 | 3- 5.5 | - Sublimate at Higher Temperature<br>- Cracks due to Sublimation<br>- CTE Mismatch | - Minimize thermally induced Stress<br>- Enhance material Compatibility factor |
| Group IV Tellurides | -$Bi_xSb_{2-x}Te_3$ /$Ag_{0.9}Pb_9Sn_9Sb_{0.6}Te_{20}$ (P)<br>-$Bi_2Te_{3-x}Se_x$ /$Ag_{0.86}Pb_{19+x}SbTe_{20}$ (N) | 100-700 | 2- 6.56 | - Sublimate and Oxidize at Higher Temperature<br>- p-type very unstable at higher Temperature<br>- Cracks due to Sublimation and Oxidation<br>- Controlling diffusion of elements from joints, electrodes, and substrates<br>-CTE tuning to reduce the effect of mismatch | - Minimize thermally induced Stress<br>- Enhance material Compatibility factor |
| Silicon-Germanium Alloys | -$Bi_{0.6}Sb_{1.4}Te_3$/$Ba_8Au_{5.3}Ge_{40.7}$/PbTe-SrTe/SiGe (P)<br>-$Bi_2Te_3$/$Ba_{0.08}La_{0.05}Yb_{0.04}Co4Sb_{12}$/$La_3Te_4$ (N) | 100 – 1100 | 5-18.2 | - Sublimate at Higher Temperature<br>- Cracks due to Sublimation and Intermetallic compounds<br>-Nano structuring to reduce the CTE mismatch effect in Segmented device | - Minimize thermally induced Stress<br>- Enhance material Compatibility factor |
| Skutterudites | -$CeFe_{3-X}Co_XSb_{12}$/$Yb_{14}MnSb_{11}$ (P)<br>-$La_{3-}XTe_4$ /$Ba_xYb_yCo_4Sb_{12}$ (N) | 200-1273 | 4-13.7 | - Sublimate and Oxidize at Higher Temperature | - Minimize thermally induced Stress |

| | | | | | |
|---|---|---|---|---|---|
| | | | | -Cracks due to Sublimation and Severe diffusion reaction between the metal electrode and SKD materials. | - Enhance material Compatibility factor |
| $Mg_2B_{IV}$ Solid Solutions | -BiTe/ $Mg_2Si$: Bi (P)<br>-BiTe/ HMS (N) | 200- 771 | 5 Upto | - Sublimate and Oxidize at Higher Temperature<br>- Cracks due to decomposition and Oxidation<br>-Encapsulation layer to protect from environmental degradation and increase fracture toughness | - Minimize thermally induced Stress<br>- Enhance material Compatibility factor |
| Silicides | -$MnSi_{1.73}$ (P)<br>- Bi0.6Sb1.4Te3, Ba8Au5.3Ge40.7 | 300-900 | 2-12.9 | - Sublimate at Higher Temperature<br>- Low Flexural strength due to metallic MnSi at grain boundaries | - Minimize thermally induced Stress<br>- Enhance material Compatibility factor |
| Clathrates | -$Bi_2Te_3$ /ErAs:$(InGaAs)_{0,8}(InAlAs)_{0,2}$ (P)<br>-$Bi_2Te_3$ /ErAs:InGaAs (N) | 300-700 | 1-5 | - Sublimate at Higher Temperature<br>- CTE Mismatch and Low lattice thermal conductivity cause structural instability | - Minimize thermally induced Stress<br>- Enhance material Compatibility factor |
| Half-Heussler Compounds | -BiTe /TAGS/ $Hf_xZr_yTi_z$- NiSbSn (P)<br>-BiTe/PbTe/$Hf_xZr_yTi_z$ - CoSbSn (N) | 300-900 | 1- 11.8 | - Sublimate and Oxidize at Higher Temperature<br>- Cracks due to Sublimation, oxidation and Intermetallic compound's reaction | - Minimize thermally induced Stress<br>- Enhance material Compatibility factor |
| Oxides | Ti0.3Zr0.35Hf0.35CoSb0.8S n0.2 /Ca2.8Lu0.15Ag0.05Co4O9+δ | 400-1100 | 5 upto | - Sublimate at Higher Temperature<br>- Mechanically weak due to poor interface | - Minimize thermally induced Stress<br>- Enhance material Compatibility factor |

## 1.5 Contemporary Approaches

Series of studies have been conducted to produce mechanically reliable and high-performance TE modules by limiting the operational stresses. All these studies have commonly pointed out lack of reliability model which can analyze, predict, and optimize TE device performance and lifespan[21][22][23]. Though most of the published work focuses on influence of TE leg design and boundary conditions, the part of integrating data into comprehensive reliability model hasn't yet proposed. Thermo-mechanical stresses do provide qualitative analysis of TEG device durability, but they don't quantify the effect of modified stresses on the device's reliability. Therefore, the literature as two aspect which are covered here regarding to dissertation work. First and the foremost, Modeling of thermomechanical stress for the devices operating above 400 C.

Apparently, due to lack of technological application, measuring precise thermally induced stresses are still challenge. In this regard, most of the researcher use Finite Element analysis based on theoretical mathematical model. When TE modules are subjected to thermal cycling, thermally induced stresses go beyond yield and tensile strength, which ultimately leads to failure of module. Several experimental studies[24][25][14] have focused on evaluating and minimizing the stresses during the operational hours in TE devices. Analytical literature starts with Timoshenko's beam theory, which is still being used to study stress behavior in multilayer thermostats and developed a fundamental relationship between temperature and stress. Suhir [26] played a key role in defining the effect of length and height on stress level, particularly in TE devices. Suhir's mathematical model, on TE legs, gives insight to understand effect of shear stress at the boundary. Malzbender's [27] work demonstrates the effect of stiffness, thickness and thermal expansion on stress level. These properties of the material are actively being utilized in Finite element analysis study. Z.H. Jin [28] continued Malzbender's model and predicted that failure can occur in multilayer leg, if length to thickness ratio increases. Whereas G. Nikolova developed a comprehensive mathematical model to study thermal and mechanical behavior of bonded layers. She has demonstrated that debonding of layers happen when module reaches at its critical shearing

stress. Naotake [27][29] develop a very comprehensive mathematical model for rectangular plate and studied their thermal-mechanical behavior at different temperature gradient.

Structural reliability of thermoelectric module is one of the key challenges. For the success of the TE technology, it has become compulsory to consider structural durability into account, especially for segmented TE modules. Despite advances in segmented TE materials, to enhance FOM, large scale production and commercial use is often impeded by the device failure [24]. These challenging aspects of the TE module demand modelling of reliability factor which includes all possible risks. Currently most qualified methods, to generalize reliability of the TEG, are

1. Accelerated Testing (AT)
2. Mean-time-between Failure (MTBF)
3. Number of Thermal cycles to failure
4. Response surface method
5. Design of Experiment Approach

These following approaches are more or less designed for specific cases and don't provide qualitative analysis of TE. The most popular and well established approach was adopted by Naveen K. Karri [24], [30], [31] and Andrew A. Wereszczak [32]–[34] in which they evaluated thermomechanical stress using brittle material failure theory based on Weibull distribution. The research has integrated Finite element analysis (FEA) with the study of boundary conditions, leg geometry, dimension, spacing and metallization. But due to lack of fracture test data and integration of precise material properties into system analysis, the model is limited to low to medium temperature (i.e., approximately about 400 C) TE device. Plus, it has been demonstrated in many studies that the shape of TE leg has less effect on probability model.

Alternative to this notion, we published a paper[35], presenting simulative results, where lognormal distribution is used to calculate failure rate. Generally lognormal distribution is used to measure the rate of failure for micro-electric devices at high temperature stress. The distribution is based on the multiple failure model, which mean that at given temperature range the TE leg in any given module undergoes a random increase of

degradation, interlayer diffusion, sublimation or oxidation, leading to complete abruptive failure [36][12], [37], [38][39]–[42]. Therefore, the use of lognormal distribution is mostly used to model components or devices that fail primarily due to stress or fatigue. Our published papers[35] has spotted another limitation of Weibull distribution. Weibull distribution has best fit data for TE devices till 400 C. For medium to high temperature TE devices, Weibull distribution fits poorly at lower tail compared to the lognormal distribution. Whereas lognormal distribution has 95% prediction for quantile compared to Weibull model.

The proposed mathematical model entails development of a model to calculate precise thermally induced stress within leg and overall. Methods integrates reliability of the TE device by introducing non-parametric lognormal distribution. The proposed work took a lognormal approach in order to study discrete and higher bond values. The alternative method “Survival function” is derived and potential analysis on reliability, specifically on TE module, is presented in our study. The model also prescribes alternative approach to model number of legs in TE system. The model calculates the optimized survival function, both segmented and unsegmented, module that has survived a specific temperature range and model gives us the mean residual life (MRL)[43]–[48] for measuring the reliability of high temperature TE modules. This measure contains two aspects of information, the lifetime of a module and the temperature at which the module has ability to work operate without any failure.

A stress-strength model-based lognormal MRL function is obtained to differentiate various characteristics of TE module to measure reliability of (segmented or unsegmented) at higher thermal stresses. This new model assists us to determine the temperature range at which the reliability of segmented device could be achieved above 90%. Additionally, an optimized Bayesian nonparametric survival function is derived to measure the probability of segmented module to survive beyond the interface stress.

# Chapter 2. Optimized Mathematical Model for Thermoelectric Devices

## 2.1 Stress- Strain Relationship

The analytical model is derived using a specific (rectangular) geometry of the TE leg and is comprised of different layers, connected perpendicularly to each other (see figure 2.1). The ceramic components are subjected to different temperatures. The temperature gradient causes nonuniform thermal expansion (or contraction) among the layers, because each material has its own thermal expansion coefficient. The nonuniform thermal expansion and use of interdiffusion layer (acting as compressive force) leads to thermally induced stresses in the leg and at interfaces between the layers. In order to calculate thermally induced stress, we treat each layer and thermoelement as elongated rectangular plates. As shown in figure 2.1, we split each layer in order to calculate thermally induced stress individually and then sum up to generate final equation. To calculate thermally induced stresses in thermoelement with a thickness of (h) and width of (L), we assume that the displacement vertically (out of plane) is small and for thermoelement we didn't take this factor into our consideration. The thickness and height stay within frame of following articles where it has been shown that shorter and rectangular shape legs are efficient as well as lower level of stress. Regarding to this fact, the ratio of thickness to height has been considered less the 0.5mm.

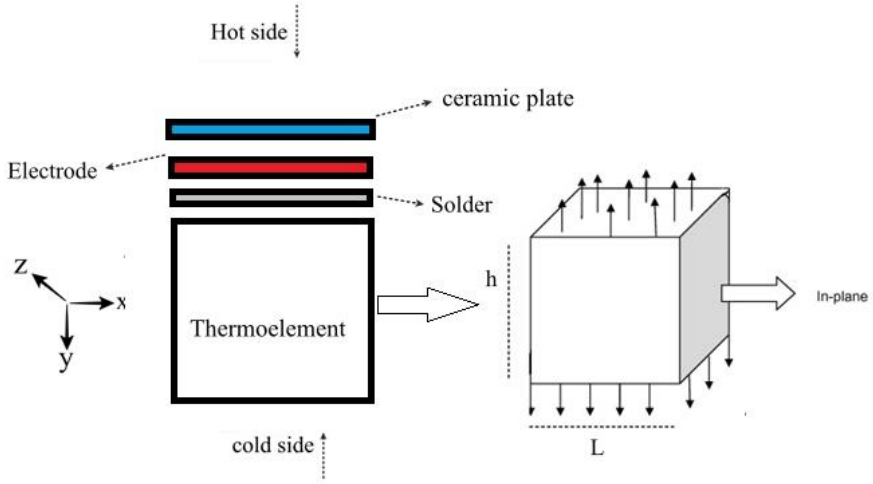


*Figure 2.1.* Basic Structure of TE leg comprised from different components

To get basic equation we introduce Kirchhoff's hypothesis[49] which states that the plane initially perpendicular to the neutral plane (z=0) of the leg and remains a plane after deformation and is perpendicular to deformed neutral plane. The coordinate system of the leg is taken as shown in figure 2.1. The boundary conditions make physically possible for leg to expand on z-axis while develop stress on y-axis.

Let *u*, *v*, and *w* be displacement components in the *x*, *y*, and *z* direction at the neutral plane (*z* = 0). Then, referring to figure 2.1, the displacement components $\acute{u}$ $\left(\frac{\partial u}{\partial x}\right)$ and $\acute{v}$ $\left(\frac{\partial v}{\partial y}\right)$ in the in-plane direction *x* and *y* at the arbitrary point of the plate are

$$\acute{u} = u - z\frac{\partial w}{\partial x}, \qquad \acute{v} = v - z\frac{\partial w}{\partial y}$$

Therefore, the strain components in the in-plane direction are

$$\epsilon_x = \frac{\partial \acute{u}}{\partial x}, \quad \epsilon_y = \frac{\partial \acute{v}}{\partial y}, \quad \epsilon_{xy} = \frac{1}{2}\left(\frac{\partial \acute{u}}{\partial y} + \frac{\partial \acute{v}}{\partial x}\right) \tag{2.1}$$

Two-dimensional stress–strain relations[50] in the in-plane directions for an isotropic thermoelement are

$$\epsilon_{xx} = \frac{1}{E}\left(\sigma_{xx} - v\sigma_{yy}\right) + \alpha\Delta T$$

$$\epsilon_{yy=}\frac{1}{E}\left(\sigma_{yy} - v\sigma_{xx}\right) + \alpha\Delta T$$

$$\epsilon_{xy} = \frac{1+v}{E}\sigma_{xy} \tag{2.2}$$

Through equations of strain (we can drive equation of stress, which is

$$\sigma_{xx} = \frac{E}{1-v^2}\left[\epsilon_{xx} + v\epsilon_{yy} - (1+v)\alpha\Delta T\right]$$
$$\sigma_{yy} = \frac{E}{1-v^2}\left[\epsilon_{yy} + v\epsilon_{xx} - (1+v)\alpha\Delta T\right]$$
$$\sigma_{xy} = \frac{E}{1+v}\epsilon_{xy} \tag{2.3}$$

By substituting eq (2.1) into eq (2.2) gives the relationship

$$\sigma_{xx} = \frac{E}{1-v^2}\left[\frac{\partial u}{\partial x} + \nu\frac{\partial v}{\partial y} - z\left(\frac{\partial^2\omega}{\partial x^2} + v\frac{\partial^2\omega}{\partial y^2}\right) - (1+v)\alpha\Delta T\right]$$
$$\sigma_{yy} = \frac{E}{1-v^2}\left[\frac{\partial \nu}{\partial y} + \nu\frac{\partial u}{\partial x} - z\left(\frac{\partial^2\omega}{\partial y^2} + v\frac{\partial^2\omega}{\partial x^2}\right) - (1+v)\alpha\Delta T\right] \tag{2.4}$$
$$\sigma_{xy} = \frac{E}{2(1+v)}\left[\frac{\partial u}{\partial y} + \nu\frac{\partial v}{\partial y} - 2z\frac{\partial^2\omega}{\partial x\partial y}\right]$$

## 2.2 Thermo-Elastic Behavior of TE Leg

Thermoelastic behavior of certain material, framed into limited boundary condition are defined by the function of stress $\sigma$, independent state of variable strain $\epsilon$ and temperature T. In order elaborate he thermoelastic behavior of the leg, we define the resultant forces per unit thickness for the thermoelement as product of stress $\sigma$,

$$F_x = \int_{-h/2}^{h/2}\sigma_x\partial z, \quad F_y = \int_{-h/2}^{h/2}\sigma_y\partial z, \quad F_{xy} = \int_{-h/2}^{h/2}\sigma_{xy}\partial z \tag{2.5}$$

And resultant moment per unit thickness for the thermoelement, as product of strain "$\epsilon$"

$$M_x = \int_{-h/2}^{h/2} \sigma_x z \partial z, \quad M_y = \int_{-h/2}^{h/2} \sigma_y z \partial z, \quad M_{xy} = \int_{-h/2}^{h/2} \sigma_{xy} z \partial z \tag{2.6}$$

Now substituting the value of stress in equation (2.5) and (2.6) and integrating accordingly, we get resultant force and moment equations

$$\begin{aligned} F_x &= \frac{Eh}{1-v^2}\left(\frac{\partial u}{\partial x} + v\frac{\partial v}{\partial y}\right) - \frac{1}{1-v}F_T \\ F_y &= \frac{Eh}{1-v^2}\left(\frac{\partial v}{\partial y} + v\frac{\partial u}{\partial x}\right) - \frac{1}{1-v}F_T \\ F_{xy} &= \frac{Eh}{2(1+v)}\left(\frac{\partial u}{\partial y} + \frac{\partial v}{\partial x}\right) \end{aligned} \tag{2.7}$$

$$\begin{aligned} M_x &= -D\left(\frac{\partial^2 w}{\partial x^2} + \frac{\partial w^2}{\partial y^2}\right) - \frac{1}{1-v}M_T \\ M_y &= -D\left(\frac{\partial^2 w}{\partial y^2} + \frac{\partial w^2}{\partial x^2}\right) - \frac{1}{1-v}M_T \\ M_{xy} &= (1-v)D\frac{\partial w^2}{\partial x \partial y} \end{aligned} \tag{2.8}$$

Here $F_T$ and $M_T$ are thermally induced stress and are defined as[51][52]

$$F_T = \alpha E \int_{-h/2}^{h/2} \Delta T dz, \quad M_T = \alpha E \int_{-h/2}^{h/2} \Delta T z dz \tag{2.9}$$

Whereas D is flexure rigidity, and it can be calculated as

$$D = \frac{Eh^3}{12(1-v^2)}$$

Now by substituting equation (2.9) into equation (2.3), we'll get stress components for rectangular Thermoelement

$$\sigma_x = \frac{1}{h}F_x + \frac{12z}{h^3}M_x + \frac{1}{1-v}\left(\frac{1}{h}F_T + \frac{12z}{h^3}M_T - \alpha E\Delta T\right)$$
$$\sigma_y = \frac{1}{h}F_y + \frac{12z}{h^3}M_y + \frac{1}{1-v}\left(\frac{1}{h}F_T + \frac{12z}{h^3}M_T - \alpha E\Delta T\right) \quad (2.10)$$
$$\sigma_{xy} = \frac{1}{h}F_{xy} - \frac{12z}{h^3}M_{xy}$$

These Equations satisfy the Kirchhoff hypothesis for in-plane stress. We now consider the equilibrium state for the plane stress for *x* and *y*. When body forces are absent, the equilibrium equations[27], [51] of the plate are given by

$$\frac{\partial\sigma_x}{\partial x} + \frac{\partial\sigma_{xy}}{\partial y} = 0, \qquad \frac{\partial\sigma_{xy}}{\partial x} + \frac{\partial\sigma_y}{\partial y} = 0 \quad (2.11)$$

Integrating equation (2.11) with respect to z direction, we get

$$\frac{\partial F_x}{\partial x} + \frac{\partial F_{xy}}{\partial y} = 0, \qquad \frac{\partial F_{xy}}{\partial x} + \frac{\partial F_y}{\partial y} = 0 \quad (2.12)$$

For the plane thermoelastic problems, we now introduce a thermal stress function $\varphi$ [53]

$$F_x = \frac{\partial^2\varphi}{\partial y^2}\ , F_y = \frac{\partial^2\varphi}{\partial x^2}\ , F_{xy} = -\frac{\partial^2\varphi}{\partial x\partial y} \quad (2.13)$$

Defining now stress function $\varphi$ for compatibility equation [26], [27], [29], [54] by considering the plane strain. Substituting equations of strain (2.2) into equation (2.10)

$$\frac{\partial^2}{\partial y^2}\left[\left\{\frac{1}{E}\left(\sigma_x - v\sigma_y\right) + \alpha\Delta T\right\}\right] + \frac{\partial^2}{\partial x^2}\left[\left\{\frac{1}{E}\left(\sigma_y - v\sigma_x\right) + \alpha\Delta T\right\}\right] = 2\frac{\partial}{\partial x \partial y}\left(\frac{1+v}{E}\sigma_{xy}\right) \tag{2.14}$$

This equation has following solution

$$\left(\frac{\partial^2}{\partial y^2} - v\frac{\partial^2}{\partial x^2}\right)F_x + \left(\frac{\partial^2}{\partial x^2} - v\frac{\partial^2}{\partial y^2}\right)F_y - 2(1+v)\frac{\partial^2}{\partial x \partial y}F_{xy} = \left(\frac{\partial^2}{\partial x^2} + \frac{\partial^2}{\partial y^2}\right)F_T \tag{2.15}$$

Now introducing eq (2.13) into equation (2.15), we get following solution

$$\nabla^2\nabla^2\varphi = -\nabla^2 F_T \tag{2.16}$$

Here $\nabla^2 = \frac{\partial^2}{\partial x^2} + \frac{\partial^2}{\partial y^2}$

The equation (2.16) is a basic equation to understand thermoelastic behavior of thermoelement, ceramic plate, electrode, and soldered layer. Figure 2.2 is compiled based on equation (2.16) in order to demonstrate the induced force in segmented and unsegmented TE device. Through this equation we can find thermally induced force for each part in plane direction. Thermally induced forces are product of difference in thermal expansion of the material which ultimately causes generation of thermally induced stresses.

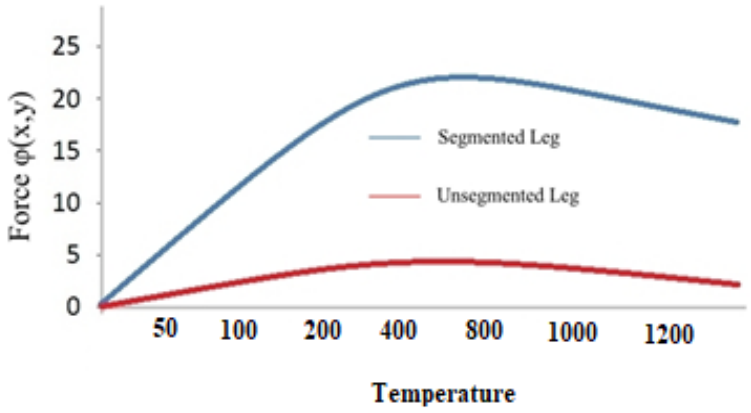


*Figure 2.2.* Force per area distribution along the thickness of the leg

Figure 2.2 is plot of average value of Bismuth Chalcogenides, Silicon- Germanium Alloys and Skutterudites for segmented and unsegmented devices. The peak of graph between 400 and 800 ◦C is for low-medium temperature segmented device's resultant forces. The devices are made of Skutterudites- Bismuth Chalcogenides materials.

## 2.3 Equation of Displacement

Different differential equations of equilibrium, strain compatibility conditions and formulas of Hooke's law form major equations for theory of elasticity. These equations are sufficient to define the stress-strain relation of an elastic structure. Additionally, solutions to any particular problem must satisfy appropriate boundary conditions. When specific temperature field is given, displacement, stress and strain are sought. Consequently, if displacement equation is given, stress, strain and external forces are sought. Respectively, we're going to develop here displacement equation in order to find thermally induced stress and strain.

Let's say $\tau_x$ and $\tau_y$ are the shearing forces per unit length for x and y direction and can be defined as function of stress

$$\tau_x = \int_{-h/2}^{h/2} \sigma_{xz} dz \quad , \quad \tau_y = \int_{-h/2}^{h/2} \sigma_{yz} dz \tag{2.17}$$

And $M_{yx}$ bending moment, which can be defined as

$$M_{yx} = \int_{-h/2}^{h/2} \sigma_{yx} z dz \tag{2.18}$$

Introducing equilibrium equations [29], [55] of moments for "x" and "y" components

$$\frac{\partial M_x}{\partial x} + \frac{\partial M_{xy}}{\partial y} - \tau_x = 0$$
$$\frac{\partial M_y}{\partial y} - \frac{\partial M_{xy}}{\partial x} - \tau_y = 0 \tag{2.19}$$

From equation (2.10) we know that

$$M_{xy} = \int_{-h/2}^{h/2} \sigma_{xy} z \partial z$$

And comparing it with above equation, we understand that

$$M_{yx} = -M_{xy}$$

Since Shear force is developed on edges, it has following equilibrium equation

$$\frac{\partial \tau_x}{\partial x} + \frac{\partial \tau_y}{\partial y} + F_P = 0 \tag{2.20}$$

Here $F_P$ denotes external load acting on the edges of the leg. Substituting equation (2.19) into equation (2.20) we get following solution

$$\frac{\partial^2 M_x}{\partial x^2} + \frac{\partial^2 M_y}{\partial y^2} - 2\frac{\partial^2 Mxy}{\partial x \partial y} + F_P = 0 \tag{2.21}$$

Now substituting equation (2.6) into equation (2.21)

$$\frac{\partial^2}{\partial x^2}\left[D\left(\frac{\partial^2 w}{\partial x^2} + v\frac{\partial^2 w}{\partial y^2}\right)\right] + \frac{\partial^2}{\partial y^2}\left[D\left(\frac{\partial^2 w}{\partial y^2} + v\frac{\partial^2 w}{\partial x^2}\right) + 2(1-v)\frac{\partial^2}{\partial x \partial y}\left(D\frac{\partial^2 w}{\partial x \partial y}\right)\right] = F_P - \frac{1}{1-v}\nabla^2 M_T \tag{2.22}$$

And with respect to displacement

$$\nabla^2\nabla^2 w = \frac{1}{D}\left(F_P - \frac{1}{1-v}\nabla^2 M_T\right) \tag{2.23}$$

Where external load is absent, the fundamental equation of displacement is reduced to

$$\nabla^2 w = -\frac{1}{D(1-v)} M_T \tag{2.24}$$

## 2.4 Boundary conditions

To develop particular thermo-mechanical solution for Thermoelement (or any layer) we need to specify their particular boundary condition. The boundary condition is the application of a force, developed by constraining. To develop a comprehensive mathematical model and simulate it, we need to specify and satisfy leg's boundary conditions. For this purpose, we have considered two different cases. Each case has its own solution and mathematical model.

### 2.4.1 First Case- Simply Supported Edges

The boundary conditions in first case are taken in absence constraining force. The rise of temperature and thermally induced stress mutually interdependent. The absence of constraining force will allow our leg to expand freely, in both x and y direction, and interact with surrounding forces. The rate of expansion and impact of surrounding forces are calculated here. Thus, this case entails following conditions

On x-axis when x=0 and x=l

$$w = 0, \qquad \frac{\partial^2 w}{\partial x^2} = -\frac{1}{(1-v)D} M_T$$

On y-axis when y=0 and y=t

$$w = 0, \qquad \frac{\partial^2 w}{\partial y} = -\frac{1}{(1-v)D} M_T$$

Now, the fundamental equation (2.24) is resolved into the following two equation system, in which we have we introduced the function of force $\phi$, the unknown force (surrounding)

$$\nabla^2 w + \frac{1}{D(1-v)} M_T = \phi(x, y) \tag{2.25}$$

$$\nabla^2 \phi = 0 \tag{2.26}$$

Equation (a) can be expended into

$$\frac{\partial^2 w}{\partial x^2} + \frac{\partial^2 w}{\partial y^2} + \frac{1}{D(1-v)} M_T = \phi(x, y) \tag{2.27}$$

In order to define force $\phi$, we introduce Boas's theorem[56][57] and accordingly define equation for *w* and $M_T$ in double trigonometric series

$$w = \sum_{m=1}^{\infty} \sum_{n=1}^{\infty} w_{mn} \sin \alpha_m x \sin \beta_n y \tag{2.28}$$

$$M_T = \sum_{m=1}^{\infty} \sum_{n=1}^{\infty} a_{mn} \sin \alpha_m x \sin \beta_n y \tag{2.29}$$

These two equations have been derived from Boas's theorem, which are continuity of integrability of trigonometric series [58], the transformation of one dimension to two-dimensional cosine series, which states

$$\emptyset(x, y) = \sum_{j-1}^{x} \sum_{k-1}^{x} a_{jk} \sin jx \sin ky$$

Through this theorem, we can also construct equation for $a_{mn}$, i.e.

$$a_{mn} = \frac{4}{ab}\int_{o}^{l}\int_{0}^{t} M_T(x,y)\sin\alpha_m x \sin\beta_n y \,\partial x \partial y \tag{2.30}$$

Now by substituting equation (2.13) into equation (2.12), we get coefficient $w_{mn}$

$$w_{mn} = \frac{a_{mn}}{{\alpha_m}^2 + {\beta_n}^2}\frac{1}{(1-v)D} \tag{2.31}$$

This gives us displacement (*w*) for a simply supported legs.

Substituting Equation (2.28) (2.29) into equation (2.9) and (2.21) we obtain the following expressions for the resultant moments and shearing forces

$$\begin{aligned} M_x &= -\sum_{m=1}^{\infty}\sum_{n=1}^{\infty} a_{mn}\frac{\beta_n^2}{{\alpha_m}^2 + {\beta_n}^2}\sin\alpha_m x \sin\beta_n y \\ M_y &= -\sum_{m=1}^{\infty}\sum_{n=1}^{\infty} a_{mn}\frac{\alpha_m^2}{{\alpha_m}^2 + {\beta_n}^2}\sin\alpha_m x \sin\beta_n y \\ M_{xy} &= \sum_{m=1}^{\infty}\sum_{n=1}^{\infty} a_{mn}\frac{\alpha_m\beta_n}{{\alpha_m}^2 + {\beta_n}^2}\cos\alpha_m x \cos\beta_n y \end{aligned} \tag{2.32}$$

$$\tau_x = 0, \qquad \tau_y = 0$$

Through equation (2.32) and (2.10) we can find stress produced in simply supported thermoelement leg. Whereas the absence of shear forces indicates that the only distortion in structure occurs is through bending moment.

### 2.4.2 Second Case-Two edges are Simply Supported and Two are Restricted

This case is more favorable for us since our TE legs are vertically (y-axes) restricted, as shown in figure 2.3, while horizontally (x-axes) free. In this case we will examine shear forces, produced on the vertical edge, bending moment on horizontal edges and thermally induced stress due to temperature gradient. Boundary conditions for the fundamental equation (2.24), in this particular case, are given as

$$w = 0, \qquad \frac{\partial w^2}{\partial x^2} = -\frac{1}{D(1-v)} M_T \qquad x = \pm\frac{l}{2}$$

$$w = 0, \qquad \frac{\partial w}{\partial y} = 0 \qquad y = \pm\frac{h}{2}$$

With respect to Neumann boundary condition [59],[60] and Boas's Theorem, we know that the displacement equation for x-axis direction, in double cosine series at particular temperature and distance, will become

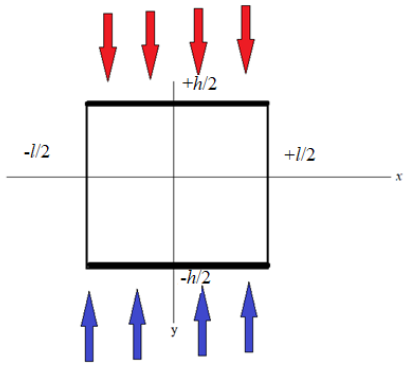


*Figure 2.3* Boundary conditions for case 2

$$w_1(x, y, T) = \sum_{m=1}^{\infty}\sum_{n=1}^{\infty} w_{mn} cos\alpha_m x cos\beta_n y \tag{2.33}$$

And the thermal moment at particular temperature

$$M_T(x,y,T) = \sum_{m=1}^{\infty}\sum_{n=1}^{\infty} a_{mn} cos\alpha_m x cos\beta_n y \tag{2.34}$$

Here $\alpha_m = \frac{m\pi}{l}, \quad \beta_n = \frac{m\pi}{h}$ and are defined by boundary conditions

Now putting the value of $w_{mn}$ from equation (2.29), we get following solution

$$w_1(x,y,T) = \sum_{m=1,3,5}^{\infty}\sum_{n=1,3,5}^{\infty}\left(\frac{1}{(1-v)D}\right)\frac{a_{mn}}{{\alpha_m}^2 + {\beta_n}^2} cos\alpha_m x cos\beta_n y \tag{2.35}$$

$$M_T(x,y,T) = \sum_{m=1,3,5}^{\infty}\sum_{n=1,3,5}^{\infty} a_{mn} cos\alpha_m x cos\beta_n y \tag{2.36}$$

Now taking again into account our boundary conditions, according to which, the elastic problem of a restricted edge ($y = \pm h/2$) causes a generation of force ($\varphi_y$) within a volume on y-axis direction. The force is distributed symmetrically and can be defined as

$$\varphi_y = \sum_{m=1,3,5}^{\infty} E_m sin\,\alpha_m y \tag{2.37}$$

Here, $E_m$is elastic constant and depends on boundary conditions. Consequently, taking into account boundary condition on free edge ($x = \pm l/2$), the displacement equation will become

$$\nabla^2\nabla^2 w_2 = 0 \tag{2.38}$$

And according to fourth-order partial differential equation, the equation (2.38) has following solution

$$w_2 = \sum_{m=1,3,5}^{\infty} [A cosh\alpha_m y + B\alpha_m y Sinh\alpha_m y] cos\, \alpha_m x \qquad (2.39)$$

Considering the boundary conditions of simply supported edge, from case 1,

$$w_2 = 0, \quad \frac{\partial^2 w}{\partial x^2} = o \qquad x = \pm\frac{l}{2}$$

$$w_2 = 0, \quad \frac{\partial^2 w}{\partial y^2} = -\frac{1}{D}\varphi_y \qquad y = \pm\frac{h}{2}$$

For $x = \pm\frac{l}{2}$

$$A cosh\gamma_m + B\gamma_m Sinh\gamma_m = 0 \qquad (2.40)$$

And for $y = \pm\frac{h}{2}$

$$A\alpha_m^2 cosh\gamma_m + B\alpha_m^2(2cosh\gamma_m + \gamma_m sinh\gamma_m) = -\frac{E_m}{D} \qquad (2.41)$$

Here

$$\gamma_m = \frac{m\pi}{2}\frac{h}{l}$$

Now, regarding to the boundary conditions of y-axis ($y = \pm\frac{h}{2}$)

$$\frac{\partial w_1}{\partial y} + \frac{\partial w_2}{\partial y} = 0$$

We can find $E_m$, that is

$$E_m = -\frac{2}{1-v}\left(\frac{\alpha_m Cosh^2\gamma_m}{\gamma_m + Sinh\gamma_m + cosh\gamma_m}\right)\sum_{n=1,3,5}^{\infty}\frac{a_{mn}\beta_n(-1)^{\frac{(n-1)}{2}}}{\alpha_m^2+\beta_n^2} \quad (2.42)$$

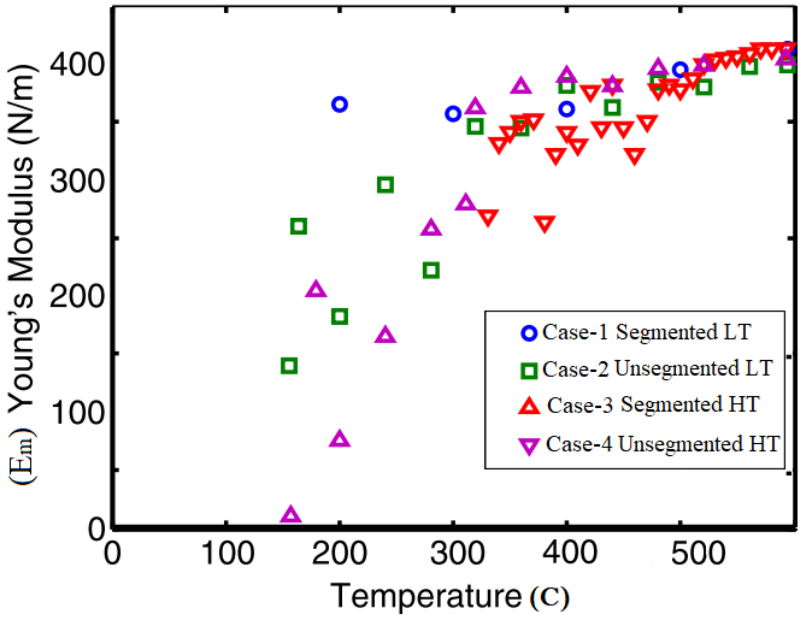


Figure 2.4 Young Modulus constant

Figure 2.4 Shows change in Young modulus constant for each device at different temperature. Equation 2.42 effectively can show stress and strain relationship for the device which has fixed boundary condition and dynamic temperature. Equation 2.42 is very different method compared to traditional way of calculating Young modulus, since it can calculate material expansion as per temperature change.

Thus, for the simply supported boundary (conditions $x = \pm\frac{l}{2}$), the resultant moment and shearing forces, due to displacement $w_2$ can be calculated through equation (2.10) and (2.19), i.e., are

$$M_x = -\frac{1}{2}\sum_{m=1,3,5}^{\infty}\frac{E_m}{cosh\gamma_m}\{(1-v)\alpha_m y sinh\alpha_m y - [2v+(1-v)\gamma_m tan\gamma_m]cosh\alpha_m y\}cos\alpha_m x$$

$$M_y = \frac{1}{2}\sum_{m=1,3,5}^{\infty}\frac{E_m}{cosh\gamma_m}\{(1-v)\alpha_m y sinh\alpha_m y + [2-(1-v)\gamma_m tan\gamma_m]cosh\alpha_m y\}cos\alpha_m x \quad (2.43)$$

$$M_{xy} = \frac{1}{2}\sum_{m=1,3,5}^{\infty}\frac{E_m}{cosh\gamma_m}[\alpha_m y cosh\alpha_m y + (1-\gamma_m tan\gamma_m)sinh\alpha_m y]sin\alpha_m x$$

$$\tau_x = -\sum_{m=1,3,5}^{\infty}\frac{E_m}{cosh\gamma_m}cosh\alpha_m y\ sin\alpha_m x$$

$$\tau_y = \sum_{m=1,3,5}^{\infty}\frac{E_m}{cosh\gamma_m}sinh\alpha_m y\ cos\alpha_m x \quad (2.44)$$

And for the restricted boundary (condition ($y = \pm\frac{h}{2}$), the displacement, resultant moment and shearing forces are

$$w = \frac{1}{(1-v)D}\sum_{m=1,3,5}^{\infty}\sum_{n=1,3,5}^{\infty}\frac{a_{mn}}{\alpha_m^2+\beta_n^2}cos\alpha_m x cos\beta_n y - \frac{1}{2D}\sum_{m=1,3,5}^{\infty}\frac{E_m}{\alpha_m^2 cosh\gamma_m}(\alpha_m y sinh\alpha_m y - \gamma_m tan\gamma_m cosh\alpha_m y)cos\alpha_m x \quad (2.45)$$

From the figure 2.5 (a) we can observe case 2, where boundaries are restricted vertically (y-direction), showing a proportional relationship between temperature and deformation occurring at the extreme edge of the leg (or component). At the edge of the leg (or component) shear stresses develop tensile nature stresses in both x and y direction, whereas resultant force, develops compressive stresses in y-direction. It can be observed that

the in segmented TE devices tensile stresses are develop within 3.5mm ≤ x ≤ 5mm and compressive stresses within 4mm ≤ y ≤ 8mm. That suggests that the constant heat supply leads development of thermal stresses and deformation within leg (or component). Both normal stresses and shear stresses in each component of the device change sharply from center to the edge, causing deformation in TE leg. In segmented TE leg, an addition of interdiffusion layers and soldering layers experience most of the deformation compared to unsegmented legs and other components. And also, sometimes interdiffusion layers undergo plastic deformation [61]. The demonstrated results of figure 2.5 are obtained using equation of displacement (eq. 2.45) for hot and cold side of the TE leg. The shown block diagram in figure 2.6 demonstrates the deformation in soldering and interdiffusion layers.

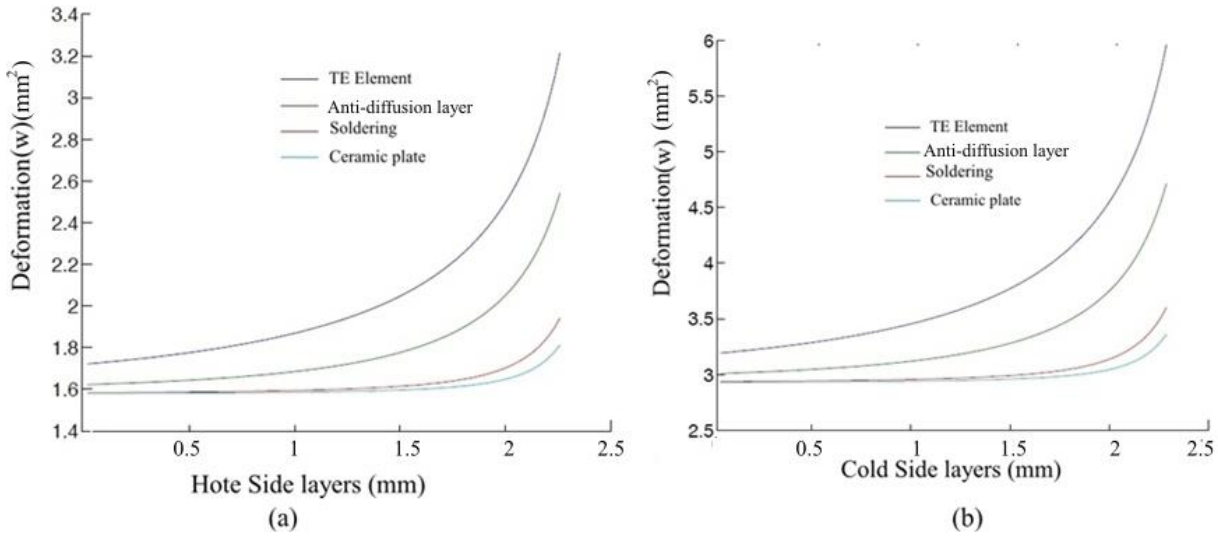


*Figure 2.5* Deformation at (a) hot end and (b) cold end with respect to their thickness

The thickness of soldering and interdiffusion later was kept between 0.7 mm≤ t ≤ 1.5 mm. Therefore, these layers deform with respect to TE element at melting point temperature above 200 C.

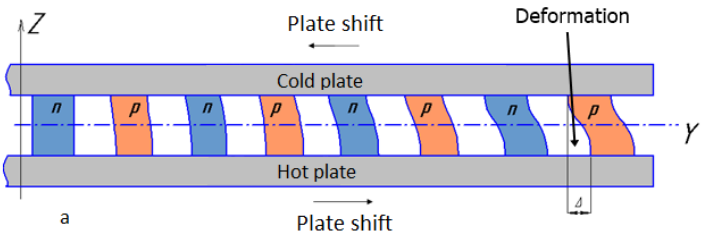


*Figure 2.6* Virtual demonstration of deformation in TE leg

Hot side-end has higher rate of plastic deformation as compared to cold side end of TE leg, causing dislocations and microcracks. We can conclude the displacement ($w$) using superposition theorem.

$$
\begin{aligned}
M_x &= -\sum_{m=1,3,5}^{\infty}\sum_{n=1,3,5}^{\infty}\frac{a_{mn}\beta_n^2}{\alpha_m^2+\beta_n^2}cos\alpha_m x cos\beta_n y - \frac{1}{2}\sum_{m=1,3,5}^{\infty}\frac{E_m}{cosh\gamma_m}\{(1-v)\alpha_m y sinh\alpha_m y - \\
&[2v+(1-v)\gamma_m tan\gamma_m]cosh\alpha_m y\}cos\alpha_m x \\
M_y &= -\sum_{m=1,3,5}^{\infty}\sum_{n=1,3,5}^{\infty}\frac{a_{mn}\alpha_m^2}{\alpha_m^2+\beta_n^2}cos\alpha_m x cos\beta_n y + \frac{1}{2}\sum_{m=1,3,5}^{\infty}\frac{E_m}{cosh\gamma_m}\{(1-v)\alpha_m y sinh\alpha_m y + \\
&[2-(1-v)\gamma_m tan\gamma_m]cosh\alpha_m y\}cos\alpha_m x \\
M_{xy} &= \sum_{m=1,3,5}^{\infty}\sum_{n=1,3,5}^{\infty}\frac{a_{mn}\alpha_m\beta_n}{\alpha_m^2+\beta_n^2}sin\alpha_m x sin\beta_n y + \frac{1}{2}(1-v))\sum_{m=1,3,5}^{\infty}\frac{E_m}{cosh\gamma_m}\{\alpha_m y cosh\alpha_m y + \\
&(1-\gamma_m tan\gamma_m)sinh\gamma_m y\}sin\alpha_m x
\end{aligned}
\tag{2.46}
$$

$$
\begin{aligned}
\tau_x &= -\sum_{m=1,3,5}^{\infty}\frac{E_m\alpha_m}{cosh\gamma_m}cosh\alpha_m y sin\,\alpha_m x \\
\tau_y &= -\sum_{m=1,3,5}^{\infty}\frac{E_m\alpha_m}{cosh\gamma_m}sinh\alpha_m y cos\,\alpha_m x
\end{aligned}
\tag{2.47}
$$

Implementing the same scenario, taken in case 1, we can find thermally induced stress from equation (2.10). Consequently, shear forces are developed on edges of the thermoelement that will lead us to next step, developing mathematical equation for interface stresses.

### 2.4.3. Multiple-Layer (Segmented) Leg

The emergence of shear forces on the edges of thermoelement, indicates the need for mathematical model for multiple-layer leg. To proceed further, we assume fundamental solution of Euler-Bernoulli beam theory [62], in which the resultant axial forces F, shear

force $\tau$ and bending moment M are related to axial normal stress ($\sigma_x$) and transverse shear stress ($\tau_{xy}$). When temperature rises to a certain degree, it causes thermally induced force along the thickness and perpendicular to width of the layer. This force is defined as a sum of resultant force and force produced due to mismatch of coefficient of thermal expansion ($\alpha$).

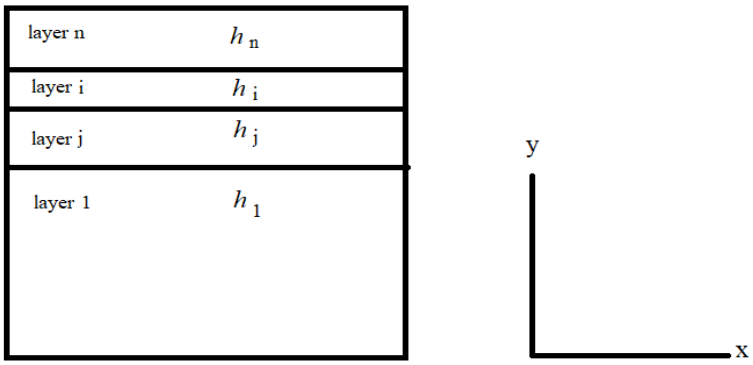


*Figure 2.7* Construction of multi-structure leg

The boundary conditions for multi-layer legs are same as for restricted leg, on y-axis,

$$F_d = F + F_\alpha$$

Here

$$F_d = h\int_0^{h_n} \sigma_y \partial y$$

$$F_d = \sum_{j=1}^{n} \int_{h_{j-1}}^{h_j} \frac{E(y,T)}{1-v^2} \alpha_j(y,T)\partial T(y)\partial y \qquad (2.48)$$

Consequently, the resultant moment is

$$M_d = M + M_\alpha$$

Here,

$$M_d = h\int_0^{h_n} \sigma_y y \partial y$$

$$M_d = \sum_{j=1}^{n} \int_{h_{j-1}}^{h_j} \int_{T_0}^{T_1} \frac{E(y,T)}{1-v^2} \alpha_j(y,T) \partial T(y) y \partial y \tag{2.49}$$

And shear force,

$$\tau_d = h\int_0^{h_n} \tau_{x,y} \partial y \tag{2.50}$$

Now introducing separation of variables method and constructing relationship between forces, moments and deformation, we get

$$\begin{bmatrix} F_d \\ M_d \end{bmatrix} = \begin{bmatrix} A & B \\ B & D \end{bmatrix} \begin{bmatrix} \epsilon_{x,0} \\ k \end{bmatrix} \tag{2.51}$$

Here A, B, D and K represent extensional coefficient, flexural-Extensional coupling coefficient, flexural stiffness coefficient and interfacial shear compliance (curvature of the leg) respectively and can be define as

$$A = \sum_{j=1}^{n} \frac{E_j(y,T)}{1-v_j^2} \left(y_j - y_{j-1}\right)$$

$$B = \frac{1}{2}\sum_{j=1}^{n} \frac{E_j(y,T)}{1-v_j^2} \left({y_j}^2 - {y^2}_{j-1}\right)$$

and

$$D = \frac{Eh^3}{12(1-v^2)}$$

Now in order to find the strain, the inverse matrix of equation (2.51) is

$$\begin{bmatrix} \epsilon_{x,0} \\ k \end{bmatrix} = \begin{bmatrix} A & B \\ B & D \end{bmatrix}^{-1} \begin{bmatrix} F_d \\ M_d \end{bmatrix} \tag{2.52}$$

And the solution for this equation

$$\epsilon_{x,0} = -\frac{D(F_d) + B(M_d)}{B^2 - AD} \tag{2.53}$$

$$k = \frac{B\ (F_d) - A(M_d)}{B^2 - AD} \tag{2.54}$$

Hence the stress between materials (at interference) and at given direction is a product of driven Young Modulus (eq 2.42) interfacial strain (here first x is direction, and second x is position), thermal expansion coefficient (where k indicates thermal expansion between two specific materials) and Temperature gradient. The mathematical expression is given as

$$\sigma_x^k = E_m \epsilon_{xx} - E_m \alpha_k \Delta T \tag{2.55}$$

The figure 2.8 shows that TE leg exposed to high heat flux generates higher thermal stresses and these stresses significantly increase by increasing number of layers inside the device. Figure 2.8 (a) shows difference of thermally induced stress between segmented and unsegmented devices. Whereas Figure 2.8 (b) demonstrates comparison of maximum stress between different TE components. Figure 3.7 is obtained through liner relationship between maximum stress and temperature. The difference in maximum stress, shown in Figure 2.8 (b), is a product of difference in thermal expansion coefficient ($\alpha$), Elastic modulus ($E$) and Poisson ratio of each material with respect to temperature distribution.

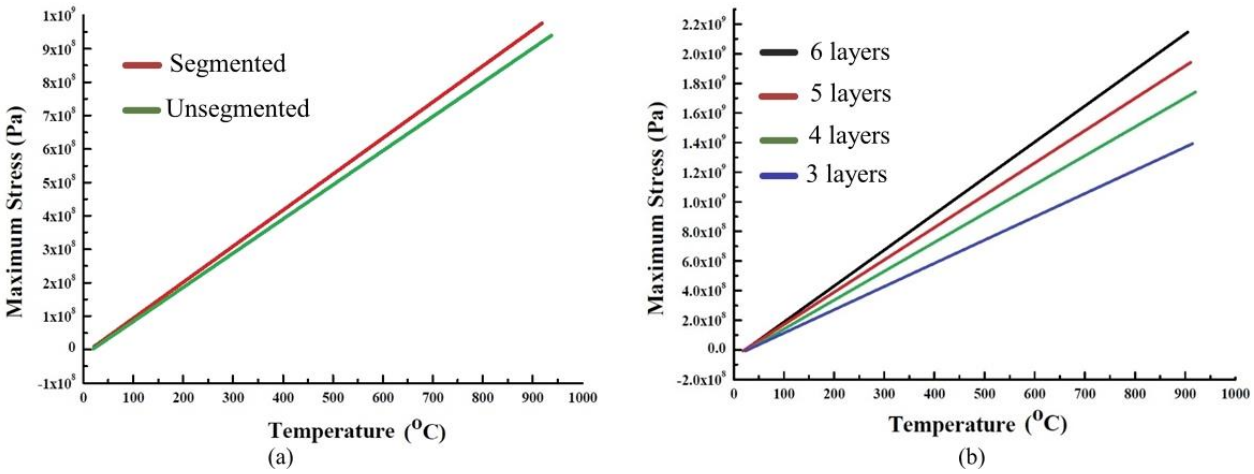


*Figure 2.8.* Comparison of (a) maximum stress, (b) maximum stress in each component

Stress modeling, particularly mathematical modeling, is effective mean of understanding thermally induced stresses in TE legs and its components, especially segmented legs. The equation of multi-leg configuration was simulated in python to obtain Pareto Front, as shown in figure 2.9, for different cases. The relationship between thermally induced stress and interfacial shearing stresses with respect to temperature for restrict boundary conditions are also demonstrated in figure 2.9 (case 2). Pareto Front of figure 2.9 (a), evaluates the thermally induced shearing stresses, within TE leg (segmented).

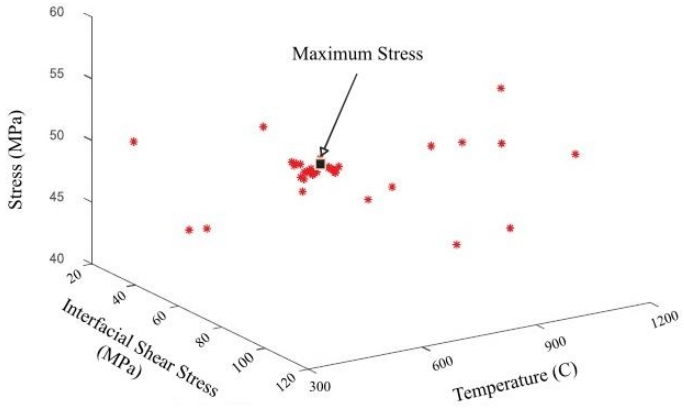


(a)

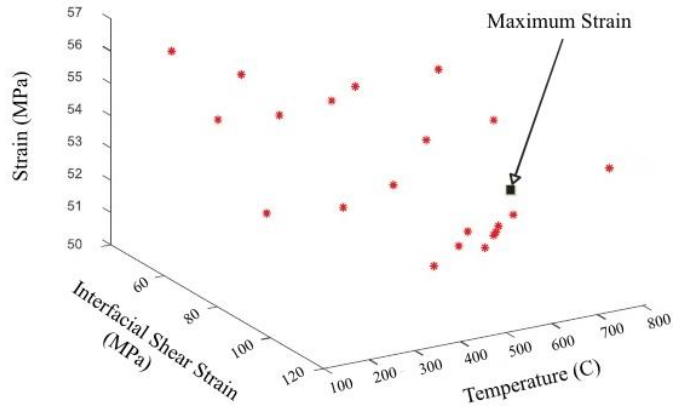


(b)

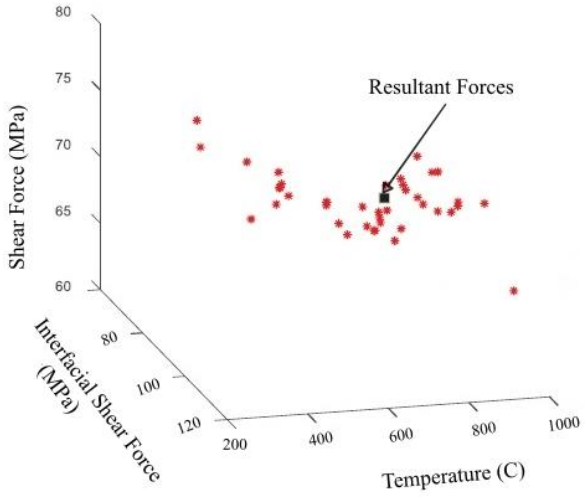


(c)

*Figure 2.9* (a) (b) (c) Pareto Front of stress-strain-temperature relationship

The concentration of stress appears at the ends of the bonded edge, where the sum of thickness for each component leads to thin and high-modulus interface. The segmented TE element, composed of Bismuth Telluride and Skutterudite materials with stiff interfaces, undergoes inter-layer diffusion after 300 C. Whereas for short interfaces, the shearing stresses are distributed along the leg (x, y direction) and the maximum shearing stress

directed towards the center of the leg. Pareto Front of figure 2.9 (b) indicates that the shearing strain of small size components with bonding (or anti-diffusion layer) causes the rise of total thermally induced stress significantly, due to difference in coefficient of thermal expansion. The comparison between figure 2.5 and figure 2.9 (b) specifies that the deformation in leg is a result of shearing strain, especially above 500 C (the melting point of Skutterudite material. The Pareto Front figure 2.9 (c) calculation is done with reference to Jin, where the temperature causing buckling failure in TE leg because of shear force derived from strength model. Analytical model indicates that thermally induced stresses values are obtain through bending moment and shear forces. Shear forces reveals the maximum normal stresses in different components of the TE leg. These shear forces, for rectangular design, contribute to maximum normal stress up to 55% at hot end and 21.7 % at cold end. Consequently, the effect of bending stresses on the TE leg specifies the change of moment of inertia with varying values of shear forces. Therefore, maximum bending stress develops a directly proportional relation to the moment of inertia. The maximum bending stress leads the shear forces in components vertically (restricted at y-axis), whereas interfacial shear forces are ignorable due to their possibility to diffuse into neighboring materials.

# Chapter 3 Optimization of TE System

## 3.1 Optimized Number of Legs of TE Device

The state of a thermodynamic system can be defined by the numbers of independent variables. Temperature is one of the independent variables. When a system is exposed to arbitrary temperature, the initial state of the system goes through transition, chasing to obtain final state[63]. The transition can be expressed through the principle of energy conservation, where

$$\frac{d}{dt}(U + K) = \frac{dW}{dt} + \frac{dQ}{dt} \tag{3.1}$$

Here $U$ is the internal energy of the system, $K$ denotes the kinetic energy of the particles, $W$ stands for the work done by the external forces, and $Q$ represents the total heat supplied to the system during the transition. The equation implies that increment in the sum of the internal and kinetic energy is directly proportion to the sum of increment in work done and heat supplied to the system during transition. The time represents the duration of the transition.

Consider a homogeneous continuous body, having an inner region $D$ with a boundary surface $c$. The functions $u_i(P, t)$ and $v_i(P, t) = \frac{\partial u_i(P,t)}{\partial t}$ denote, respectively, the displacement and velocity components of the particle at a position $P$, at time $t$ , and $p(P, t)$ and $\varepsilon (P, t)$ are the density and the internal energy per unit volume, respectively, of the particle located at $P$, at time $t$ . The kinetic energy $K$ of the body at time $t$ is defined as

$$K = \frac{1}{2}\int_{\mathrm{D}} p\, v_i v_i \, dV \tag{3.2}$$

The internal energy $U$ of the body at time $t$ is given by

$$U = \int_{\mathrm{D}} \varepsilon \, dV \tag{3.3}$$

The power of the external forces is

$$\frac{dW}{dt} = \int_{\mathrm{D}} F_i \, v_i \, dV + \int_{\mathrm{c}} p_i v_i \, dA \tag{3.4}$$

where $F_i$ denotes the component of the body force and $p_i$ the component of the surface traction applied at the boundary surface $c$. Using Cauchy fundamental relation[64] and Gauss' divergence theorem[65] the second term on the right-hand side of Eq. (3.4) becomes

$$\int_{\mathrm{c}} p_i v_i \, dA = \int_{\mathrm{c}} \sigma_{ji} n_j v_i \, dA = \int_{\mathrm{D}} \left(\sigma_{ij} v_i\right)_{,j} dV = \int_{\mathrm{D}} \left(\sigma_{ij,j} v_i + \sigma_{ij} v_{i,j}\right) dV$$

Then equation (3.4) will reduce to

$$\frac{dW}{dt} = \int_{\mathrm{D}} \left(\sigma_{ij,j} + F_i\right) v_i dV + \int_{\mathrm{D}} \sigma_{ij} v_{i,j} \, dV \tag{3.5}$$

The total rate of energy transferred into $D$ and due to internal heating is

$$\frac{dQ}{dt} = \int_{\mathrm{c}} q_i n_i \, dA + \int_{\mathrm{D}} Q^* \, dV \tag{3.6}$$

Where $q_i$ denotes the component of heat flux per unit time and unit area transferred from D across surface c, $n_i$ is the outer unit normal and $Q^*$ for the heat generation in unit

time and area in volume. Since internal heating is negligible compared to heat flux from outside the system, the second term will become zero and by applying Gauss' divergence theorem, equation (3.6) will become

$$\frac{dQ}{dt} = \int_{\mathrm{D}} q_{i,i}\, dV \tag{3.7}$$

In order to expand the basic equation (3.1), we can substitute equation (3.2), (3.3), (3.5), (3.7) and get equation of system subjected to stress component per heat flux and unit volume. The equation will become

$$\frac{d}{dt}\left(\frac{1}{2}\int_{\mathrm{D}} p\, v_i v_i\, dV + \int_{\mathrm{D}} \varepsilon\, dV\right) = \int_{\mathrm{D}} (\sigma_{ij,j} + F_i) v_i dV + \int_{\mathrm{D}} \sigma_{ij} v_{i,j}\, dV - \int_{\mathrm{D}} q_{i,i} dV \tag{3.8}$$

When a system encounters deformation, the mass of the body doesn't vary due to principle of mass conservation, which can be applied on above equation

$$\frac{d}{dt}\int_{\mathrm{D}} p\, dV = 0 \tag{3.9}$$

If we assume that density of the TE device doesn't vary, we can also apply that

$$\frac{d}{dt}(pdV) = 0 \tag{3.10}$$

Equation (3.9) is called the equation of local conservation of mass [66] and it reduces our equation (3.8) further and the first term on the left-hand side of Eq. (3.8) will be

$$\frac{d}{dt}\int_{\mathrm{D}}\frac{1}{2}p\,v_i v_i\,dV=\int_{\mathrm{D}}p\,v_i\dot{v}_\iota\,dV+\frac{1}{2}\int_{\mathrm{D}}v_i v_i\frac{d}{dt}(\rho dV) \tag{3.11}$$

The equation mass conservation also implies $\frac{d}{dt}\int_{\mathrm{D}}\frac{1}{2}\rho\,v_i v_i\,dV=\int_{\mathrm{D}}\rho\,v_i\dot{v}_\iota\,dV$, leading us to our next equation, which is,

$$\int_{\mathrm{D}}\rho\,v_i\dot{v}_\iota\,dV+\int_{\mathrm{D}}\dot{\varepsilon}\,dV=\int_{\mathrm{D}}\left(\sigma_{ij,j}+F_i\right)v_i dV+\int_{\mathrm{D}}\sigma_{ij}v_{i,j}\,dV-\int_{\mathrm{D}}q_{i,i}dV$$

Or

$$\int_{\mathrm{D}}\left(\sigma_{ij,j}+F_i-\rho\dot{v}_\iota\right)v_i dV+\int_{\mathrm{D}}(\sigma_{ij}v_{i,j}-q_{i,i}-\dot{\varepsilon})dV=0 \tag{3.12}$$

The integration of first integral denotes the equation of motion, which applies that the integrand of the equation is zero. That is $\int_{\mathrm{D}}\left(\sigma_{ij,j}+F_i-p\dot{v}_\iota\right)v_i\,dV=0$. Therefore, Eq. (3.12) reduces to

$$\int_{\mathrm{D}}(\sigma_{ij}v_{i,j}-q_{i,i}-\dot{\varepsilon})dV=0 \tag{3.13}$$

Equation (3.13) should be valid for every part of the system and the integrand in Eq. (3.13) is identically zero at every point of the system. Thus, we can attain the principle of energy conservation and our basic relationship between stress components, heat flux and internal energy is obtained as

$$\dot{\varepsilon}=\sigma_{ij}v_{i,j}-q_{i,i} \tag{3.14}$$

We may write $v_{i,j}$ in terms of its symmetric and antisymmetric portions:

$$v_{i,j} = \frac{1}{2}\left(v_{i,j} + v_{j,i}\right) + \frac{1}{2}\left(v_{i,j} - v_{j,i}\right) = \dot{\varepsilon}_{ij} + \dot{w}_{ij} \tag{3.15}$$

Here

$$\dot{\varepsilon}_{ij} = \tfrac{1}{2}\left(v_{i,j} + v_{j,i}\right) \quad , \quad \dot{w}_{ij} = \tfrac{1}{2}\left(v_{i,j} - v_{j,i}\right)$$

By use of the symmetry of the stress components $\sigma ij = \sigma ji$, the first term on the right-hand side of Eq. (3.14) reduces to

$$\sigma_{ij} v_{i,j} = \frac{1}{2}\left(\sigma_{ij} v_{i,j} + \sigma_{ij} v_{j,i}\right) = \frac{1}{2}\sigma_{ij}\left(v_{i,j} + v_{j,i}\right) = \sigma_{ij}\dot{\varepsilon}_{ij} \tag{3.16}$$

So, the principle of energy conservation goes further as

$$\dot{\varepsilon} = \sigma_{ij}\dot{\varepsilon}_{ij} - q_{i,i}$$

Here $\dot{\varepsilon} = \frac{d}{dt}\varepsilon$, $q_{i,i}$ can be expressed as heat in and out. The stress component ($\sigma_{ij}$) has been expressed above, where i,j can be expressed in form of axis (xx, yy, zz). By rearranging above equation, we can obtain follows expression.

$$\dot{\varepsilon} = \sigma_{xx}\dot{\varepsilon} - q_{in,out}$$

Therefore,

$$q_{in,out} = \dot{\varepsilon}(\sigma_{xx} - 1) \tag{3.17}$$

Expressing change in internal energy ($\frac{d}{dt}\varepsilon$) with joule density, where movement of phonon produces electricity due to transfer of heat per unit time[67]. This result is directly proportional to the change of potential of the device and inversely proportional to internal resistance[68]. Thus, the following expression for change in internal energy implies

$$\frac{d}{dt}\varepsilon = \frac{d}{dt}\left(\frac{v^2 t}{R}\right) = \frac{v^2}{R}$$

Assuming that x-axis stress component for the given device is comparatively very high and deduction of small amount is negligible, i.e., $\sigma_{xx} - 1 \cong \sigma_{xx}$. According to maximum stress principle, the overall stress is product of two components. Which means $\sigma_{xx}\sigma_{yy} = \sigma_T$ and the x-component stress can be obtain as $\sigma_{xx} = \frac{\sigma_T}{\sigma_{yy}}$. While on another hand, we have expressed the heat exchange can be expressed in form of power (P) as $q_{in,out} = q_1 - q_0 = P$. Compiling all condition into single equation, the equation (3.17) becomes

$$P = \frac{v^2}{R}\left(\frac{\sigma_T}{\sigma_{yy}}\right) \tag{3.18}$$

Utilizing the existing literature[69], the method of describing number (N) of legs for TE leg are mathematically expressed as

$$N = \frac{v}{2\alpha\Delta T} * \frac{R+1}{R} \tag{3.19}$$

In this equation *v* stands for voltage potential, $\alpha$ Seebeck coefficient, $\Delta T$ temperature difference between cold and hot end and R stands for the transition to the dimensionless variable, which has the meaning of the ratio of the load resistance **($R_{load}$)** to the internal

resistance **($R_{leg}$)** of the thermal column. In order to introduce stress-based equation to find number of TE legs, we can find voltage as

$$v = \sqrt{PR\frac{\sigma_{yy}}{\sigma_T}} \tag{3.20}$$

## 3.2 Simulation and Results

The obtained results have been studied to validate numerically modeled equation to get optimized number of legs and characteristics of the TE devices. The results and discussion include SiGe, $Bi_2Te_3$-based alloys and $CoSb_3$-based filled skutterudites. This includes values of maximum power, maximum efficiency and maximum stress by comparing different configurations of thermoelectric modules. Optimized number of legs of the thermoelectric device combined with devices material segmentation are analyzed based on three performance parameters (i.e., power, efficiency and stress). In this regard boundary condition, material compatibility and optimum number of legs are adopted to get maximum power and efficiency with minimum thermal stress. A graphical presentation of the comparison between various configuration of thermoelectric modules based on numerically calculated optimal number of thermoelectric legs shown in figure 3.1. The graph includes comparison between conventional (unsegmented) and segmented devices. For this purpose, conventional $Bi_2Te_3$ and SiGe and segmented $Bi_2Te_3$-based alloys and $CoSb_3$-based filled skutterudites.

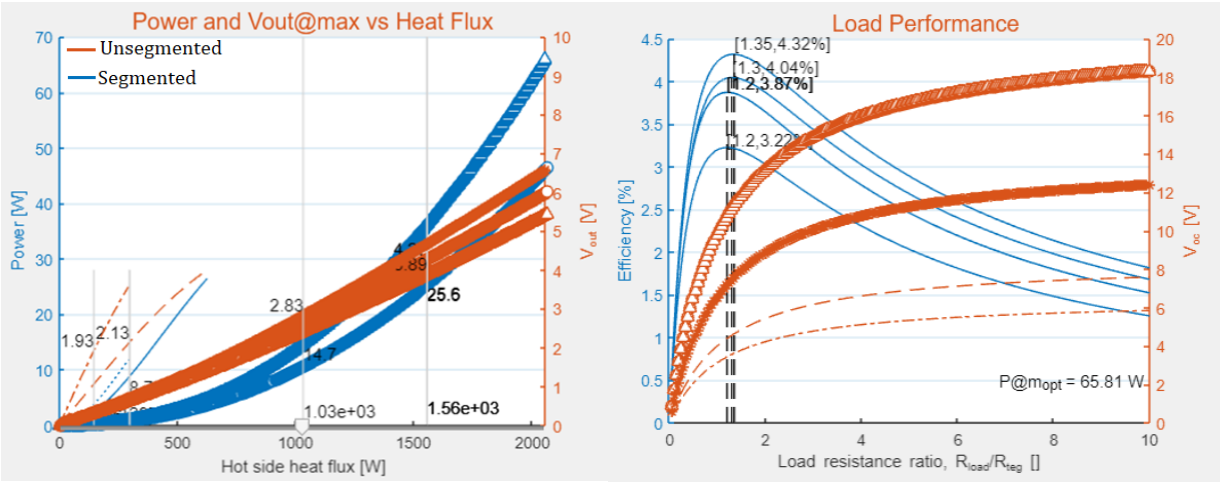


(a) (b)

Figure 3.1 MATLAB Optimal results based on average parameters method ($Bi_2Te_3$-based alloys)

As shown in figure 3.1 (a), unsegmented device $Bi_2Te_3$ has 5.7 V, providing 35 W and SiGe has 6.8 V with power output of maximum 50 W. Whereas Figure 3.1 (b) shows efficiency based on R, that is ratio of the load resistance ($R_{load}$) to the internal resistance ($R_{leg}$).

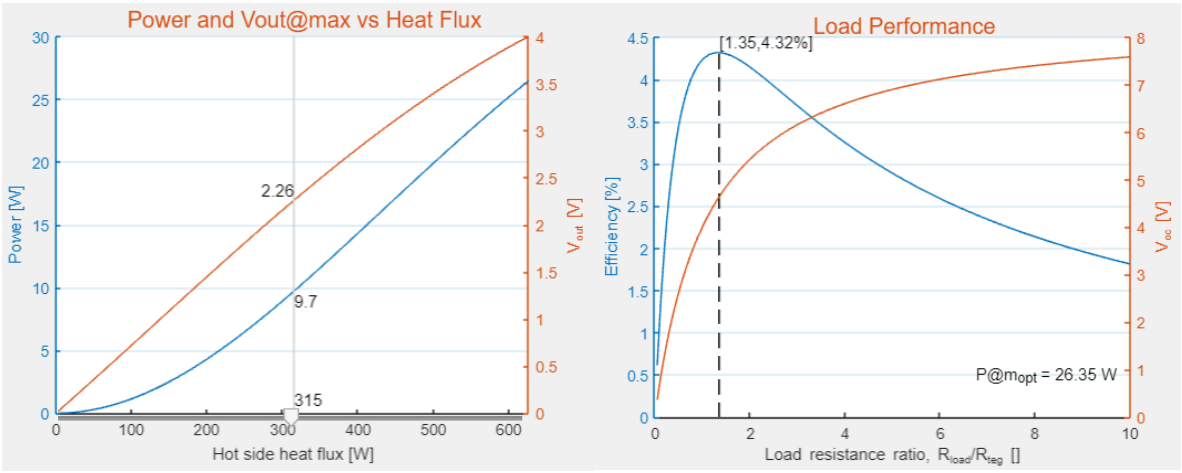


(a) (b)

Figure 3.2. $Bi_2Te_3$-based alloys and $CoSb_3$-based filled skutterudites

Whereas figure 3.2 presents graphical plot of segmented device by utilizing bismuth telluride and Skutterudite materials. The plotted graph show module derived values through simulation and calculation. The maximum power for the device is 25W at temperature gradient for this output is 300 C (i.e., between 150 C to 500 C). The optimum calculate

voltage, current, power is 7.5 V, 5.08 A and 65W. The maximum voltage was 15.33 at difference of 400 C and efficiency was almost 8%.

The optimized equation (equation 3.20) was applied on $Bi_2Te_3$ device with 126 legs. The device has 21 W, R = 1.23, and $\alpha = 1.18 * 10^{-4}$. The device boundaries were vertically restricted, whereas, horizontally free. Thermally induced on the vertical ends were 70 MPa, whereas total stress of the device was 80 MPa. The temperature gradient ($\Delta T$) was 280 C between cold and hot end. This gives us (also shown in figure 3.3)

$$\sqrt{21 * 1.23 * \frac{70}{80}} = v$$

$$v = 4.833$$

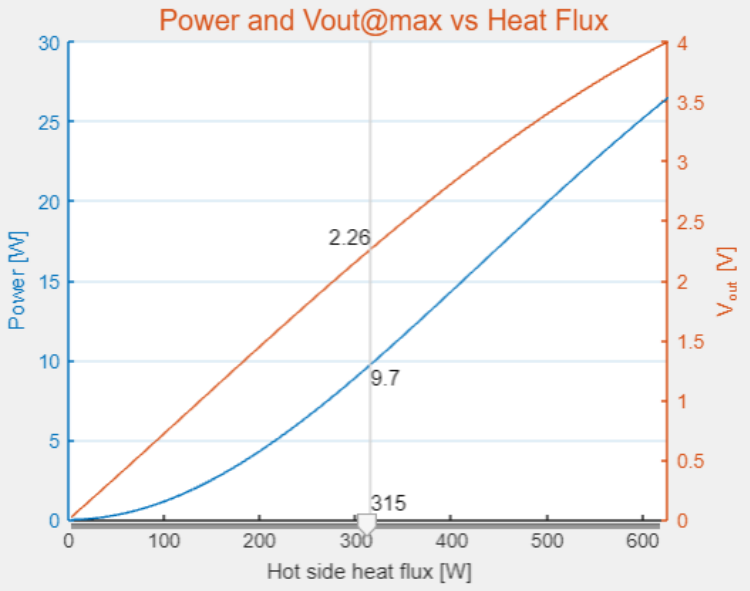


Figure 3.3 Voltage potential after applying equation 3.20

This gives us new numbers of legs, that compensates thermally induced stress

$$N = \frac{4.833}{2 * 1.18 * 10^{-4} * 280} * \frac{1.233 + 1}{1.233}$$

N= 132

The equation gives provide alternative approach. The Optimization in the device

tends to increase number of legs from 126 to 132 legs, which is almost ±4.5 % increase in order to gain voltage potential of 5.5 V. The optimization requires increase of space between each leg. The recommended spacing between the thermoelectric legs is ±0.5 to ±0.7mm. The space between $Bi_2Te_3$ was taken as 0.5mm and after optimization the spacing between each leg was 0.5225 mm. That is ±0.01 % increase of space between each leg.

The obtain Optimized approach also shown that effect of thermally induced stresses were reduced by decreasing number of leg and increase of spacing between each leg. The mathematical equation of deriving space between two legs has been presented in the following literature [70], [71]. Figure 3.3 (a), in this regard, demonstrates the power output for different low to high temperature TE materials. The materials used to get data in figure 3.3 (a) are shown in table 3.3.

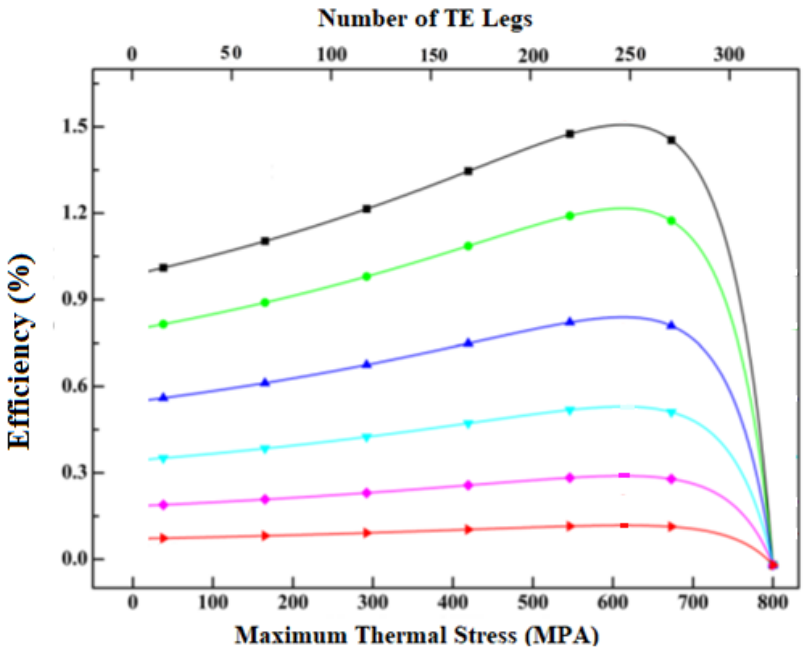


Figure 3.4. Stress-based number of legs for TE device

The optimum number of legs were fixed at 300. The optimization in each device was increase of spacing (i.e., 0.01%). Efficiency of each thermoelectric was maintained between 200 to 260 legs. The experimental results have shown optimal number of legs for each device, maintaining the optimized space. As device configuration was altered, the efficiency was changed accordingly.

Table 3.1 Material used in Figure 3.1 (a) and their color

| **Material Type** | **Color** | **Temperature Range** |
|---|---|---|
| Bismuth Chalcogenides | Red | 100 – 250°C |
| Group IV Tellurides | Violet | 200-600 |
| Silicon-Germanium Alloys | Cyan | 600C – 1000°C |
| Segmented $Mg_2B_{IV}$ Solid Solutions | Blue | 200-800 |
| Segmentation of Skutterudites with Group IV Tellurides | Green | 200-800 |
| High Temperature<br>$CeFe_4Sb_{12}$(p-type)<br>$Zn_4Sb_3$(p-type)<br>TAGS (p-type) | Black | 700-1100 |

Figure 3.5 demonstrates an average difference between segmented and unsegmented for small, gathered data. The peak drop of graph shown in figure 3.4 and 3.5 (a & b) is due to power output as the device approaches to thermal failure at given stress. It was also noticed that when the boundaries are fixed (vertically and horizontally), device develops compressive stress, causing spallation of the leg. Whereas, when the boundaries are horizontally flexible, the device mostly develops tensile stress and device mostly compensates thermally induced stresses, i.e., almost $\pm$37%. The optimization of the devices according to obtained mathematical equation, the results are very different from conventional literature. Figure 3.5 demonstrates that optimum number of legs are vary with the device design. The segmentation (for smaller devices) has 60 number of legs that can sustain steady operational hours compared to unsegmented device.

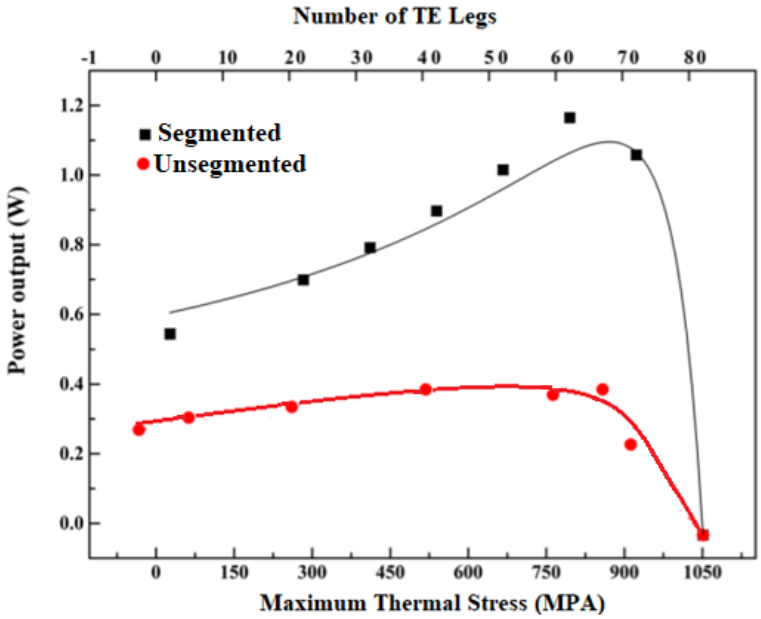


Figure 3.5 – The comparison between Segmented and Unsegmented TE device

Unsegmented devices, whereas, has 57 number of legs. In order to study the effective measurements, Finite element analysis were conducted.

## 3.2 Finite Element Analysis

The influence optimization on the length and height ratio of any given cross-sectional area is shown in figure 3.6. It can be seen that the variation tendency of thermally induced stress at leg size 1.4 is different from other leg sizes as the temperature increases. The simulation results uphold the leg size mentioned in chapter 2, where dimensions are mentioned. For unsegmented devices, thermally induced stresses minorly vary compared to segmented devices. Plus, the stress concentration is higher on hot sides compared to cold sides. Thus, the variation tendency of thermally induced stress per temperature change decrease as we increase the leg size. The main reason for this has been discussed in figure 3.8, where it has been shown that the leg bends at larger leg size. This provides insight that leg size must be chosen according to stress concentration.

Figure 3.6, in that case, shows us more optimized relationship between temperature and stress, where the change of size also changes local electrical current density and local thermal resistivity. The electrical current density becomes larger at a smaller leg size which

generates more thermally induces stresses in the volume. This phenomenon is called joule heating effect. By choosing proper number of legs, space between them and size can minimize the thermally induced stress. The example shown in the figure 3.7 & 3.8, for unsegmented and segmented p-n TE module, has dimension of 4 x 4 x 8 $mm^3$ with optimized calculation, spacing of 1.5 mm. The electrode is made from 0.5mm copper and the thickness of barrier layer (for segmented device) is 0.3mm alumina. The boundary conditions are taken according to case-2 (mentioned in chapter 2)

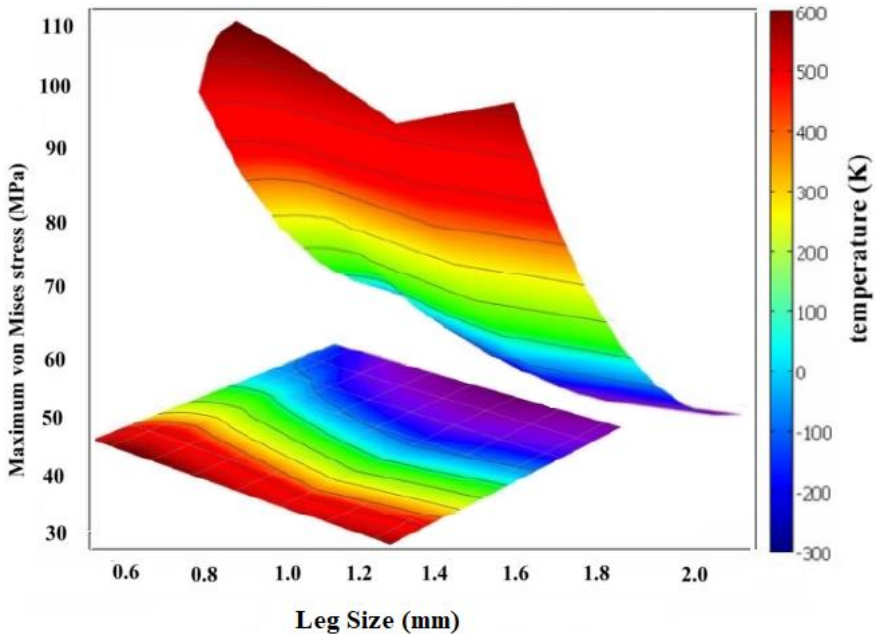


Figure 3.6 Variation of Von Mises stress with leg size and temperature for cold and hot side

In connection with figure 3.6, figure 3.7 shows the effect of thermal expansion in thermocouple under varying temperature and thermally induced stress. The case study has been demonstrated above and the deformed frame is highlighted in red color. Especially in case of Segmented device, where red is contact point for two different materials. The current density in that case varies from 1 to 3 A. The original geometry is shown on left side of the figure and the displacement due to thermally induced stress is position on right side.

The given change in the module's length, y-direction, is due to two main factors, i.e., thermally induced stress and change in current density. By utilizing above given model, thermoelectric, and thermomechanical effects can be analyzed simultaneously. This enables us to study thermoelectric effect along the thermomechanical characteristics. For instant, the

effect of change in electric resistivity and increases stress concentration on edges makes leg more vulnerable to expand [72], [73]. The increase in resistivity lowers at hot end causes increase in temperature, hence causing increase in thermally induced stresses.

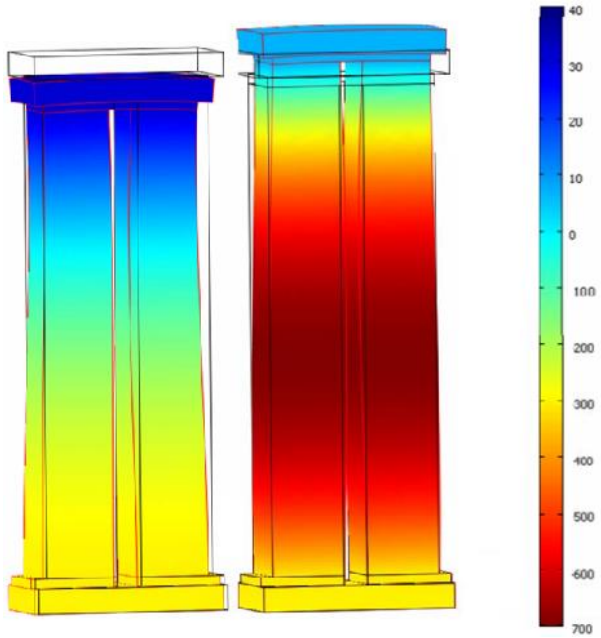


Figure 3.7 Thermal expansion of TE leg under temperature gradient by using boundary condition in case 1

In this regard, figure 3.8, in connection with figure 3.6, shows the temperature distribution and effect of thermal expansion (induced stress) on TE leg where boundaries are bounded. Proving Suhir assumption, the TE legs encounter tensile stress on boundaries due to bending force. We have realized that varying resistivity within thermal couple and complete leg, the thermoelectric leg bend asymmetrically at varying temperature distribution due to tensile and compressive nature thermally induced stresses. Figure 3.8 shows the Von Mises stress within the module at 370 (MPa) for Bismuth telluride-based segmented modules.

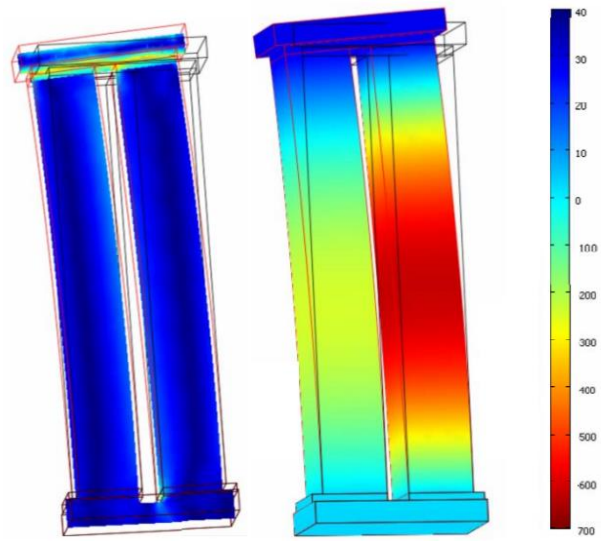

Figure 3.8 Thermal bending under higher resistivity and temperature gradient.

Above shown demonstration is obtained by use COMSOL Multiphysics and calculation are made for arbitrary geometries. Whereas figure 3.9 demonstrate the change in overall thermally induced stress by varying with number of TE legs and spacing between them. Where figure 3.9 (a) shows power output as per temperature distribution in device, where spacing between each leg was increased as per optimized mathematical model. whereas (b) shows the change in thermally induced stresses by increasing number of legs for power production.

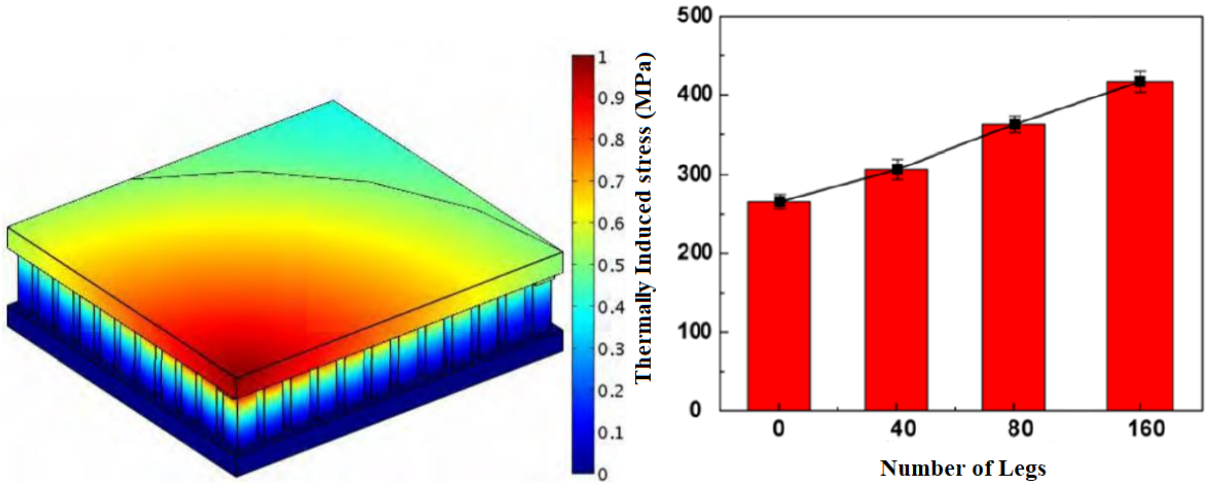


(a) (b)

Figure 3.9 Thermoelectric mapping for multileg module

For all configurations of the TE modules, numerically predicted number of legs, space between them and their relative stress were validated ±5 % error and ±10 % error

with their maximum efficiency values. Regardless of their arrangement and material selection, leg size, space between them and number has 10% effect on maximum power and efficiency. However, by increasing space between the legs, in unsegmented devices, do decrease maximum stress of the overall device. Whereas segmented thermoelectric devices show higher power and efficiency but lower maximum stress by increasing space between the legs as per optimized model. The case study of $Bi_2Te_3$-based alloys and $CoSb_3$-based filled skutterudites segmentation, it has been seen that by increasing 0.01% space between the legs and decreasing $\pm$4.5% number of legs, the maximum thermal stress was reduced from 350 MPa to 300 MPa.

# Chapter 4. Developing the Optimized Reliability Model for Thermoelectric System

Choice between different distribution can change the estimated reliability at larger extend. With regard to estimate the strength and stress, mathematical models are developed to locate the magnitude of stress in a component and its concentration map. In electronic industry, where the size of the given sample is small enough to discriminate between the two-distribution functions to find probability of correct selection.

## 4.1. Analytical Model

For a given set of operating conditions, the reliability is defined as the probability that a system survives for some specific period of time. In our case, we drive our survival function on random variable "thermal stress ($\sigma$)" at specific temperature "T". In order to operate efficiently, the generated thermal stress in TE module must be lower than the strength (s) of the overall module. The condition of reliability is that the TE module survives within modeled strength. This condition can be mathematical expressed as $S = P(s > \sigma) = \int_{\sigma_o}^{\infty} f(s)ds$. Here $\sigma_0$ is initial mechanical stress before the temperature effect and S is survival function. The survival function (S) of any TE module, with a probability that stress is less than the strength, where stress and strength are two independent variables, for all the possible values of the strength can be computed as

$$S = \int_0^{\infty} f_\sigma(\sigma)\left[\int_0^{s} f_s(s)d\sigma\right]ds \tag{4.1}$$

Then the failure function can be given as case that the value of stress is higher than the strength of the device, that is, $F = 1 - S = P(s \leq \sigma)$. And for independent values of stress ($\sigma$) and strength (s) variables, the failure function is given as

$$F = \int_0^{\infty} F(s).f_{\sigma}(\sigma)\, d\sigma \tag{4.2}$$

Since TE module is temperature dependent device, we assume here interface random real number (y) which is interim thermal stress at which module operates without any interruption, that is, $y = s - \sigma$. If we assume that $\sigma$ and *s* are non-negative independent random variables, then the ability to operate without interruption at interface temperature is given by survival function, i.e., S (y > 0) and the P.D.F of the failure function (y=0) can be determined through following solution

$$F_y(y)dy = f_s(s)ds.\int_{\sigma}^{\infty} f_{\sigma}(\sigma)d\sigma \tag{4.3}$$

In equation 4.3 the value of strength is a fixed variable whereas the value of stress has a random magnitude. In this scenario the sustainability of the device is assumed that all possible value of $\sigma$ are less than the value of *s* i.e. ($s > \sigma$). By assuming the range of $\sigma$ from $0 \rightarrow \infty$, the equation (4.3) can be solved as,

$$f_y(y) = \int_0^{\infty} f_s(y+\sigma).f_{\sigma}(\sigma)d\sigma \tag{4.4}$$

Based on equation (4.4) reliability of the TE module can measured through survival function, given as $S = \int_0^\infty f_y(y)dy$, i.e.,

$$S = \int_0^\infty \int_0^\infty f_s(y+\sigma).f_\sigma(\sigma)d\sigma$$

And the probability of failure can be written as

$$F = 1 - S = \int_{-\infty}^0 \int_0^\infty f_s(y+\sigma).f_\sigma(\sigma)d\sigma dy \tag{4.5}$$

When we consider the reliability of segmented Module, the survival function of a system with multiple layers with multiple possible failure mode,

$$\text{S}= 1 - \prod_{i=1}^{\varphi} F_{n_i}F_{p_i} \tag{4.6}$$

Here, S, $\varphi$ and $F_{n_i}F_{p_i}$ present over all module survival function of TE module, number of significant failure mode and significant failure mode of n and p type TE leg with *i* number of layers respectively. As elaborated above that we study here segmented TE modules for high temperature operating atmosphere, we take lognormal distribution, instead of Weibull distribution. The strength-stress density function for lognormal distribution[74][48] is derived as

$$f_y = \frac{1}{y\delta\sqrt{2\pi}} exp\left[-\frac{1}{2\delta^2}(\ln y - \mu)^2\right] \tag{4.7}$$

Here, y > 0, and the parameters μ and $\delta$ are the mean and the standard deviation, respectively, of the variable ln y. If we take log of interference condition, i.e., $\ln y = \ln s - \ln \sigma$, we get mean log values to get probability plot. The condition is $\bar{y} = \frac{\bar{s}}{\bar{\sigma}}$, where bar shows average log value for thermal stress and strength. Here the mean log value for strength is taken as ultimate stress at which the component materials in form of segmentation can survive at modeled temperature. The system is reliable if the probability of survival function is equal to 4.1 and probability of module to survive can be given as

$$S = P\left(\frac{s}{\sigma} > 1\right) = P(y > 1) = \int_1^{\infty} f_y(y)\, dy \tag{4.8}$$

The lognormal distribution provides distribution of a random variable whose logarithm is normally distributed. The stress-strength model, with lognormal distribution (for both, the stress, and the strength) has widely replaced the normal distribution model due to more realistic properties. The positiveness of its values and the positive skewness of its shape provide more predictable results compare to normal distribution.

## 4.2 Mean Residual Life (MRL) for Lognormal Distribution

In reliability analysis, lifetimes are mostly taken as random variables when probability distributions are considered. In thermoelectric field most famous distribution used in reliability analysis is Weibull distribution, which is the most suitable model for modules operating gradient is T > 300 C. But rising demand of high temperature modules limits Weibull's distribution and requires new methods to predict accurately operating life of TE modules, especially segmented modules. In order to develop a mathematical model, there are five main characteristics which must be define by the reliability model and those are PDF, CDF, failure rate, survival function and MRL function. In this chapter we'll include MRL function in order to develop a condensed information to measure precise reliability of the (un)-segmented TE module. The main purpose of MRL is to measure mean life for the

given device at random thermal stress value, i.e., the stage where TE component works before the module faces abruptive failure. This gives us two aspects of module, its lifetime and the mean thermal stress ($\sigma$), at given temperature gradient, at which module operates without halt.

Suppose $\sigma$ is a continuous non-negative random variable with CDF F($\sigma_y$), PDF $f$ ($\sigma_y$) and survival S($\sigma_y$)= 1− F ($\sigma_y$). To define residual life random variable at threshold thermal stress ($\sigma_{Th}$), the life expectancy would be $\sigma_{Th}$= $\sigma - \sigma_y | \sigma > \sigma_y$. This implies that mean residual life can be calculate as

$$M(\sigma_y) = E\left(\sigma - \sigma_y \middle| \sigma > \sigma_y\right) = \frac{1}{S(\sigma_y)} \int_{\sigma_y}^{\infty} S(y)dy \qquad \sigma_y \geq 0 \quad (4.9)$$

The lognormal distribution belongs to those distribution which have no closed form of survival function, so we will use equation (4.8) to obtain the MRL function for lognormal distribution. In this regard, the PDF and CDF of a lognormal are given as

$$f(\sigma) = \frac{1}{\sigma\sqrt{2\pi\delta^2}} exp\left[-\frac{1}{2}\left[\left(\frac{\ln \sigma_y - \mu}{\delta}\right)\right]^2\right] \quad (4.10)$$

$$\mathrm{F}(\sigma_y) = \int_0^{\sigma_y} \frac{1}{\sigma_y\sqrt{2\pi\delta^2}} exp\left[-\frac{1}{2}\left[\left(\frac{\ln \sigma_y - \mu}{\delta}\right)\right]^2\right] \partial\sigma_y \quad (4.11)$$

Therefore, the survival function TE module can be written as

$$S(\sigma) = 1 - \varphi\left[\frac{\ln \sigma - \mu}{\delta}\right] \quad (4.12)$$

Let assume that $z_\sigma = \frac{\ln \sigma - \mu}{\delta}$, then $\sigma = exp\,[z_\sigma \delta + \mu]$ and $\partial\sigma = \sigma exp\,[z_\sigma \delta + \mu] dz_\sigma$.

Main residual life for lognormal distribution will become

$$M(\sigma) = e^{\left(\frac{\mu+\delta^2}{2}\right)} \frac{\left[1 - \varphi\left[\frac{\ln \sigma_y - (\mu + \delta^2)}{\delta}\right]\right]}{1 - \varphi\left(\frac{\ln \sigma_y - \mu}{\delta}\right)} - \sigma \tag{4.13}$$

Figure 4.1 provides comparison between PDF (top left), CDF (bottom left), Survival function (top right) and MRL function (bottom right). The PDF shows that unsegmented device has maxima at 75 MPa, with probability of 0.45 and whereas segmented device has maxima at 90 MPa, with probability of failure of 0.65. That case reflects drop of survival function sharply before segmented device, noting the difference of 15%. The results are conformed in CDF graph where survival graph repeats with more-less $\pm$10% error. MRL function demonstrates reported number of TE modules that survive at specific thermal stress. The comparative study has shown no transformation and both lognormal MRL and survival functions, shows fitting graph for higher value of scale ($\delta$) and location ($\mu$) parameters. The domains of the survival functions, based on equation (4.12) for $\sigma \leq \sigma_y$ can take on values from 0 to infinity, however for $1 < \sigma_y < 0$ goes from 0 to $\sigma_{Th}/\sigma$.

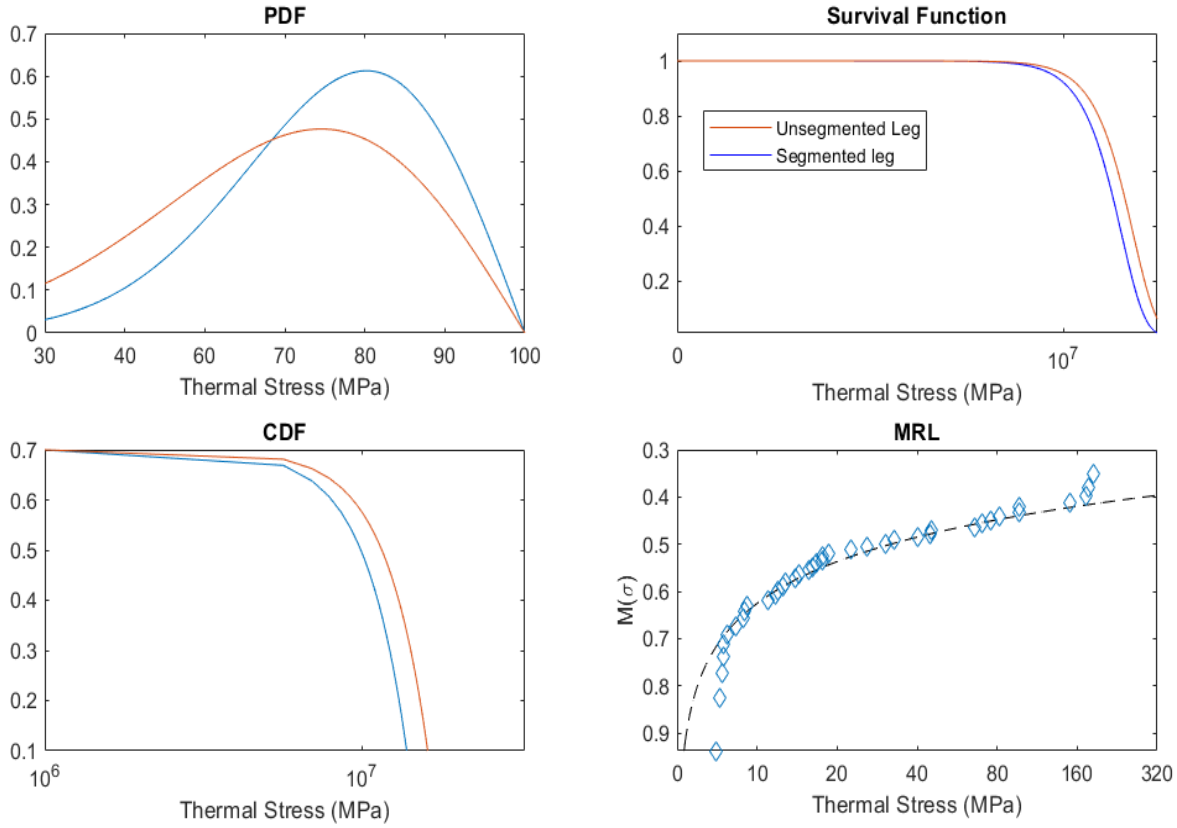


*Figure 4.1 Comparison between PDF, CDF, Survival Function and Mean residual life of segmented and unsegmented TE leg*

This presented method is known as parametric method, where all the given assumptions can be verified [75]. The function can describe the failure behavior of the devices, which is life distribution of the device. Although parametric approaches allow us more to obtain more information based on assumed model distribution but there are two main restrictions. Firstly, the distribution is merely an approximation and extrapolation of life for the prediction does not always (necessarily) succeed. And secondly, parameters of given distribution not always converge observed data, especially when the size of the device is small.

In that regard we have chosen to implement nonparametric analysis. Nonparametric analysis allows us to characterize life data without assuming an underlying distribution. Nonparametric method helps us in reliability modelling in two ways. (i) Verifying the hypotheses and (ii) estimating the distribution function. That means that nonparametric method provides us a model free estimate of reliability, which in our case survival function and CDF of the device.

## 4.3 Non-Parametric Lognormal Survival Function

Nonparametric models, compared to parametric modelling, are mostly used to analyze failure data to estimate the MRL function. Under extreme right censorship, the nonparametric model can provide an innovative method to deal with discrete and nonlinear censoring data. The relationship between nonparametric MRL and failure rate function can assist us to develop a better reliability model and effective system. Consequently, nonparametric Survival function aims to measure sustainability of a device based on their failure behaviors. We used a Dirichlet process for obtaining a common nonparametric lognormal survival function. In this regard we take density of survival function ($\acute{S}$) at threshold stress ($\sigma_{Th}$) with the respect of interference and strength stress. i.e.

$$\acute{S}(\sigma_y, G) = \int K\ (\sigma_y; \sigma_S) d\mathrm{G}(\sigma_{Th}) \tag{4.14}$$

Here K is a lognormal distribution for the kernel, G($\sigma_{Th}$) is nonparametric vector defined at threshold stress where we can still find our TE modules operating, the moment before module confronts abruptive failure. The nonparametric lognormal-Kernel distribution, for the discrete data based on stress-strength data distribution, can be given as

$$K\left(\sigma_y; \sigma_S = (\mu, \delta^2)\right) = \frac{1}{\sigma_y\sqrt{2\pi\delta^2}} exp\left[-\frac{1}{2}\left(\frac{\ln\sigma_y - \mu}{\delta}\right)^2\right] \tag{4.15}$$

And nonparametric vector for a module to operate at threshold stress (surviving stress) can be defined as

$$G(\sigma_{Th}) = \sum_{\sigma=1}^{\infty} \omega_{\sigma} \delta_{f(\sigma)}(\sigma_{Th}) \quad (4.16)$$

Here $f(\sigma)$ presents independent stress distributed identically over the module. And $\delta_{f(\sigma)}$= {1,2….} is the parametric indicative function of stress, which is the baseline distribution. $\omega_{\sigma}$ present stick-breaking of discreteness and explicitly used to give random probability of discrete distribution. Since the distribution is random itself, its precision is derived from location parameter, define as $\{\delta_{\sigma}\}_{\sigma=1}^{\infty}$ and shape of survival function $\acute{S}(\sigma_y, G)$. The expansion of equation (4.13), we can locate the survival function curve, at $\sigma_y$ and $G(\sigma_{Th})$

$$\acute{S}\left(\sigma_y \middle| G(\sigma_{Th})\right) = \sum_{l=1}^{N} \rho \sigma_{Th} \text{ LN } \left(\sigma_y; \mu, \delta^2\right) \quad (4.17)$$

Here $\rho$ comes from Bayesian inference to include posterior probability, which presents maximum likelihood of survival function derived from failure rate data. It is given as $\rho = E_{v_i} \prod_{v=i}^{i-1}(1 - E_{v_{\sigma_y}})$, where $E_{v_i}$volumetric elastic constant of $i^{\text{th}}$ layer at $\sigma_y$ and $v_{\sigma_y} = \beta(1, \alpha)$. $\beta$ and $\alpha$ are two positive shapes defined as per Dirichlet process and *i* is the total number of components in the model. The nonparametric lognormal distribution mixed with Kernel distribution as per Dirichlet process model, for positive real number, is transformed as Y= log $(\sigma)$ −log $(\sigma_y)$. The nonparametric survival probability for unsegmented module, to survival within domain of threshold stress but higher than interference stress, can be given as

$$\acute{S}(\sigma_y \leq \sigma \leq \sigma_{Th}; G) = Pr(\sigma \leq e^Y; G) \quad (4.18)$$

Respectively for segmented TE modules, the nonparametric probability can be given

as

$$\acute{S}\left(\sigma_y \leq \sigma \leq \sigma_{Th}; G\right) = \sum_{i\geq 1}^{i} \rho\, \varphi\left(\frac{Y-\mu_i}{\delta_i}\right) \tag{4.19}$$

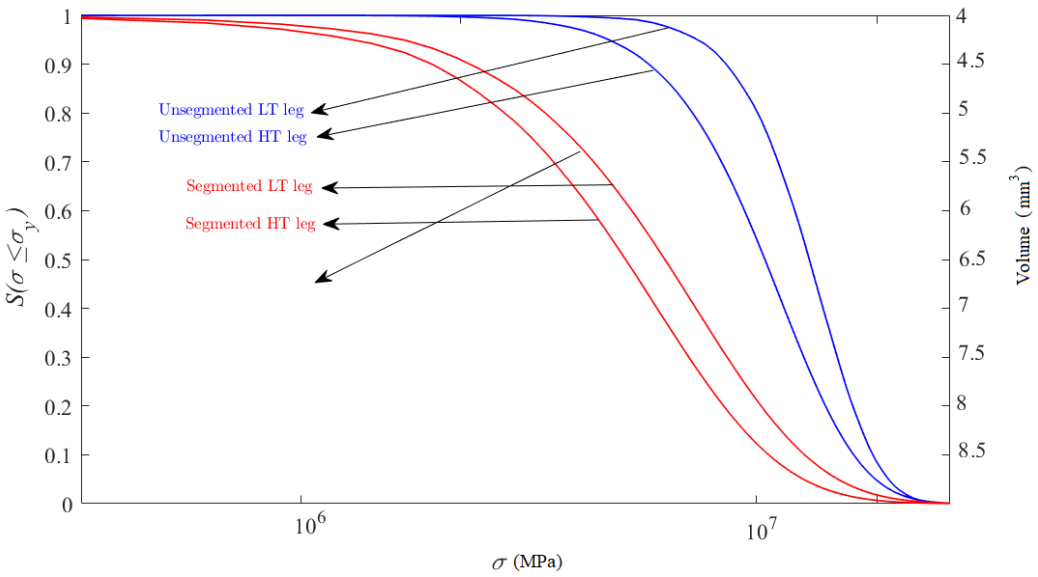


*Figure 4.2 Comparative Nonparametric Survival Function graph for Segmented and Unsegmented*

Figure 4.2 shows the evaluation of survival function based obtained results for segmented and unsegmented TE legs. TE module working on high and low temperature result different ratio of reliability. Low temperature unsegmented TE modules demonstrated higher rate of survival on given standard ($4mm^3$) leg volume. One of the major reasons is that unsegmented TE module has low adverse effect from thermal expansion compared to segmented TE module. At given leg volume unsegmented modules has 95% survival rate within range of $10 \leq \sigma < 60$ (MPa). Whereas the 95% of survival rate for low temperature segmented TE module exists only between $0 \leq \sigma < 30$ (MPa), due to mismatch of thermal expansion between different materials. The main difference between simple MRL and Survival function and nonparametric survival function is rapid decline in curve of Figure 4.2 compared to figure 4.1. MRL has definite method to predict reliability of module based on failure rate data whereas nonparametric survival function can give us precise dimensions (volume) and thermally induce stress to produce reliable characteristics for segmented and unsegmented TE modules. Hence more intuitive conditions (especially boundary conditions

of TE leg) are produced as alternatives on given survival curves. This makes easy for us to obtain graphical MRL function-based reliability to analyze survival function on sufficient conditions.

## 4.4 Comparative Discussions and Results

### 4.4.1 Lognormal or Weibull Distribution

To construct a qualitative reliability model for thermoelectric devices, we calculate the failure probability for different devices at different temperature gradient. For the probability distribution we can utilized both, Weibull and lognormal distribution. The Weibull distribution is most widely being used in ceramic and glass industry for developing probabilistic tensile strength of material. At lower temperature, Weibull model is relative, and failure can be defined but becomes less accurate when temperature increases [76]–[78]and the size of the device (sample) decreases. That is because change in stress during excessive loading, the device is a subject of fatigue failure, which vary from static loading or temperature. As an alternative to Weibull distribution, lognormal is also widely used, especially when the stress varies continuously. In this regard, discussion around both methods is done to understand adequate probability of failure.

### 4.4.2 MATLAB Results

Probability of failure is calculated through Weibull and Lognormal distribution through MATLAB. Stress was set as main random variable and the values of stresses are obtained from tensile, bending and compression tests. Figure 4.3 shows Weibull probability function to estimate failure of different TE leg during tensile, bending and compression tests. The obtained data is distinguished through different lines and colors (blue, red and orange color respectively). Each line and color indicate stress values obtained during experiments. Values (as shown in Figure. 4.3a) of stress vary from 10 to 50 MPa with shape of 7.4 MPa

and scale 25 MPa for Bismuth telluride. Survival and hazard rate graph (b & c) show high probability of survival of leg at tensile stress as compared to bending and compression stress. Whereas the probability plot (d) shows the probability of failure of device as whole. Weibull's Probability plot shown in figure 4.3 d is relatively taken in regard of constant atmosphere temperature and static loading.

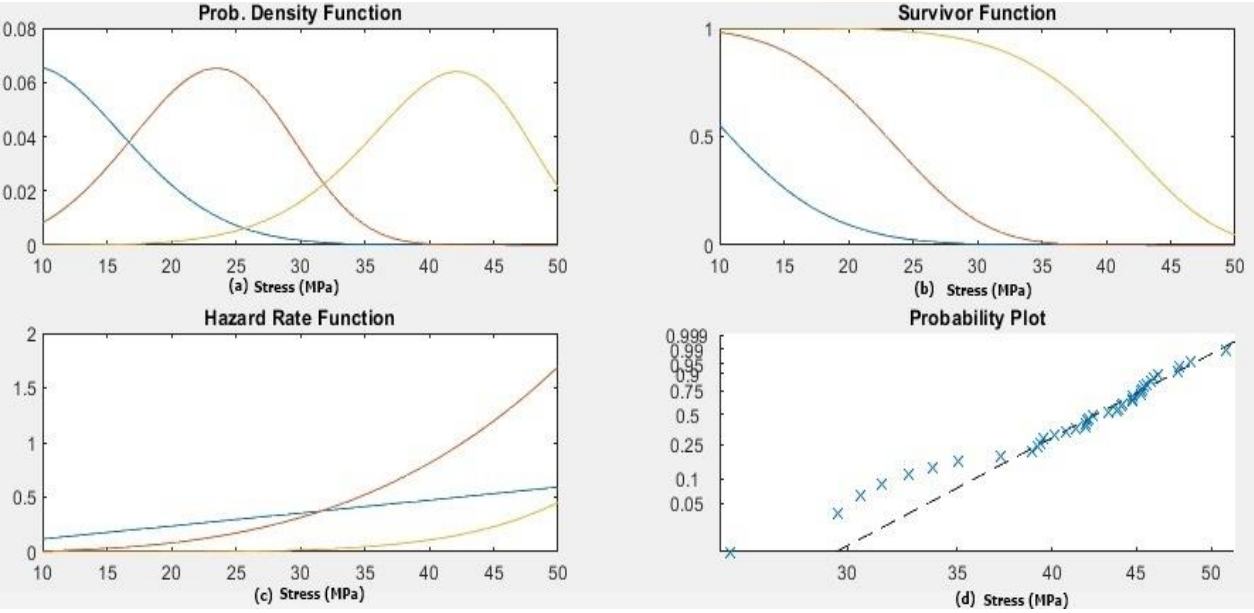


*Figure 4.3 Weibull's Distribution Graphs*

The comparison between figure 4.1 and figure 4.3 shows us significant difference between two methods. We'll express that different more clearly in figure 4.4. That specific comparison, life distribution of the TE device is lognormal distribution. The Shape value, 7.4 MPa, is big as shape parameter of Weibull distribution. It shows that wear-out mechanism doesn't prevail, and we can't conform in the failure analysis. Thermoelectric device, contrary to the assumption of Weibull distribution, follows lognormal distribution because it entails higher stress in a small (comparatively) size of TE device.

In regard to static loading where only extreme load (force) will cause damage, figure 4.4a and 4.4b are presented but the differences are very minor. By observing figure 4. 4 closely, each graph represents different range for probability. Figure 4.4a shows failure zone from 50 to 66 MPa, whereas failure zone in figure 4.4b starts from 45 MPA till 66 MPa. That comparison conforms that our sample doesn't fit in Weibull's assumption, i.e., wear-

out, of device. The raise in temperature, especially during compression test, Weibull manifest its effect very slightly. Whereas lognormal distribution (see shown in figure 4.4b & 4.5), show that clear difference between dynamic (varying stress) and static (constant stress) loading. By plotting data at same graph sheet (figure 4.5), Weibull distribution has 50% of failure prediction at 66 MPa, whereas lognormal gives 80% probability of failure at the same stress level.

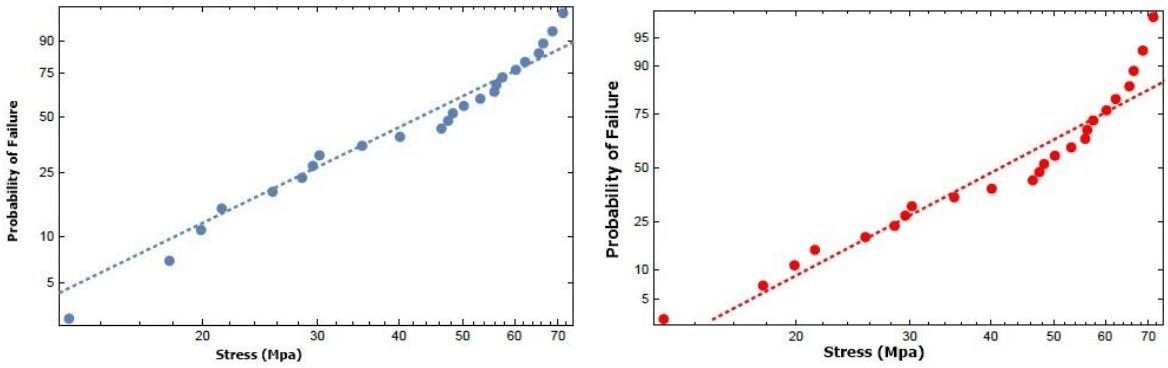


(a) (b)

*Figure.4.4 (a) Probability distribution function of Weibull and (b) Probability distribution function of lognormal*

Lognormal presents significantly precise expression of data because during experiments, most of legs encountered damage, crack, or deformation at 60 (and above) MPa. In this regard, we noted stress and failure of leg at each level for two different sides i.e., hot and cold side.

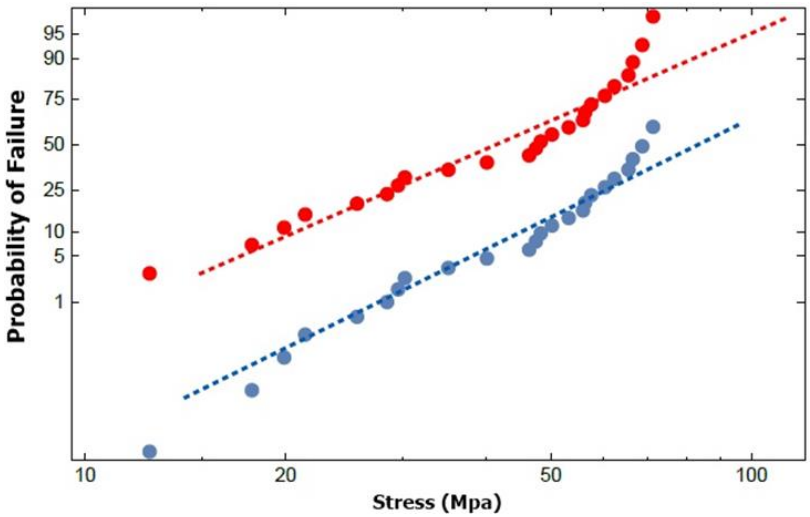


*Figure4.5 lognormal vs Weibull distribution*

The percentile failure of TE legs compiled through experimental results are shown in Figure 4.6, is expressed through lognormal distribution function. In this figure we have shown percentage of failure of legs at different temperatures. The blue line shows low temperature experiments and red shows high temperature experiments. It was noticed that the legs are more vulnerable to failure at higher temperature as compared to lower temperature. Applicability of lognormal distribution in this phenomenon is valid due to fatigue effect on legs.

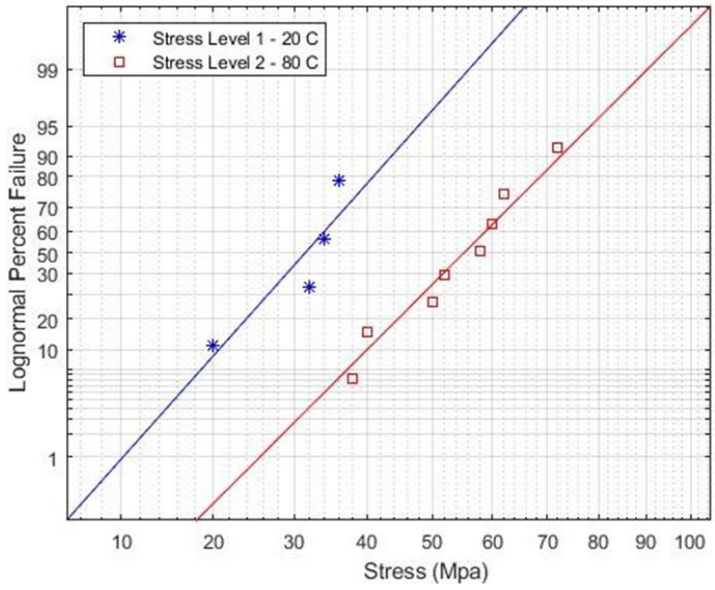


*Figure. 4.6 Lognormal distribution-based percentage failure of TE modules,*

### 4.4.3 Reliability Model (Python and MATLAB)

The influence of temperature on thermoelectric module and its material properties plays a significant role to predict reliability as outlined in the introduction. The analytical model corresponds to stress- strength covariance to obtain probability of survival and MRL of the module. The temperature gradient along the TE leg, between cold and hot sides, leads significant changes by influencing thermal conductivity. Two main aspects that govern the reliability of the module are (i) amount of heat absorbed and (ii) material property changes due to heat distribution along the module. We above illustrated the linear relationship

between temperature distribution and thermal stress generation, here we have notice that there is minor bow, shown in figure 4.7 (a) in the temperature-stress relationship (in segmented cases). The inclusion of Thomson and joule heat in temperature distribution profile leads to this bow in graph (shown in figure 4.7).

The Figure .7(b) corresponding to temperature profiles by considering contribution of boundary conditions at each end (hot and cold) for the emergence of deviation from linear temperature profile at maximum efficiency. The simulated results show the temperature profile dependence on material properties, which contribute nonconstancy, leading temperature line bending, especially on hot side. Thomson heat generation (or absorption) gradient, in double integration $\left(k(T)\frac{\partial^2 T}{\partial y^2}\right)$, fills the loss of heat, causing a bow on the gradient line.

For visualization, the effect of Thomson heat generation (absorption) on stress-strength covariance profile, based on temperature gradient, is obtained for nonparametric lognormal model and compared with obtain simple Monte Carlo simulation (see figure 4.8).

The simulation results demonstrate that bending with torsion and phase displacement, varying with length to thickness ratio, have influence over the maximum thermal shearing and mechanical shearing stresses. Figure (a) shows positions of maximum covariance between stress (shearing) and strength for a stable (segmented and unsegmented) TE module using general stress-strength relationship through Monte Carlo simulation.

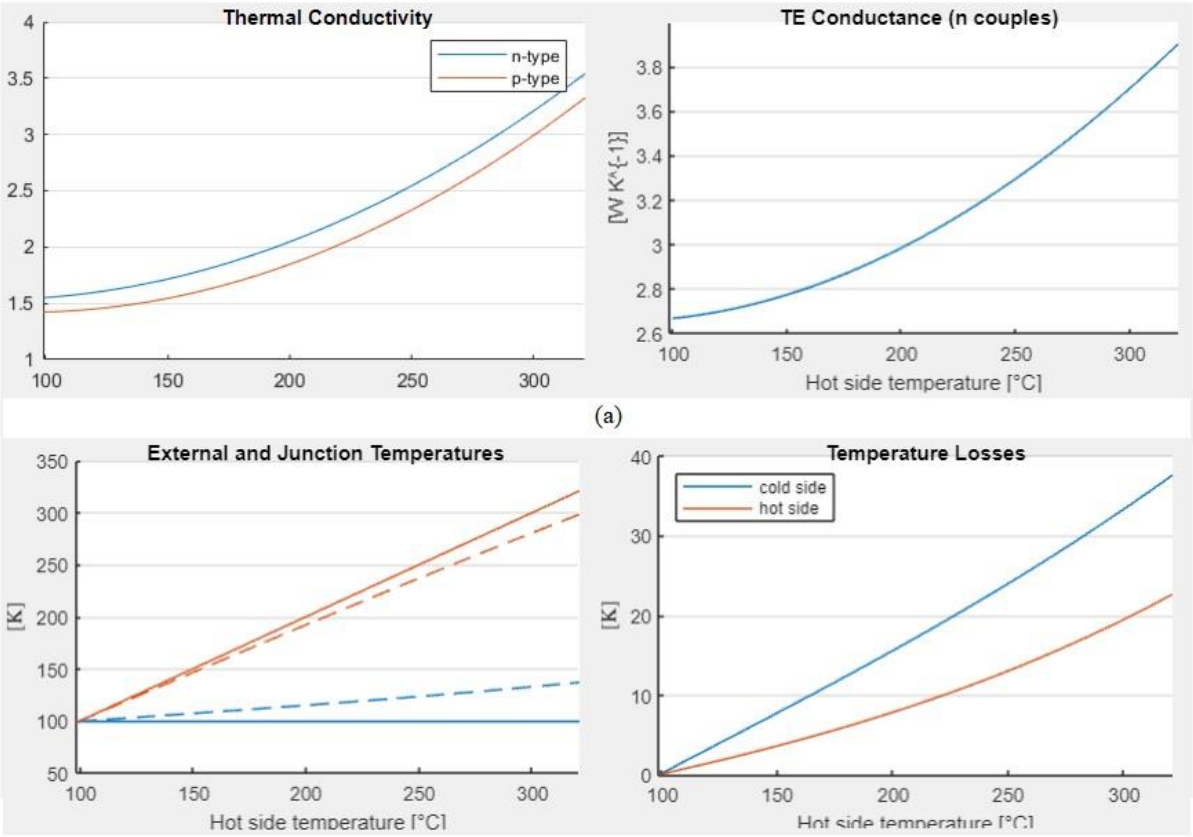


*Figure 4.7 Temperature Profile of Segmented TE module*

Whereas figure 4.8(b) presents the covariance profile for high and low temperature segmented TE modules under highly induced thermal stresses, where the maximum covariance corresponds to the critical position. For the ratio of thermal shearing stresses to the strength, at significant bending stresses, the plane of maximum covariance occurs from 300 MPa onwards (*specific case of segmentation using bismuth telluride material*). The plane of maximum covariance varies from material to material and module to module. The resemblance between graph (a) and (b) shows the relevancy of nonparametric lognormal distribution to obtain critical stress for segmented TE module through covariance plane.

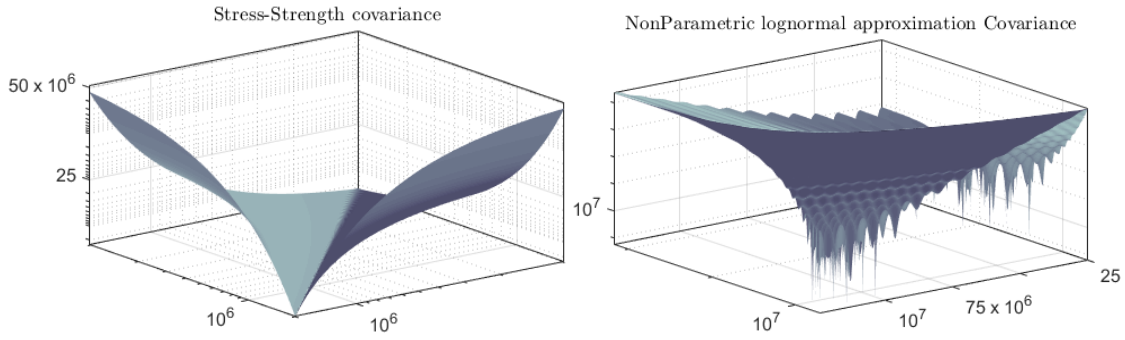


(a) (b)

*Figure 4.8 Stress Strength Covariance*

On further investigation, the demonstrated figure 4.9 shows relevance vector regression on stress-strength covariance. The optimized nonparametric lognormal distribution model, developed to understand stress-strength covariance, was simulated under Fast Multi-output relevance vector regression (MRVR)[79] in MATLAB. Figure 4.9 illustrate the distribution of Survival function in domain of threshold stress. A noteworthy observation is that the probability of survival function encompasses characteristics of upside-down bathtub shape for individual module threshold stress discrete analysis. The distribution of failure data has same characteristics for shape of survival function as Figure 4.2. The deviations are different when compared with high temperature segmented (SKD) and relatively decreases after 300 MPa when compared to low temperature TE modules (bismuth telluride). This has significant implications on TE system design and optimization of discrete data distribution to apply nonparametric lognormal survival function.

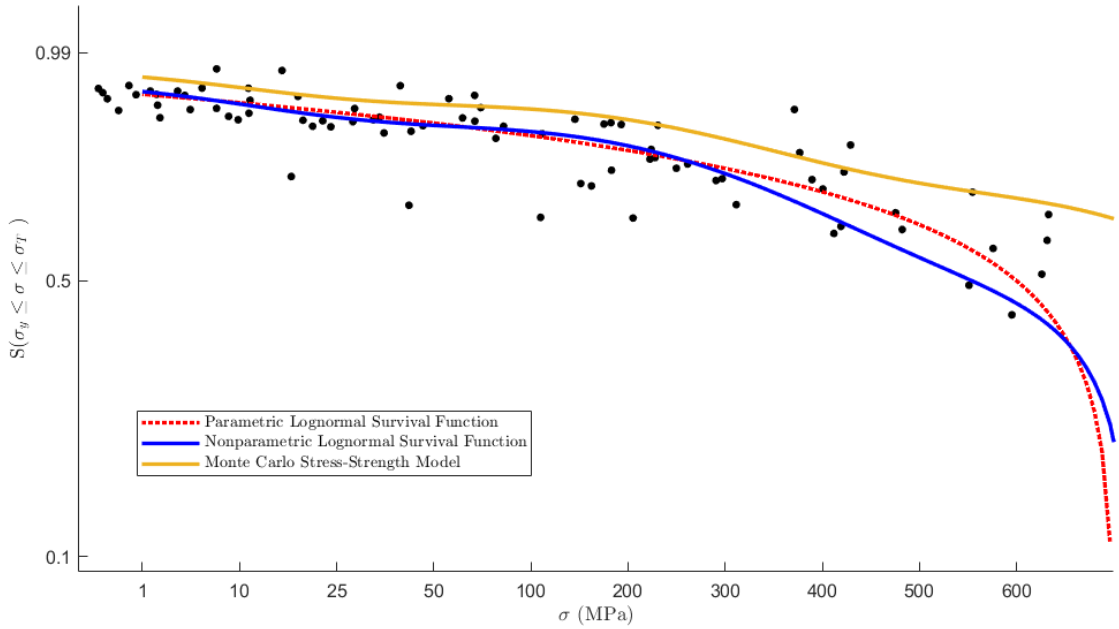


*Figure 4.9 Comparison of Monte Carlo simulation with Parametric and Nonparametric Survival Functions*

Figure 4.10 illustrates the nonparametric model, at 200, 300,500, 700 and 900 MPa stress data to approximate the appropriate priors for segmented and unsegmented modules. We used interference random variable *y*, under the random stress σ. The range of the unsegmented high temperature TE module on the log scale was (3.69356, 8.2986), extending the prior variance about 0.85. The shape parameter was set 2 so that the unsegmented high temperature module could have finite variance. Whereas for segmented high temperature module, following the same approach, the range on the log scale was set on (4.646774, 6.350078) so the expansion of prior variance is 0.55. Number of components varies from 4-9, depending on the module. Posterior estimates for the densities for the segmented and unsegmented (low and high temperature) are shown in the Figure 4.10.

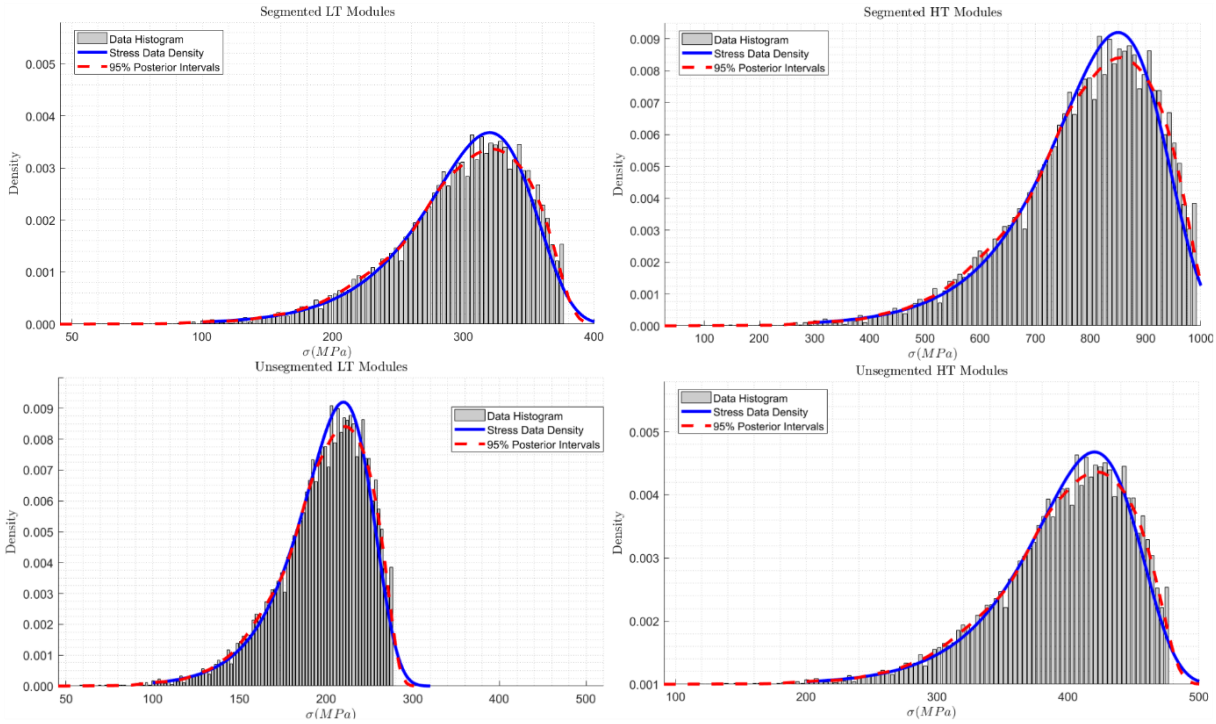


*Figure 4.10 Relative frequency histogram and densities of survival function for segmented and unsegmented modules under the Nonparametric model.*

Nonparametric lognormal function is able to describe the peaks and valleys that the parametric model can't. There is a slight discrepancy from the point of estimate and the density of the data around 900-1000 (MPa). But nevertheless, the data density remains within the estimated interval for given model. By comparing the densities regarding to different temperatures under nonparametric lognormal function gives us a clear insight to understand mean residual life. Figure 4.11 in that respect points interval estimates of the posterior density for survival function for segmented (Low and High Temperature) and unsegmented (high temperature).

Looking at the estimated densities we can see that segmented high temperature module has lowest surviving life compared to segmented low temperature module. The survival function estimates show that after 400 MPa the survival curve monotonically decreases. Subsequently the underlying explanation is that failure rate function at thermal stress ($\sigma \geq \sigma_y$) is finite for nonparametric survival model which distinguishes it from other existing models with infinite initial failure rates. If modules are stressed to failure lower than $\sigma_y$, then it is difficult to distinguish between lognormal and Weibull distribution. If Its above

then $\sigma_y$, then the probability of making a correct choice is fair, especially for small sizes samples and nonparametric lognormal module becomes quite good.

The subsequent a comparative investigation was conducted for the probability of failure for various thickness of segmented TE leg. The probability of failure for Weibull's distribution, Monte Carlo simulation and nonparametric survival function, for both low and high temperature modules are shown in Figure 4.12. The Monte Carlo simulation-based technique assists to distinguish different distributions and predict reliability based on empirically determined failure data [80]–[82].

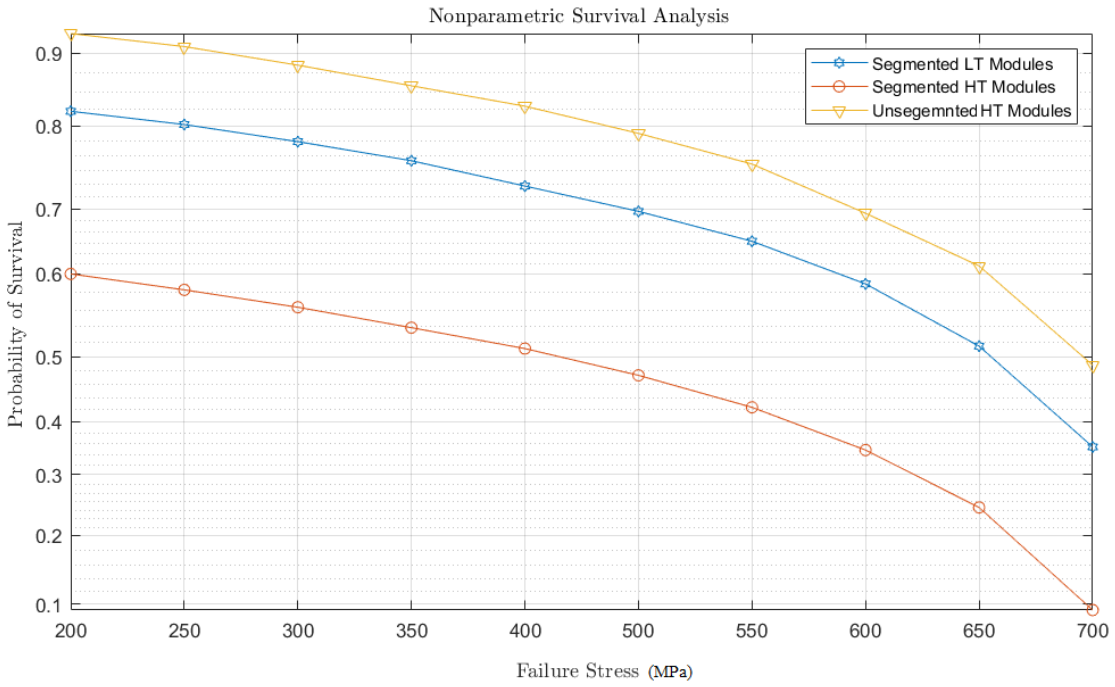


*Figure 4.11 Probability of Survival for segmented (Low and High Temperature) and unsegmented TE devices (high temperature)*

Especially distinguishing between nonparametric lognormal and Weibull distribution is of interest here because both are used to model probability of failure. The changing the in thickness corresponds to temperature very closely, producing varying probability map.

We used the posterior predictive survival approach, introduced by Gelfand and Gosh[83] to compare Weibull's model to the nonparametric lognormal mixture model. The comparative method is used to minimize expectation of specified survival function under

posterior predictive distribution model to replicate response observed in data. For both segmented HT and LT, the nonparametric lognormal mixture model performs significantly better than the Weibull's model. The comparison of distribution regarding to thickness of the thermoelectric leg provides us insight for modeling devices. This aspect ultimately changes the prospect of sizing the legs. We have noticed that unsegmented TE legs can survive between 4-5 (mm) with probability of failure of 30%, whereas the segmented TE legs can survive between 6-7 (mm) with probability of failure of 35%.

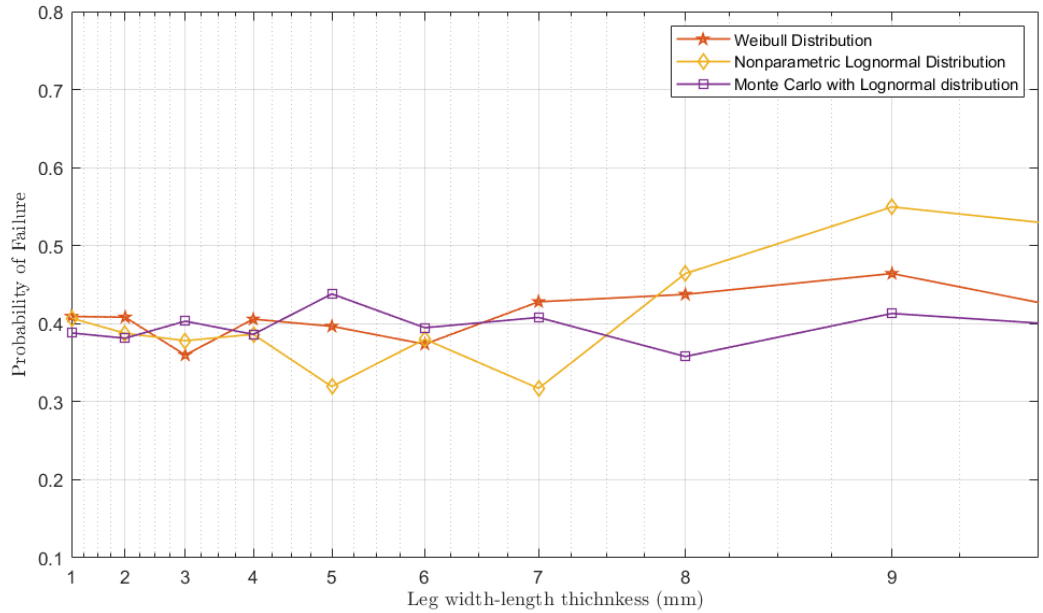


*Figure 4.12 Comparative Probability Analysis between Weibull, Monte Carlo and Nonparametric distributions*

As Shown in graph that onwards, the probability of failure enhances up to 60% for nonparametric lognormal distribution whereas 45% for Weibull distribution. The result of the comparison supports our earlier argument that nonparametric lognormal survival function is indeed a better model for these circumstances compared to Weibull model.

### 4.4.4 COMSOL Solution

Different literature [11, 19] demonstrated the similar results, where interface boundary conditions, spacing between leg and metallization of interface influence stresses

in the TE leg. The conducted simulation has particular focus on boundary conditions and spacing between each leg. Fixed boundary conditions (Case 1) have been widely seen in low temperature modules, whereas free boundary conditions (Case 2) are appropriate for medium to high temperature modules. In our configuration the hot ends of the leg are assumed to be free to expand whereas cold ends are considered to be bounded. Figure 4.13, in this regard, shows the influence of the boundary conditions on the reliability of a TE module couple with varying length size. The results are presented for the probability of failure by using equations of nonparametric survival function. The failure probability for p and n-types of legs have almost similar average as per the change in temperature gradient.

The probability of failure is directly proportional to the magnitude of stress. The stresses at cold and hot end of the leg are shown in figure 4.14 (a) and (b). The simulation results show the map of distribution within the TE leg. The distribution map shows particular observation related to compressive and tensile nature of stress. It has been noticed that compressive load contributes more to peak maximum principle stress in the legs (hence influences the probability of the failure) compared to tensile stresses. The reduction of tensile stresses is CTE mismatch at the interference under boundary condition (especially fixed). In this regard figure 4.15 shows maximum principle stresses, divided into three different zones.

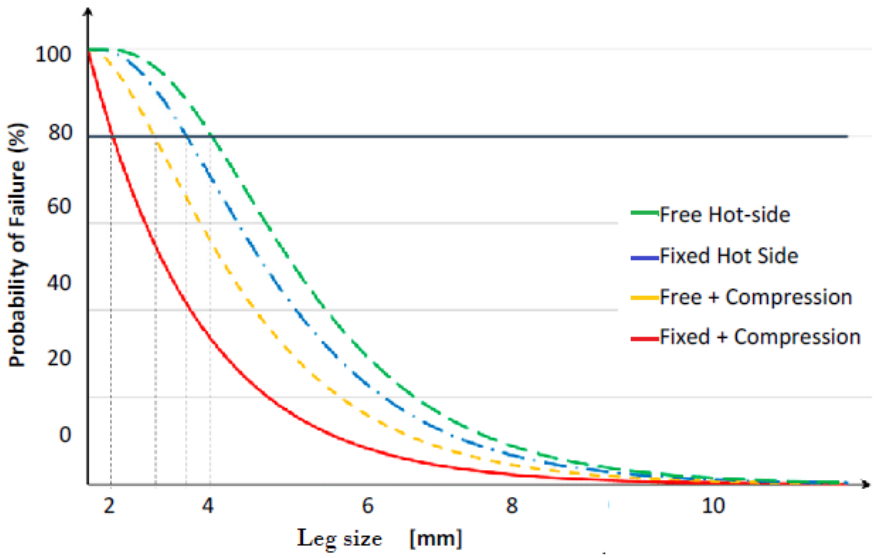


Figure 4.13 Effect of Boundary condition on Reliability of the device

The size of leg varies from 3mm to 7mm, and stress zones (A to C) vary as per change in leg size. The three zones indicate the maximum principle stress as per change in size of leg. Zone A is compressive zone, in which hike in stress is due to compressive stress and it is different for segmented and unsegmented module. In Zone A the main source of stress comes from hot end, and it shifts down to cold end, where constrain makes contribution. In this case, as shown in figure 4.16 legs tend more towards spallation outwards. The arc of the expansion (x-axis) is also dependent on temperature gradient. For zone A type of devices, the spacing between each leg was increase, which significantly increased the efficiency of the leg. Whereas Zone B devices are mostly segmented and include diffusion barrier layers and interconnected metallization. The work of Suhir and Erturun et al.[14], [84] has demonstrate the importance of spacing between each leg and its impact on stress. Zone B corresponds with their study, which shows that by increasing the leg size from 3 mm to 5 mm and spacing between (range between 1.5 to 2.5 mm) each leg can compensate compressive and tensile stress.

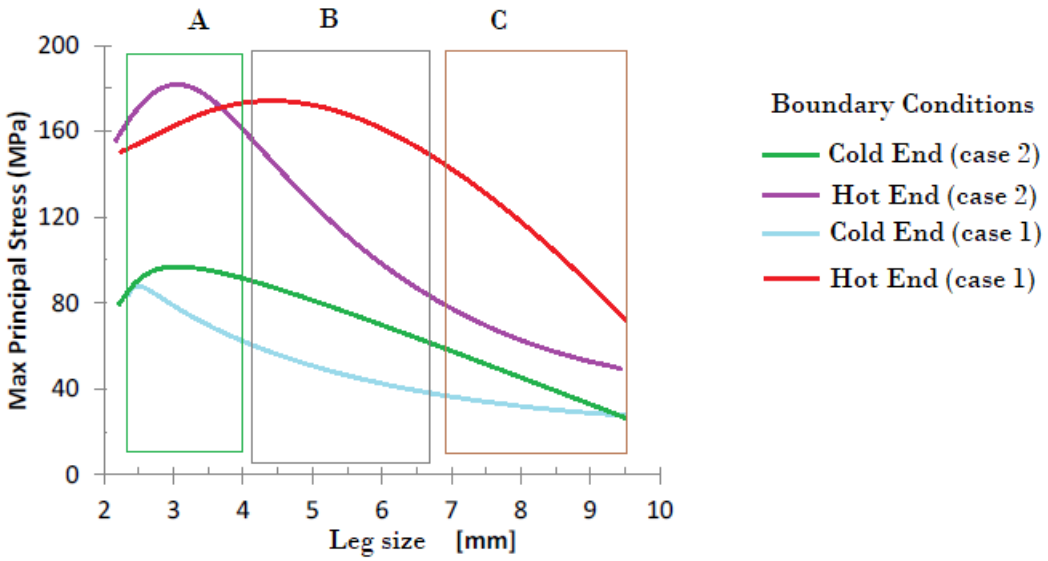


Figure 4.14. Effect on thermo-mechanical stress regarding to their boundary conditions

Whereas the zone C represents the tensile nature stress. By increasing the leg size from 6mm to 9 mm, the tensile stress, strain, and shearing strain stress dominates. Tensile stresses cause deformation and dislocation in the leg (as shown in figure 4.15).

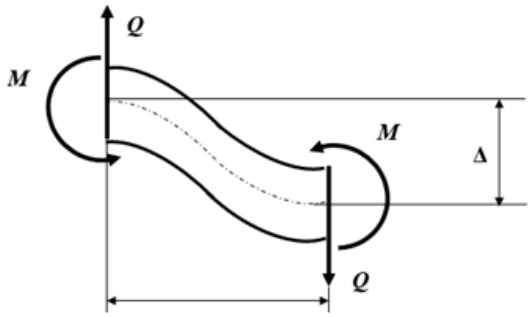


Figure 4.15 Visual Presentation of Deformation of leg

Figure 4.15 also provides visual insight of the peak von-Mises stress in the legs and influence of tensile (shear stress) on the maximum principle stress. The simulation study shows the influence of these factors on the reliability of TE device and how can these factors be minimized, that is, by increase space between them. Whereas figure 4.16 presents the results regarding to the leg spacing study. The figure shows that leg spacing has minor influence on the overall stress level of the TE device. While the maximum principle stresses reduce by increase leg spacing. This factor has significant effect on hot side of the leg. Since unconstrained expansion on x-axis direction, allow legs to radiate extensive heat or spall without deformation (slightly). The simulations were conducted with 4mm (unsegmented) and 6 mm (segmented) leg length and 1.5 mm (for unsegmented) and 2.5 mm (segmented) spacing. The parameters for figure 4.16 are derived from SKD materials and calculated for medium temperature gradient. The experimental results are configured in such a manner that increasing spacing between each leg assist to avoid heat concentration between legs and allows consistent exchange of heat with surrounding and within leg simultaneously.

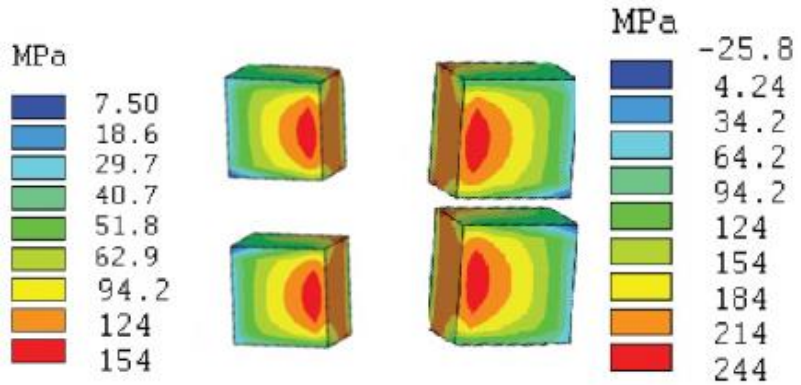


*Figure 4.16 Change in maximum stress by increasing space between each leg*

This factor is taken into consideration while calculating reliability of the TE device. It has been significantly noticed that by increasing the space between the legs and allocating them appropriate size can significantly optimize the reliability of the device.

## Conclusion

1. The model optimizes the Naotake plate theory, to analyze thermo-mechanical behavior of the thermoelectric device under optimized boundary condition, geometry, and space between legs. The model concludes that the reliability of segmented thermoelectric devices, operating at intermediate temperature, could be enhanced by using free-end boundary case. Whereas, unsegmented devices work longer under both, free and constraints, boundary conditions.
2. The simulation results evaluate the length to thickness ratio, compressive-tensile stresses, and equation of deformation. The model describes the impact of extension-bending, flexural stiffness, and Elastic constant on thermally induced stress. The calculated stresses are used to calculate specific number of thermoelectric legs in a thermoelectric system. Compared to previous methods, our model claims 13% reduction in number of legs.
3. The model calculates optimal maximum thermo-mechanical stresses between components, on edge and within volume. Two precise cases are presented based on boundary conditions. Case 1 (free boundary conditions) shows that though maximum stress has reduced but device encounter bending, spallation and dislocation during operational hours. Whereas Case 2 (vertically restricted and horizontally free) demonstrated that maximum stress develops vertically, whereas horizontal expansion tends to relief leg. The simulated results shows that segmented devices encounter compressive stresses, whereas unsegmented encounter tensile nature stresses. In this regard, a new model has been introduced to calculate number of legs by including stress into consideration. The model has shown that by increasing space between each leg, about 0.01 %, can compensate maximum stress. (done)
4. Currently available literature uses Weibull distribution and Mean-time-between-failure (MTBF) to calculate reliability of the thermoelectric device. Our comparative discussion shows that whether they don't fit (especially in case of segmented devices) or can't predict life of device with not more than 80% accuracy. Our model, compared to existing methods, uses parametric and non-parametric lognormal distribution to measure

lifetime of operating devices. The obtained lognormal mean residual life provides 80% accuracy on the “estimated mean value”, whereas survival function, driven from non-parametric lognormal distribution, gives 90% accuracy on thermo-mechanical durability.

## References


[1] "Global Thermoelectric Generators Market by Application (Waste Heat Recovery, Energy Harvesting, Direct Power Generation, Co-Generation), Temperature (<80c, 80-500c, >500c) Wattage, Type, Material, Vertical, Component, Region - Forecast to 2026- Product I," 2021. [Online]. Available: https://www.researchandmarkets.com/reports/5406454/global-thermoelectric-generators-market-by?utm_source=GNOM&utm_medium=PressRelease&utm_code=5nd6dx&utm_campaign=1582688+-+Global+Thermoelectric+Generators+Market+Report+2021%3A+Winners+of+the+Market+are+G.

[2] C. Gayner and K. K. Kar, "Progress in Materials Science Recent advances in thermoelectric materials," *Prog. Mater. Sci.*, vol. 83, pp. 330–382, 2016, doi: 10.1016/j.pmatsci.2016.07.002.

[3] H. J. Goldsmid, "Springer Series in Materials Science 121 Introduction to Thermoelectricity," Accessed: Dec. 15, 2021. [Online]. Available: http://www.springer.com/series/856.

[4] N. Generation *et al.*, "Engineering of Novel Thermoelectric Materials and Devices for Next Generation, Long Life, 20% Efficient Space Power Systems," pp. 1–6, 2013.

[5] R. P. Chasmar and R. Stratton, "The Thermoelectric Figure of Merit and its Relation to Thermoelectric Generators," *undefined*, vol. 7, no. 1, pp. 52–72, Jul. 1959, doi: 10.1080/00207215908937186.

[6] H. T. Problems and T. Stresses, "Heat transfer problems and thermal stresses," pp. 1–14.

[7] B. Qi, H. Zhang, X. Y. Huang, S. Q. Bai, and X. Shi, "Thermoelectric Devices for Power Generation : Recent Progress and Future Challenges **," no. 2, 2016, doi: 10.1002/adem.201500333.

[8] M. K. Kashyap and R. Singla, "Beyond 3D-traditional materials thermoelectric materials," *Thermoelectr. Adv. Thermoelectr. Mater.*, pp. 163–193, Jan. 2021, doi:

10.1016/B978-0-12-819984-8.00007-2.

[9] M. Apostol, “Generalized theory of thermoelectric figure of merit,” pp. 3–5, 2008, doi: 10.1063/1.2974789.

[10] M. Oçko, S. Žonja, and M. Ivanda, “Thermoelectric materials: Problems and perspectives,” *MIPRO 2010 - 33rd Int. Conv. Inf. Commun. Technol. Electron. Microelectron. Proc.*, pp. 16–21, 2010.

[11] L. I. Anatychuk and O. J. Luste, “On the reliability of thermoelectric cooling and generator modules,” *Int. Conf. Thermoelectr. ICT, Proc.*, pp. 101–104, 1998.

[12] J. A. Nesbitt, E. J. Opila, and M. V Nathal, “In Situ Growth of a Yb 2 O 3 Layer for Sublimation Suppression for Yb 14 MnSb 11 Thermoelectric Material for Space Power Applications,” vol. 41, no. 6, pp. 1267–1273, 2012, doi: 10.1007/s11664-011-1875-7.

[13] P. Ponnusamy, H. Kamila, E. Müller, and J. de Boor, “Efficiency as a performance metric for material optimization in thermoelectric generators,” *J. Phys. Energy*, vol. 3, no. 4, p. 044006, Oct. 2021, doi: 10.1088/2515-7655/AC293E.

[14] U. Erturun, K. Erermis, and K. Mossi, “Influence of leg sizing and spacing on power generation and thermal stresses of thermoelectric devices,” *Appl. Energy*, vol. 159, pp. 19–27, 2015, doi: 10.1016/j.apenergy.2015.08.112.

[15] A. B. Zhang, B. L. Wang, J. Wang, and J. K. Du, “International Journal of Thermal Sciences Two-dimensional problem of thermoelectric materials with an elliptic hole or a rigid inclusion,” vol. 117, pp. 184–195, 2017, doi: 10.1016/j.ijthermalsci.2017.03.020.

[16] H. Ngan, V. Nong, D. Version, and V. Nong, “Design and Optimization of Effective Segmented Thermoelectric Generator for Waste Heat Recovery,” 2015.

[17] H. Wu, A. T. Wu, P. Wei, and S. Chen, “Interfacial reactions in thermoelectric modules,” *Mater. Res. Lett.*, vol. 0, no. 0, pp. 1–5, 2018, doi: 10.1080/21663831.2018.1436092.

[18] H. Tian, X. Sun, Q. Jia, X. Liang, G. Shu, and X. Wang, “Comparison and parameter optimization of a segmented thermoelectric generator by using the high temperature

exhaust of a diesel engine," *Energy*, vol. 84, pp. 121–130, 2015, doi: 10.1016/j.energy.2015.02.063.

[19] H. Tian, N. Jiang, Q. Jia, X. Sun, G. Shu, and X. Liang, "Comparison of Segmented and Traditional Thermoelectric Generator for Waste Heat Recovery of Diesel Engine," *Energy Procedia*, vol. 75, pp. 590–596, 2015, doi: 10.1016/j.egypro.2015.07.461.

[20] T. Ursell, "Compatibility of segmented thermoelectric generators Compatibility of Segmented Thermoelectric Generators," no. July, 2014, doi: 10.1109/ICT.2002.1190349.

[21] "Mathematical Modelling of Thermo-Mechanical Stresses Arising in Rectangular Supports of Thermoelectric Modules." https://www.elibrary.ru/item.asp?id=45717006 (accessed Nov. 02, 2022).

[22] Y. Tian, Z. Miao, X. Meng, W. Yan, and M. Zhu, "Thermo-mechanical analysis of thermoelectric devices based on single p-n pair," *Energy Procedia*, vol. 158, pp. 1559–1564, 2019, doi: 10.1016/j.egypro.2019.01.366.

[23] X. Li, L. Cui, L. Zhang, and Z. Wang, "Heat reliability analysis of thermoelectric generators (TEG) based on heat transfer process," *IOP Conf. Ser. Mater. Sci. Eng.*, vol. 1043, no. 2, p. 022036, Jan. 2021, doi: 10.1088/1757-899X/1043/2/022036.

[24] N. K. Karri and C. Mo, "Structural Reliability Evaluation of Thermoelectric Generator Modules : Influence of End Conditions , Leg Geometry , Metallization , and Processing Temperatures," vol. 47, no. 10, 2018, doi: 10.1007/s11664-018-6505-1.

[25] T. Pan, T. Gong, W. Yang, and Y. Wu, "Numerical Study on the Thermal Stress and its Formation Mechanism of a Thermoelectric Device," *J. Therm. Sci.*, vol. 27, no. 3, pp. 249–258, 2018, doi: 10.1007/s11630-018-1006-3.

[26] E. Suhir, *Structural Analysis in Microelectronic and Fiber-Optic Systems: Basic Principles of Engineering Elastictiy and Fundamentals of Structural Analysis (Volume-I)*. 2012.

[27] N. Noda *et al.*, *THERMAL STRESSES 2nd Edition*, vol. 53, no. 9. 2003.

[28] Z. H. Jin, “Thermal stresses in a multilayered thin film thermoelectric structure,” *Microelectron. Reliab.*, vol. 54, no. 6–7, pp. 1363–1368, 2014, doi: 10.1016/j.microrel.2014.02.028.

[29] N. Noda, R. B. Hetnarski, Y. Tanigawa, N. Noda, R. B. Hetnarski, and Y. Tanigawa, “Basic Equations of Thermoelasticity,” *Therm. Stress.*, pp. 137–178, 2018, doi: 10.1201/9780203735831-4.

[30] N. K. Karri and C. Mo, “Reliable Thermoelectric Module Design under Opposing Requirements from Structural and Thermoelectric Considerations,” *J. Electron. Mater.*, vol. 47, no. 6, pp. 3127–3135, 2018, doi: 10.1007/s11664-017-5934-6.

[31] N. K. Karri and C. Mo, “Geometry optimization for structural reliability and performance of a thermoelectric generator,” *SN Appl. Sci.*, vol. 1, no. 9, pp. 1–17, 2019, doi: 10.1007/s42452-019-1120-1.

[32] O. M. Jadaan and A. A. Wereszczak, “Probabilistic Mechanical Reliability Prediction of Thermoelectric Legs Under contract DE-AC05-00OR22725,” 2009.

[33] A. A. Wereszczak and E. D. Case, *Mechanical Response of Thermoelectric Materials*, no. May. 2015.

[34] A. A. Wereszczak *et al.*, “Thermoelectric Mechanical Reliability,” *Electron. Mater. Lett.*, vol. 7, no. 1, p. 952, 2011, doi: 10.1007/s13391-011-0917-x.

[35] S. Sattar, “Measuring Probability of Failure of Thermoelectric Legs through Lognormal and Weibull Distribution,” *J. Phys. Conf. Ser.*, vol. 1560, no. 1, 2020, doi: 10.1088/1742-6596/1560/1/012025.

[36] G. Skomedal, N. R. Kristiansen, R. Sottong, and H. Middleton, “Evaluation of Thermoelectric Performance and Durability of Functionalized Skutterudite Legs,” vol. 46, no. 4, pp. 2438–2450, 2017, doi: 10.1007/s11664-017-5309-z.

[37] Y. Mozharivskyj, A. O. Pecharsky, S. Bud’ko, and G. J. Miller, “A Promising Thermoelectric Material: Zn4Sb3 or Zn6-δSb5. Its Composition, Structure, Stability, and Polymorphs. Structure and Stability of Zn1-δSb,” *Chem. Mater.*, vol. 16, no. 8, pp. 1580–1589, 2004, doi: 10.1021/cm035274a.

[38] S. Sattar and A. Osipkov, “Understanding reliability of the thermoelectric devices for

space application," in *Advances in the Astronautical Sciences*, 2020, vol. 170.

[39] S. Hyun, Y. Kim, and C. Yoo, "Oxidation suppression characteristics of the YSZ coating on Mg 2 Si thermoelectric legs," *Ceram. Int.*, vol. 42, no. 8, pp. 10279–10288, 2016, doi: 10.1016/j.ceramint.2016.03.161.

[40] Y. Li, B. He, J. P. Heremans, and J. Zhao, "High-temperature oxidation behavior of thermoelectric SnSe," vol. 669, pp. 224–231, 2016, doi: 10.1016/j.jallcom.2016.01.258.

[41] K. Zawadzka, E. Godlewska, K. Mars, M. Nocun, A. Kryshtal, and A. Czyrska-filemonowicz, "Enhancement of oxidation resistance of CoSb 3 thermoelectric material by glass coating," *Mater. Des.*, vol. 119, pp. 65–75, 2017, doi: 10.1016/j.matdes.2017.01.055.

[42] K. C. Lukas, W. S. Liu, Q. Jie, Z. F. Ren, and C. P. Opeil, "Thermal stability of thermoelectric materials via in situ resistivity measurements," *Rev. Sci. Instrum.*, vol. 83, no. 11, pp. 1–14, 2012, doi: 10.1063/1.4767904.

[43] R. C. Gupta and D. M. Bradley, "On Representing the Mean Residual Life in Terms of the Failure Rate," pp. 1–13, 2004, [Online]. Available: http://arxiv.org/abs/math/0411297.

[44] W. J. Hall and J. A. Wellner, "Estimation of Mean Residual Life," *Stat. Model. Biol. Syst.*, pp. 169–189, 2020, doi: 10.1007/978-3-030-34675-1_10.

[45] V. Poynor and A. Kottas, "Nonparametric Bayesian inference for mean residual life functions in survival analysis," *Biostatistics*, vol. 20, no. 2, pp. 240–255, 2019, doi: 10.1093/biostatistics/kxx075.

[46] L. C. Tang, Y. Lu, and E. P. Chew, "Mean residual life of lifetime distributions," *IEEE Trans. Reliab.*, vol. 48, no. 1, pp. 73–78, 1999, doi: 10.1109/24.765930.

[47] S. Yan, A. T. Submitted, F. O. R. The, D. Of, and D. Of, "Reliability Modeling and Analysis With Mean Residual Life," 2009.

[48] R. C. Gupta and S. Lvin, "Reliability functions of generalized log-normal model," *Math. Comput. Model.*, vol. 42, no. 9–10, pp. 939–946, 2005, doi: 10.1016/j.mcm.2005.06.005.

[49] O. Ozenda and E. G. Virga, “On the Kirchhoff-Love Hypothesis (Revised and Vindicated),” *J. Elast.*, vol. 143, no. 2, pp. 359–384, 2021, doi: 10.1007/s10659-021-09819-7.

[50] D. W. A. Rees, “Stress and Strain Transformation,” *Mech. Solids Struct.*, pp. 1–42, 2000, doi: 10.1142/9781860943065_0001.

[51] T. F. Johnson and W. D. Pilkey, “Accurate Thermal Stresses for Beams : Normal Stress,” pp. 3–6, 1954.

[52] E. Carrera, F. A. Fazzolari, and M. Cinefra, “Chapter 4 - Fundamental of mechanics of beams, plates and shells,” in *Thermal Stress Analysis of Beams, Plates and Shells*, E. Carrera, F. A. Fazzolari, and M. Cinefra, Eds. Oxford: Academic Press, 2017, pp. 91–116.

[53] M. H. SADD, “7 - Two-Dimensional Formulation,” in *Elasticity*, M. H. SADD, Ed. Burlington: Academic Press, 2005, pp. 123–138.

[54] H. Song, K. Song, and C. Gao, “Temperature and thermal stress around an elliptic functional defect in a thermoelectric material,” *Mech. Mater.*, vol. 130, no. January, pp. 58–64, 2019, doi: 10.1016/j.mechmat.2019.01.008.

[55] Y. Demirel and V. Gerbaud, “Fundamentals of Equilibrium Thermodynamics,” *Nonequilibrium Thermodyn.*, pp. 1–85, Jan. 2019, doi: 10.1016/B978-0-444-64112-0.00001-0.

[56] N. Levinson, “A theorem of Boas,” *https://doi.org/10.1215/S0012-7094-41-00811-6*, vol. 8, no. 1, pp. 181–182, Mar. 1941, doi: 10.1215/S0012-7094-41-00811-6.

[57] T. Morita and K. I. Sato, “Boas’ formula and sampling theorem,” *Axioms*, vol. 4, no. 1, pp. 71–83, 2015, doi: 10.3390/axioms4010071.

[58] M. Ricz, “On the lntegrability of Double,” pp. 452–465, 1991.

[59] J. Henry and A. M. Ramos, “3 - Complements to the Model Problem,” in *Factorization of Boundary Value Problems Using the Invariant Embedding Method*, J. Henry and A. M. Ramos, Eds. Elsevier, 2016, pp. 41–67.

[60] N. D. Katopodes, “Basic Concepts,” *Free. Flow*, pp. 2–79, Jan. 2019, doi: 10.1016/B978-0-12-815485-4.00007-3.

[61] G. G. Garrett, “Introduction To Fracture Mechanics.,” *Civ Eng S Afr*, vol. 19, no. 10, pp. 223–227, 1977.

[62] O. A. Bauchau and J. I. Craig, “Euler-Bernoulli beam theory,” in *Structural Analysis*, O. A. Bauchau and J. I. Craig, Eds. Dordrecht: Springer Netherlands, 2009, pp. 173–221.

[63] K. S. Schmitz, “Five Important Equations in Thermodynamics,” *Phys. Chem.*, pp. 41–98, Jan. 2017, doi: 10.1016/B978-0-12-800514-9.00002-X.

[64] IVAR STAKGOLD, “THE CAUCHY RELATIONS IN A MOLECULAR THEORY OF ELASTICITY on JSTOR,” *Quarterly of Applied Mathematics, Vol. 8, No. 2*. https://www.jstor.org/stable/43633803 (accessed Nov. 02, 2022).

[65] V. Benci and L. Luperi Baglini, “A generalization of Gauss’ divergence theorem,” 2015.

[66] S. Sun and T. Zhang, *Reservoir Simulations: Machine Learning and Modeling*. Elsevier, 2020.

[67] W.-M. Liu, X.-G. Zhao, and L. Ke, “Thermal generation of shift electric current You may also like Intrinsic Localization of Bloch Electrons in dc-ac Electric Fields,” 2020, doi: 10.1088/1367-2630/ab64af.

[68] K. W. Böer and U. W. Pohl, “Phonon-Induced Thermal Properties,” *Semicond. Phys.*, pp. 151–179, 2018, doi: 10.1007/978-3-319-69150-3_5.

[69] O. V. (Oleg V. Marchenko, L. S. (Lev S. Beliâèv, and Sibirskiĭ ėnergeticheskiĭ institut im. L.A. Melent′eva., “Metody rascheta termoėlektricheskikh generatorov,” p. 218.

[70] E. Suhir and A. Shakouri, “Predicted thermal stress in a multileg thermoelectric module (TEM) design,” *J. Appl. Mech. Trans. ASME*, vol. 80, no. 2, pp. 1–12, 2013, doi: 10.1115/1.4007524.

[71] E. Suhir and A. Shakouri, “Assembly bonded at the ends: Could thinner and longer legs result in a lower thermal stress in a thermoelectric module design,” *J. Appl. Mech. Trans. ASME*, vol. 79, no. 6, 2012, doi: 10.1115/1.4006597.

[72] T. Ming *et al.*, “Numerical analysis on the thermal behavior of a segmented

thermoelectric generator," *Int. J. Hydrogen Energy*, vol. 42, no. 5, pp. 3521–3535, 2017, doi: 10.1016/j.ijhydene.2016.11.021.

[73] M. Shioya, S. Yasui, and A. Takaku, "Relation between interfacial shear strength and tensile strength of carbon fiber/resin composite strands," *Compos. Interfaces*, vol. 6, no. 4, pp. 305–323, 1999, doi: 10.1163/156855498X00333.

[74] E. Bridget and M. Abiodun, "Inference on Stress-Strength Reliability for Log-Normal Distribution based on Lower Record Values," vol. 22, no. July, pp. 77–97, 2017.

[75] W. Kuo, W.-T. K. Chien, and T. Kim, "Reliability, Yield, and Stress Burn-In," *Reliab. Yield, Stress Burn.*, 1998, doi: 10.1007/978-1-4615-5671-8.

[76] T. L. Distribution, "The Lognormal Distribution," pp. 277–279.

[77] R. C. Gupta, N. Kannan, and A. Raychaudhuri, "Analysis of lognormal survival data," *Math. Biosci.*, vol. 139, no. 2, pp. 103–115, 1997, doi: 10.1016/S0025-5564(96)00133-2.

[78] A. D. Telang and V. Mariappan, "Hazard Rate of Lognormal Distribution : An Investigation," vol. 4, no. 2, pp. 103–108, 2008.

[79] Y. Ha and H. Zhang, "Fast multi-output relevance vector regression," *Econ. Model.*, vol. 81, pp. 217–230, 2019, doi: 10.1016/j.econmod.2019.04.007.

[80] F. Innal, "Monte Carlo (MC) simulation for system reliability," *NTNU -Trondheim*, no. Mc, pp. 10–12, 2015.

[81] S. Abrar, S. Bobba, and S. M. Rehman, "Probability study on the thermal stress distribution in the thick HK40 stainless steel pipe using finite element method," no. December 2018, pp. 1–20, 2019, doi: 10.3390/designs3010009.

[82] S. Bobba, S. Abrar, and S. M. Rehman, "Probability Study on the Thermal Stress Distribution in Thick HK40 Stainless Steel Pipe Using Finite Element Method," pp. 1–26, 2019, doi: 10.3390/designs3010009.

[83] A. E. Gelfand and S. K. Ghosh, "Model choice: A minimum posterior predictive loss approach," *Biometrika*, vol. 85, no. 1, pp. 1–11, 1998, doi: 10.1093/biomet/85.1.1.

[84] U. Erturun, K. Erermis, and K. Mossi, "Effect of various leg geometries on thermo-

mechanical and power generation performance of thermoelectric devices," *Appl. Therm. Eng.*, vol. 73, no. 1, pp. 128–141, 2014, doi: 10.1016/j.applthermaleng.2014.07.027.